ABSTRACT

Optimization of Muscle Physiological Parameters for a Computer Model
of the Human Shoulder Girdle

Joel D. White, M.S.B.M.E.

Mentors: Brian A. Garner, Ph.D.
Carolyn P. Skurla, Ph.D.

The shoulder girdle serves as the platform for all human upper extremity movement and plays an integral role in providing the large range of motion of the shoulder joint. However, computer models representing human upper-extremity biomechanics have suffered from a lack of published data relating to the shoulder girdle. The aim of this study was to validate an existing human upper-extremity model in light of newly-published strength data for twelve shoulder shrugging exercises at various shoulder girdle positions. The three-dimensional model accounted for motions of the clavicle, scapula, and humerus, and was actuated by 19 muscle bundles. The model was used to simulate each of the reported shrugging exercises, while the model's muscle physiological parameters were optimized to minimize error between the simulated and experimental strength measures. The optimized model accurately reproduced the experimental shoulder elevation and depression strengths, but tended to overachieve for retraction and underachieve for protraction exercises.

Optimization of Muscle Physiological Parameters for a Computer Model
of the Human Shoulder Girdle

by

Joel D. White, B.S.M.E

A Thesis

Approved by the Department of Mechanical Engineering

____
William Jordan, Ph.D., Chairperson

Submitted to the Graduate Faculty of
Baylor University in Partial Fulfillment of the
Requirements for the Degree
of
Masters of Science in Biomedical Engineering

Approved by the Thesis Committee

____
Brian A. Garner, Ph.D., Chairperson

____
Carolyn P. Skurla, Ph.D.

____
Jaeho Shim, Ph.D.

Accepted by the Graduate School
May 2011

____
J. Larry Lyon, Ph.D., Dean

Page bearing signatures is kept on file in the Graduate School.

Copyright © 2011 by Joel D. White

All rights reserved

TABLE OF CONTENTS

LIST OF FIGURES

LIST OF TABLES

LIST OF ABBREVIATIONS

CT	Computed Tomography
MRI	Medical Resonance Imaging
VHP	Visible Human Project
VHM	Visible Human Male

Muscle Parameter Abbreviations:

Lom	Optimal Muscle-Fiber Length
Lst	Tendon Slack Length
Fom	Peak Isometric Force

Muscle Abbreviations:

Subclav	Subclavius
Subscap	Subscapularis
SerantsS	Serratus Anterior (Superior)
SerantM	Serratus Anterior (Middle)
SerantI	Serratus Anterior (Inferior)
TrapC	Trapezius (C1-C6)
TrapC7	Trapezius (C7)
TrapT1	Trapezius (T1)
TrapT	Trapezius (T2-T7)
Lvs	Levator Scapulae
Rmn	Rhomboid Minor
RmjT2	Rhomboid Major (T1-T2)
RmjT3	Rhomboid Major (T3-T4)
Pmn	Pectoralis Minor
PmjC	Pectoralis Major (Clavicular)
PmjS	Pectoralis Major (Sternal)
PmjR	Pectoralis Major (Ribs)
LtdT	Latissimus Dorsi (Thoracic)
LtdL	Latissimus Dorsi (Lumbar)
LtdI	Latissimus Dorsi (Illiac)
Tmj	Teres Major

ACKNOWLEDGMENTS

I would like to express my appreciation to my advisors Dr. Garner and Dr. Skurla for guiding me through this process, and to Dr. Shim for serving on my committee. I very much appreciate the time that each of you has invested in my education and am thankful for the great time I had working with each of you. Dr. Garner, I am thankful for your patience and understanding as I learned from you. Dr. Skurla, thank you for your feedback and constant support.

I am grateful to God for blessing me with the means and ability to achieve this education. My wife has been a constant support and encouragement to me during this process. Her patience, understanding, and support have been an amazing blessing, and I want to thank her for everything she has done to help me accomplish this goal . I would also like to thank my parents for investing their lives in my growth and for their immense support of my education throughout my life. My family has been a huge blessing and encouragement to me and I am very thankful for them.

I would like to thank my colleagues for their encouragement, time, and help throughout the entire graduate school process.

CHAPTER ONE

Introduction

Musculoskeletal Modeling

Importance of Modeling

Accurate models of the body are developed to simulate how the body will react in all types of environments. Models are important for several reasons. First, models can estimate internal mechanics, such as muscle forces, that are impossible or impractical to measure experimentally. Second, models can simulate a variety of scenarios that would be much more cost and time intensive using experimental methods. Finally, models can be used to simulate situations in which a real person's safety would be put into jeopardy. Experiments in extreme or dangerous environments can be safely simulated without risk of harm to researchers or subjects. However, the utility of a model depends on how accurately it represents the real system.

Applications

Modeling of the human musculoskeletal system has applications in both research and clinical environments. Musculoskeletal models can be used to simulate surgeries to determine best practices for doctors. Changes in the muscle and tendon properties can drastically influence the patient's range of motion and strength. The effects of muscles being cut or tendons being attached at differing sites on the bone could be calculated prior to surgeries, reducing guesswork by the surgeon and providing optimal results for the patient. Models can be made to simulate many types of exercises, providing important information on how a subject would react to changes to their body or their environment.

Purpose

The purpose of this research is to simulate previously performed maximal isometric strength exercises reported in Garner and Shim [1], compare the model's strength to those of human subjects, and optimize the model's muscle physiological parameters to reduce error between the two. We hypothesize that the optimized model will be able to accurately simulate the exercise experiments, and that the computed muscle physiological parameters will stay within reasonable physiological bounds.

Musculoskeletal System of the Shoulder Girdle

In this study, a detailed musculoskeletal model of the shoulder girdle was developed. The descriptions of the bones, muscles, and joints that were used in this model were all derived from the same anatomical database that was provided by the National Library of Medicine Visible Human Male project [2].

An understanding of musculoskeletal biomechanics is necessary for grasping important features needed for work with a computer model of the human shoulder girdle. The musculoskeletal system of the human body is comprised of two overarching systems; the passive system and the active system. These two systems work together to move the body in a very efficient manner while still allowing for a broad range of motions and activities to be possible.

The passive system consists of components that cannot produce force on their own but generate forces in response to forces produced by the active system. These components include the skeleton, cartilage, ligaments, and other connective tissues. The skeletal system provides the primary structure within the body. Cartilage is a strong, semi-flexible tissue that provides structure in some areas of the body and is found in joints, where it provides a smooth articulating surface as well as cushioning for bones during movement. Ligaments are strong and flexible connective tissues that connect bones together. Tendons are fibrous connective tissues that attach muscle to bone. These connections help maintain stability in the skeletal system and provide constraints for joints' range of motion.

The active system consists entirely of muscle tissue. Muscle is a fibrous tissue that contracts when stimulated by the nervous system. This contraction is the basis for all major force-generation and movement in the body. These forces are then transmitted from the muscle to the skeletal system by the tendons, which allow the body to control its posture, body movements, and maintain its balance.

The skeletal system provides the primary structure within the body while the muscular system produces forces between bones and moments about joints. These joint moments then give rise to the locomotion of the body. Each muscle-tendon unit is fixed to the skeleton in two places: the origin and the insertion points. The pathways between these points are generally curved paths because they wrap over underlying surfaces such as bone, other muscles, or other tissues. The geometries of these muscle pathways are dependent on the shapes of the bones and tissues, as well as the joint positions [3].

Anatomy of the Shoulder Girdle

Importance

The shoulder girdle is a complex system, comprised of four joints and multiple muscles to help move and stabilize the extremely flexible joint [4, 5]. The human shoulder is a set of joints that produces the largest range of motion in the human body [6]. The shoulder girdle is extremely important in extending the range of motion for this joint system. If the shoulder girdle is fixed, then the humerus can only be elevated 120 degrees [6]. When the shoulder girdle is included in the kinematic model, the range of motion is substantially increased. The complexity of this movement is many times oversimplified or neglected in models of the shoulder and shoulder girdle. The movement articulates with no fixed center of rotation and is therefore difficult to illustrate [7]. Complex articulations between the bones allow for wide range of motion, and large muscles give the shoulder the stability that it needs to operate effectively. A detailed description of the shoulder girdle is presented in two sections: the components of the skeletal system, and the components of the muscular system.

Skeletal System

The skeletal system of the shoulder girdle is made up of three primary components, which forms a serial linkage connecting the trunk of the body to the arm. These include the clavicle, scapula, and the proximal end of the humerus (Figure 1) [4, 8] Many of the muscles that articulate these bones also attach to the humerus, sternum, and numerous vertebra.

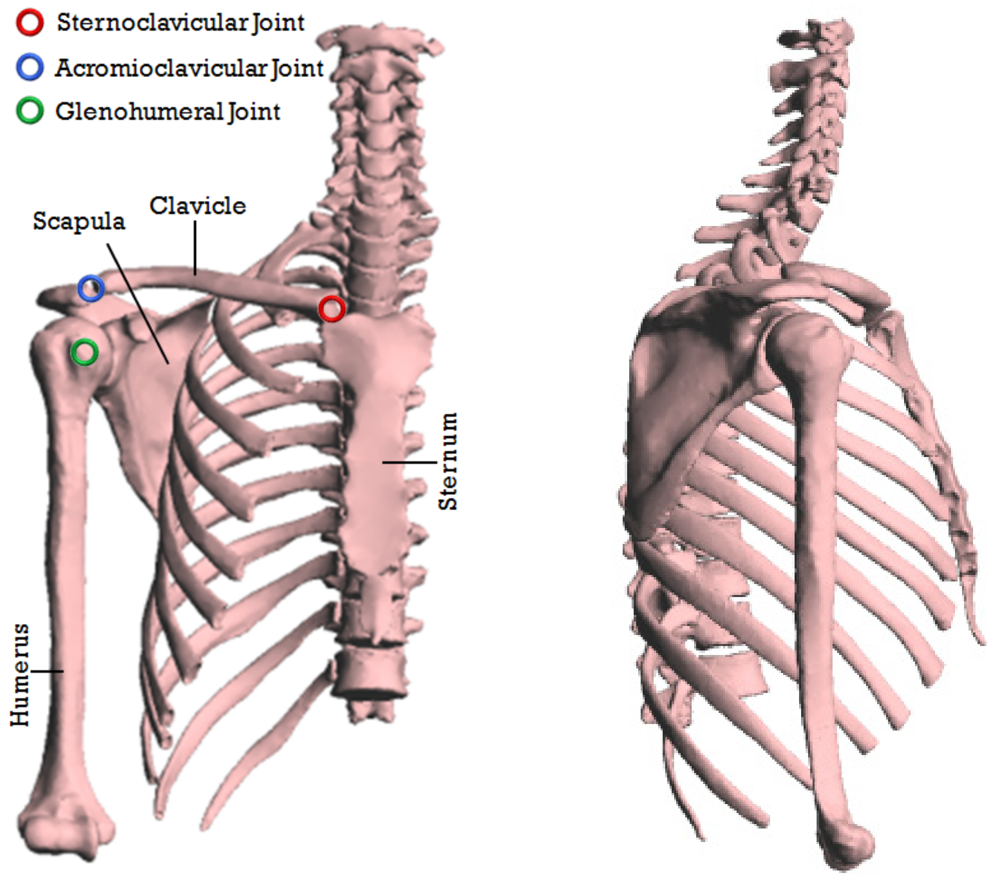

Figure 1: Anterior-posterior and right medial-lateral views of the skeletal system of the shoulder girdle with primary bones and joints labeled

The clavicle is the connecting link between the scapula and the sternum (Figure 2), and acts to hold the arm laterally away from the torso. The sternoclavicular joint behaves like a ball and socket joint, so it allows the clavicle to swivel and pivot, and supports the shoulder shrugging motion [9]. The sternoclavicular joint is also the only joint which directly attaches the skeletal system of the shoulder and arm to the rest of the body.

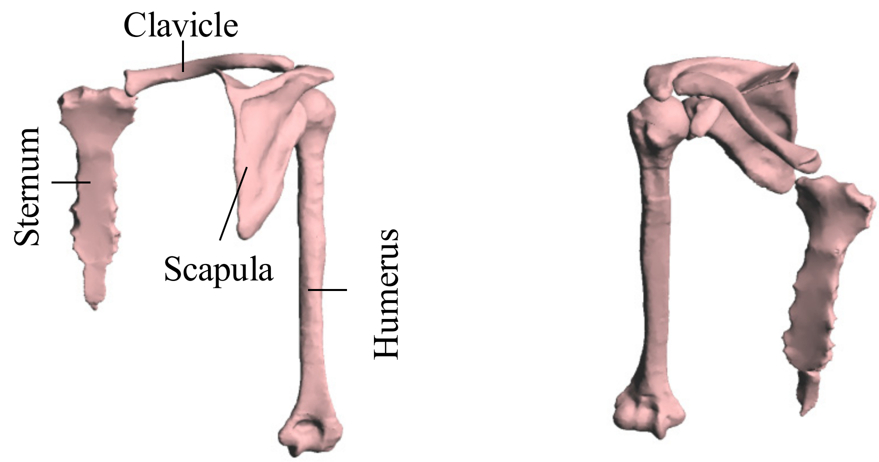

Figure 2: Posterior-anterior view and oblique views of the skeletal models of sternum, clavicle, scapula, and humerus

The scapula attaches to the distal end of the clavicle at the acromioclavicular joint, which also behaves like a ball and socket joint. The scapula is a broad, flat bone that slides along the posterior of the thorax. The muscle groups that attach to the scapula are the largest of the shoulder girdle and so are considered the primary muscles of the shoulder girdle. The articulation between the scapula and the thorax is sometimes considered a joint and has been named the scapulothoracic joint. The glenohumeral joint is a ball and socket joint located on the far lateral side of the scapula. It is a concave structure into which the proximal end of the humerus (ie, humeral head) fits and articulates. The glenohumeral joint provides the widest range of motion and is also the least stable joint of the shoulder.

The humerus is the longest bone in the arm, and provides over half the length of the arm. The proximal end of the humerus articulates in the glenoid fossa of the scapula, and the distal end of the humerus articulates at the elbow with the radius and ulna.

Muscular System

The muscular system of the shoulder girdle is extensive because it spans numerous joint systems. The model created consisted of 11 different muscles, with several being broken up into multiple muscle bundles. The muscles of the shoulder girdle that were modeled include: the subclavius, subscapularis, serratus anterior, trapezius, levator scapulae, rhomboid minor and major, latissimus dorsi, teres major, pectoralis major, and the pectoralis minor. The serratus anterior, trapezius, rhomboid major, pectoralis major, and latissimus dorsi muscles were broken up into multiple muscle bundles to more accurately model their muscle pathways. Figure 3 and Figure 4 (shown below) provide anterior and posterior diagrams of the muscular systems of the upper body.

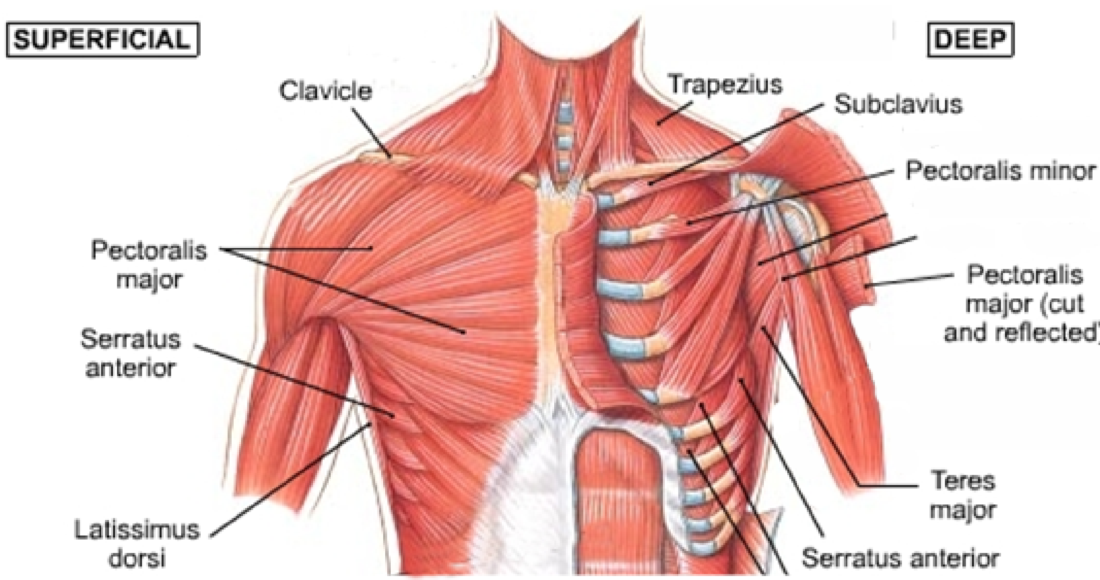

Figure 3: Muscular system anterior view [10]

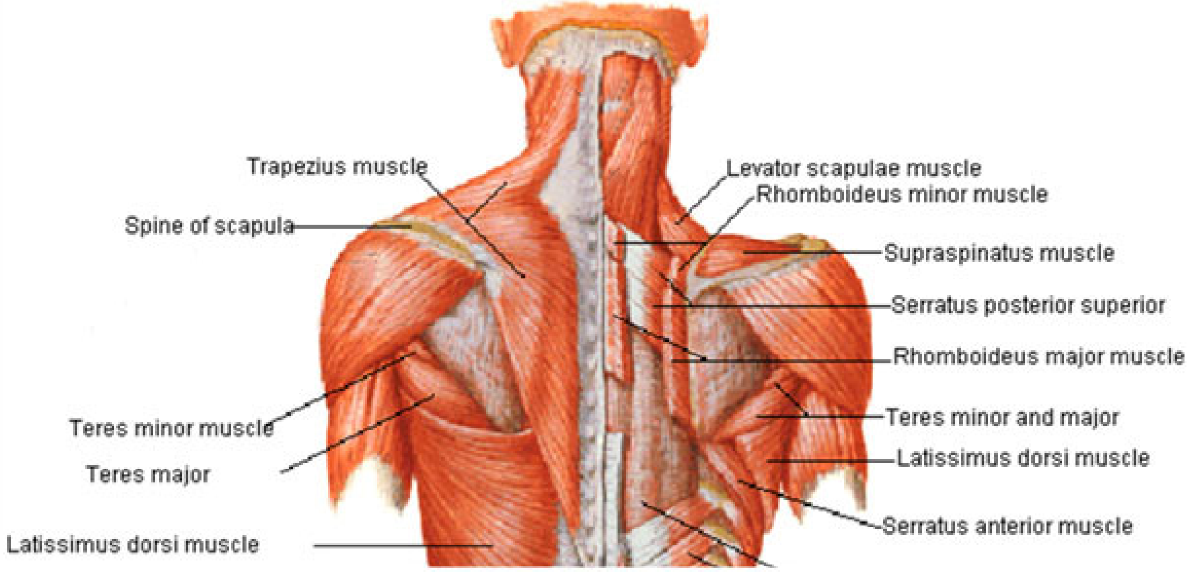

Figure 4: Muscular system posterior view [10]

Musculoskeletal Biomechanics

Modeling of Human Biomechanics

Musculoskeletal models of the human body commonly describe four systems in the body. Models generally have representations of the bone and joint mechanics, each muscle's line of action, the muscle physiological properties, and muscle activation dynamics. The bone and joint mechanics describe how the rigid structures of the body interact with each other, and the muscle lines of action prescribe the paths of the muscles with relation to the skeletal and joint structures. These muscles produce force when activated by electrical impulses sent to the muscular system when triggered by the brain. The physiological properties for the muscles determine the physical characteristics of each muscle and how they react when activated.

Muscle physiology

Muscles contract when activated, and their capacity to produce force varies with their length. Their force-length relationship can be displayed as a bell-type curve, as is shown in Figure 5. The force produced when the muscle is activated is shown as a solid line, and has the maximum force produced in the middle of the curve. The active force produced decreases as the muscle fiber length shortens or lengthens from this optimal length. The passive (or parallel elastic) force contribution is displayed as a dotted line in the figure. This passive force is produced regardless of activation level whenever the muscle fibers are lengthened beyond the optimal length. This is due to the fact that the muscle fibers are being stretched and have an elastic response to the force being applied on them. The combined total muscle force (dashed line) is the sum of the active and passive components.

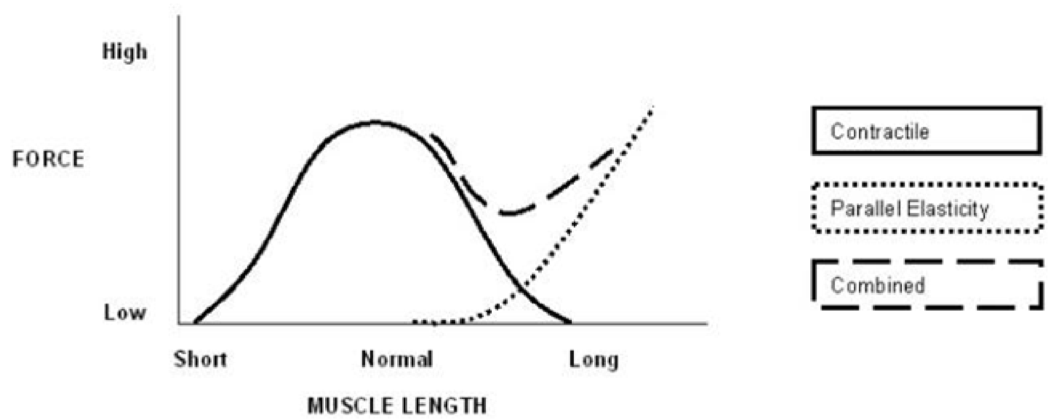

Figure 5: Muscle Force-Length Curve. Contractile force also known as active force curve and parallel elasticity also known as passive force contribution. [11]

The specific muscle physiological properties that determine the amount of force produced by a muscle will be discussed in further detail later in chapter three. In general, these properties prescribe the lengths of muscle and tendon that make up the musculotendon unit, the volume of the muscle, and the amount of force that the muscle can produce.

Thesis Overview

Chapter two provides a brief overview of previous research associated with the muscles of the shoulder girdle and computer modeling of the shoulder girdle. Chapter three describes the previous development of the specific computer model used in this project. Chapter four describes the methodology and results of the experiment conducted by Garner and Shim [1] which will be simulated in the current project. Chapter five describes the methodology performed in this project. Chapter six presents the results found after the exercises were simulated. Chapter seven discusses the results and possible applications, and chapter eight provides conclusions drawn from this work.

CHAPTER TWO

Previous Studies

Over the past decade, musculoskeletal modeling has become increasingly more popular for predicting the forces transmitted by muscles, ligaments and articular surfaces during kinematic tasks [3, 12, 13]. This increase in interest is due to several factors: the advent of more accurate modeling methods, the acceptance of these kinematic models for use in the medical and sports marketplace, and most importantly, the increase in computational power. The accuracy of these models' analysis is dependent on the accurate prediction of the position of the muscle paths with respect to the joint, which determines the muscle length, moment arm, and torque [12, 14]. The creation of more sophisticated modeling methods allows for more accurate representation of complex muscle pathways, but these methods are more computationally expensive. As computational power continues to increase, more sophisticated modeling methods will be able to be used to create increasingly accurate kinematic models of the body.

In order for a biomechanical model to be useful, its muscle pathways must be able to accurately emulate the physiological lines of action of the muscles for all positions of the subject and must address the problems of muscle wrapping for all joint positions [15]. These moment arms are often determined experimentally through tendon-joint displacement, geometric or direct load measurement [16]. The moment arms of the shoulder have been the subject of numerous studies [6, 17-19], but the precise definitions of the moment arms for the shoulder girdle have proven difficult to determine, due to the complexity of the shoulder articulation and limitations in measurement techniques [19].

Previous Research

The current study has been strongly motivated by the lack of published works concerning the shoulder girdle. While there are many sources concerned with the study of the musculoskeletal kinematics surrounding the glenohumeral joint [15, 17, 18, 20] and many acknowledge the importance of the contribution of the shoulder girdle[6, 7, 20], most have not studied the shoulder girdle itself, its muscle pathways, nor addressed the important muscle physiological properties that affect shoulder girdle strength.

Kuechle and Newman [18] studied the instantaneous moment arms of 10 muscles in the shoulder during glenohumeral rotation at four selected humeral positions using tendon excursion and joint displacement data [18]. Twelve cadaveric forequarter specimens were used, and a configuration of potentiometers attached to muscle bundles were used to measure the muscle excursions during humeral exercises at each position.

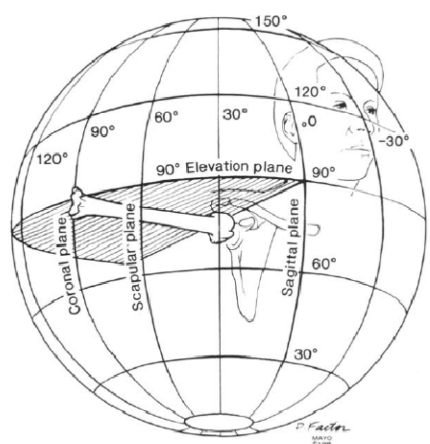

Figure 6: Representation of shoulder motions demonstrated in each plane [18]

Four glenohumeral movements were investigated. These included three humeral elevations (in the Coronal, Scapular, and Sagittal planes) and one horizontal humerus motion at a constant 90 degree humeral elevation [18]. The planes used are shown in Figure 6 above. The motion driven in this procedure does not provide especially beneficial data for shoulder girdle excursion because the primary aim of the study was for glenohumeral rotation, not shoulder girdle excursion. Kuechle *et al* [19] also studied the moment arms of the same shoulder muscles during axial rotation of the glenohumeral joint at four positions using the same experimental set up. The resulting muscle moment arms were not compared to other literature.

Klopcar, Tomsic, and Lenarcic [7] studied the effects of the shoulder girdle on the kinematics of the whole shoulder system. Because the majority of human shoulder models do not use the shoulder girdle as part of their kinematic model, Klopcar et al [7] developed a kinematic model to demonstrate the full range of motion that is reachable with a mobile arm and shoulder girdle. This study modeled the full arm reachable workspace with an emphasis on the shoulder girdle's kinematics in order to quantify the volume that is reachable by a fully mobile shoulder girdle and arm [7]. Their research, however, was only concerned with determining what areas can be reached by the arm and shoulder articulation and not with creating a model that included the muscle contributions.

Klopcar and Lenarcic also studied the relationship between the scapular motion in the shoulder girdle and humeral elevation [6]. A motion tracking device was used to track infrared markers attached to bony landmarks on the skin. Ten subjects (five men and five women) were seated with their back against a support to eliminate spine rotation. The subjects then elevated their arms in four anatomical planes anterior and posterior of the body (as is seen in Figure 7) while their motions were tracked.

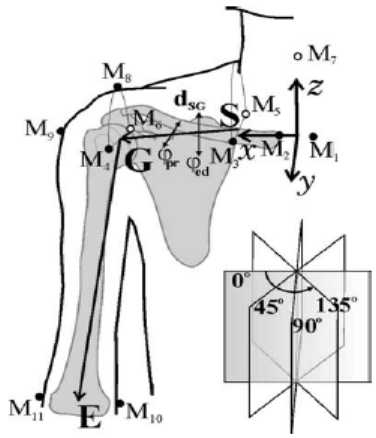

Figure 7: Shoulder reference points (M1-M11) and four anatomical planes used in motion analysis by Klopcar and Lenarcic [6]

The results showed that "the relative movement between the shoulder girdle and humerus segment is always repeated the same way [6]." This relationship was observed not only for each subject, but between all subjects studied. The relationship studied is important because it proves that kinematic models of the shoulder girdle can be used in conjunction with models of the arm with a constant kinematic relationship.

Williams et al [21] studied methods for determining the maximal isometric strength of stabilizing muscles for protraction and retraction exercises. The objective was to determine the reliability of each of the four methods used to measure strength. A stationary tension dynamometer was used to measure the force produced by thirty female adults for all four methods. Two positions (shown in Figure 8 below) for each type of exercise were compared, one requiring the use of stabilizing muscles in the glenohumeral joint and rotator cuff muscles, and the other isolating the muscles in the shoulder girdle. "Good agreement" was found between Bland-Altman plots for both methods of measurement for protraction strength but a "weaker agreement" was found for retraction strength measurements [21].

Figure 8: Scapular Retraction Exercises described in Williams et al [21]with and without use of glenohumeral joint and rotator cuff muscle

Langenderfer et al [22] determined the muscle physiological parameters for muscles crossing the shoulder and elbow of two cadaveric specimens. Sarcomere lengths were measured using laser diffraction, and the mean sarcomere lengths for each muscle were used to estimate the optimal muscle length. Statistical power for detecting the optimal muscle lengths as a function of the sample size was determined. One hundred and twenty measurements were taken for each muscle. The specimens were carefully dissected and overall muscle, tendon, muscle belly, and fascicle lengths were measured. Tendon and muscle volumes were measured by water immersion [22]. Summarized results for 24 muscle bundles included the tendon length, tendon area, physiological cross sectional area (PCSA), pennation angle, muscle length, fascicle length, mean sarcomere length, optimal fascicle length, and optimal muscle length. This study generated important data for use in developing computer models of the musculature of the upper body. Many of the muscles modeled apply to the current study.

Audenert [12] augmented the standard obstacle-set muscle path modeling method to create a method to find solutions for complex muscle pathways that were unstable in previous forms of the obstacle set method. They published algorithms that can be used for special wrapping cases which previous papers had not addressed, specifically a wrapping condition for the head of the humerus. The humerus was modeled as a sphere-topped cylinder with a sphere of a radius differing from the radius of the cylinder sitting atop the cylinder [12]. They formulated the optimization algorithm so that only one parameter was unknown, allowing for a simplified one-dimensional search algorithm. The approach and solution are novel because the sphere-capped cylinder modeled by Garner and Pandy [23] was assumed to have a sphere and cylinder of equal radius.

Gao *et. al* [3] presented a muscle path modeling method similar to the obstacle set method. The line-of-action was assumed to be a massless, taut string that rides on the surfaces of the re-constructed bones. This model was developed specifically to model complex boney structures, such as condyles. They also noted that the obstacle set method requires prior prediction of the location of muscle via points, whereas their model does not. This model is said to be computationally efficient enough to be run on personal computers and has only one model for all muscles. The geometric bone data required for the model can be derived from available computerized geometric models of the bones. They stated that a high level of accuracy can be reached by increasing the number of cross-sectional slices used in the reconstruction of the bone surfaces. Friction between muscles and bones are ignored, and muscles are assumed to touch bone surfaces directly. Geometric and frictional interactions between muscles were also ignored [3]. The algorithms used were also included in the paper, and effective moment arms were compared with experimental data from literature to good results for values above 25 degrees of flexion [3].

Scepi *et al* [13] created a three-dimensional model of the shoulder girdle utilizing a commercial software package (Solid Dynamics System) used primarily in robotics science. Fourteen muscles were modeled geometrically using a straight line modeling method. Muscle forces generated were not a function of muscle length. A static study in reverse dynamics was performed, and the forces produced in seven of the muscles were examined. Calculations were said to have given “few reliable results at the start of [the] abduction of the arm (from 0 to 10 degrees) [13]” although the force-angle curves generated for the deltoid and supraspinatus muscles were similarly shaped to others reported in literature. Overall, this study does not seem to provide compelling results or show any form of validation to other published data.

CHAPTER THREE

Previous Development of the Current Computer Model

The work done in this experiment is a continuation of the works performed by many other researchers, but with a specific offshoot from many previous projects by Dr. Garner [1, 5, 23-26]. There have been significant advances in computer modeling of the musculoskeletal system over the past decade, and several standard methods have been developed upon which others have built. Many of these computer models have been developed using the Visible Human Project's (VHP) [2] male and female databases as the structure from which the muscular and skeletal systems have been constructed. The National Library of Medicine provided the images from the Visible Human Projects.

Visible Human Project Overview

The Visible Human Project (VHP) is part of an initiative that the United States National Library of Medicine has sponsored to create "complete, anatomically detailed, three-dimensional representations of the normal male and female human bodies [2]." Transverse computed tomography (CT), magnetic resonance imaging (MRI), and cryosection images of a male cadaver were generated. The cadaver cryosection images were sectioned at one millimeter intervals along the length of the body.

Significance of VHP

Having an anatomically correct representation of the human body from which computer models can be based is highly important. In academia it is important to have a consistent anatomical model for comparison of related research, and the Visible

Human Project has provided a standard with which to start. Having one standard does, however, pose a problem because there is a large variance in anatomical characteristics over the breadth of the population. Because of this variance, studies that are carried out using the VHP male dataset may not accurately represent the whole of the population. This is especially true because the subject used in the project was larger than average in both stature and muscle tone.

Kinematic model of upper body

Bone Models

Garner and Pandy's first project was the creation of a kinematic model of the upper limb that was based off the VHP image dataset [24]. They used the high-resolution medical images available from the National Library of Medicine to construct the skeletal structure. Geometries of the skeletal structure were used to construct joint models that allowed it to be used as a kinematic model [24][25]. Bone surfaces in each image from the right side of the body were identified using a thresholding algorithm and were reconstructed using a surface reconstruction algorithm [27]. All the bones were reconstructed from CT (Computed Tomography) images except bones which fell outside of the frame of the CT images (the humerus, ulna, and radius) which were reconstructed from the color cryosection images. The bone surfaces were reconstructed (Figure 9) in the form of triangular meshes, which were then decimated to reduce the number of points. This greatly reduced the amount of data stored for each bone file. The bone surfaces were viewed and manipulated using an in-house interactive computer software program, which allowed the user to define or obtain coordinates from any point on the bone surface [24]. Bones on the right side of the upper body were modeled using this method.

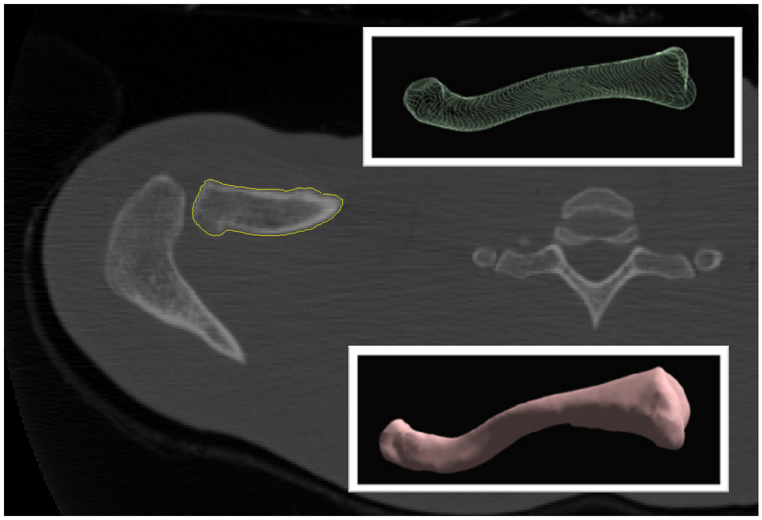

Figure 9: Example of clavicle bone reconstruction from CT scan.
The two-dimensional contours of each cross sectional slice were stacked to compile a three dimensional line model. This line model was then used to generate a surface model for each bone.

The constructed model included seven individual joints from the thorax to the hand for a combined thirteen total degrees of freedom. The thorax was assumed to be stationary while all the other bones moved relative to it, according to their joint constraints. All centers of joint rotation were determined by inspecting the articulating surfaces of the bones. A depiction of the joint centers' positions after calculation is shown in Figure 10. Additionally, a constraint was created to accurately depict the articulation of the scapula on the posterior rib cage. Reference frames for each bone were defined, and a full skeletal model of the upper body was compiled [24]. The skeletal model, joints, and constraints created in this model were used as the basis for our current model.

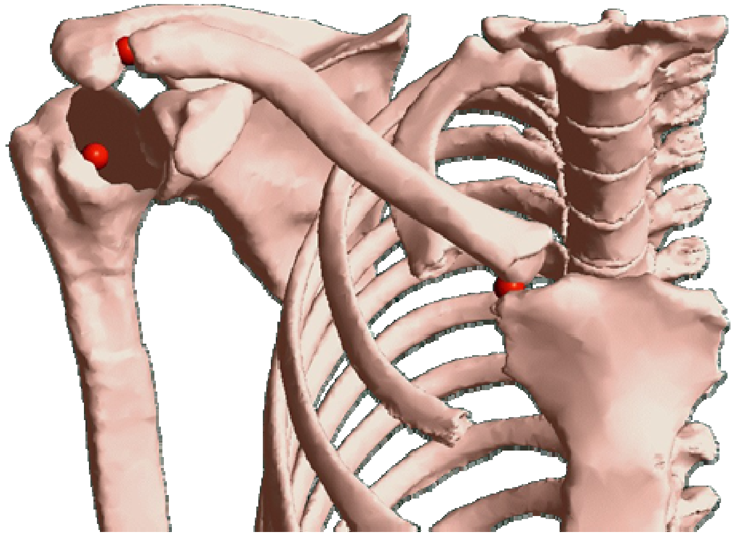

Figure 10: Positions of joint centers calculated from surface geometry

Obstacle-Set Method

Garner and Pandy [23] documented the Obstacle-Set method to represent the pathways of muscles in computer models. This method is based on the principle that the muscle force acts primarily at the cross-sectional centroid of the muscle [23]. The muscle path is calculated by assuming that the line of action for the muscle is the path minimum potential energy. This pathway can wrap and slide around frictionless objects (or obstacles) that give the muscles curved, anatomically-correct pathways. The obstacle is defined as “a regular-shaped rigid body that is used to model the shape of a constraining anatomical structure [23].” Spheres and cylinders are defined as obstacles for each individual muscle pathway, and the muscles wrap around them as the kinematic model joints move. It was proposed that any muscle path can be modeled using one or several of the following types of obstacles: a single sphere, a single cylinder, a double cylinder, or a cylinder with the end capped with a sphere, called a “stub”. Examples of the cylinder and double-cylinder obstacles are shown below in Figure 11. The Obstacle-

Set method is powerful because it can be used to calculate the pathways of the muscles for all joint positions and can calculate muscle paths for muscles that cross joints with multiple degrees of freedom. It is also a computationally efficient method of solving for complex muscle paths.

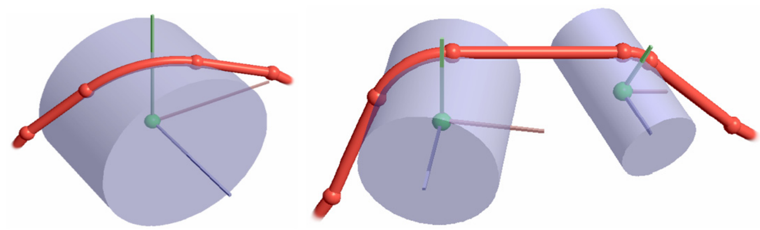

Figure 11: Examples of single and double cylinder obstacles with muscle wrapping used in the obstacle set method [23]

The obstacle set algorithm was used to model the upper limb [23]. The muscle paths of the triceps brachii and deltoid muscles in the arm were modeled, and the moment arm values generated were compared to values in the literature obtained from human cadavers [23]. An image of the model used is shown in Figure 12. Garner stated that "good agreement between model and experiment over the full range of elbow flexion indicates that the paths of [the three heads of the triceps brachii] are represented accurately in the model [23]." Results for the model of the deltoid were also favorable, though the large, fan shaped muscles were more difficult to model accurately.

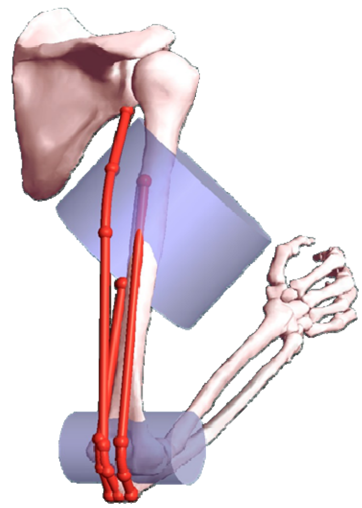

Figure 12: Obstacle set model of the human elbow joint [23][28]

This method is computationally efficient, and therefore allows for real-time changes to the model and kinematics. Calculations can be run simultaneously with graphical representations of the simulation, and this method allows for anatomically-derived solutions. The obstacle set method is able to accurately generate muscle pathways with motions that involve multiple degrees of freedom while remaining computationally simple.

Musculoskeletal Model

Garner and Pandy combined these techniques create a musculoskeletal model of the full upper limb [25]. The kinematic model created [24]was joined with the obstacle-set method for representing the muscle pathways [23], and a musculoskeletal model was developed with 42 muscle bundles representing 26 muscle groups in the upper limb . Each musculotendon actuator had four physiological parameters specified to define its function. These included the maximum isometric force (Fom), optimal fiber length (Lom), pennation angle (α), and tendon slack length (Lst). Pennation angle values were based on experimental data reported in literature [25]. Muscle volumes were computed by calculating cross-sectional areas of each muscle from the VHM database images by multiplying the image thickness by the cross sectional area. Muscle volumes were then used to limit the amount of peak isometric force able to be generated. Minimum and maximum physiological values for Lom and Lst were also defined. Muscle moment arms for shoulder, elbow, and wrist were calculated and compared to literature. The calculated values were consistent with published values [9]. The obstacle-set parameters used to model each muscle path were also published [25].

The muscle geometries used in the current research were based off of the model developed by Garner and Pandy [24]. The origins and insertions of each muscle path were found by inspecting cross-sectional images of the muscles acquired from the VHP dataset, and the centroids of the contact area were calculated. The obstacles used to define the muscle paths were oriented based on physiological shapes observed using the VHP dataset and their positions and sizes were validated by muscle moment arm data. These geometries were kept virtually unchanged for the current model aside from one minor adjustment. The radius associated with the Serratus Anterior Superior muscle's obstacle was slightly reduced so that muscle pathway errors did not occur in the low depression exercise position.

Muscle Physiological Parameters

Several muscle parameters were defined to provide an accurate description of the performance of the muscle when activated. The pennation angle, optimal muscle fiber length, tendon slack length, and maximum isometric force are all muscle parameters that must be known for a muscle to be modeled. Muscle volumes and peak cross sectional area are also defined in many cases. Muscle volumes were known in the current study and were used to constrain the calculated peak isometric forces in this model.

Muscle volume describes the total geometric quantity measured for a muscle bundle. The volume associated with a muscle is a function of both its length and its physiological cross-sectional area (PCSA).

The optimal fiber length (L_o^M) is the muscle length at which the muscle will produce the most force when activated. The position of the optimal fiber length on the force length curve is displayed as L_o^M in Figure 14 below. A muscle would match the optimal fiber length to produce the best possible force during activation. If the muscle length to optimal fiber ratio L/Lom is below 60 or above 140, very small amounts of force will be able to be produced. Muscle fiber length to optimal fiber length ratios close to 100% produce the most force when activated, and deviations from the muscle optimal muscle fiber length decrease the amount of force produced. The curve for parallel elasticity (or passive force produced) is generated when muscles are used at the far range of their usable length. The active (contractile) and passive (parallel) force curves combine to form the total force produced. The muscle force-length curve is shown below in Figure 13.

The maximum isometric force (F_o^M) describes the amount of linear strength that a muscle can generate if it is not producing motion (i.e. the joint is static). This is directly related to the physiological cross sectional area (the size of the muscle). This parameter must be defined so that the strength of the muscle is known. The position of the maximum isometric force is displayed on the muscle force-length curve in Figure 13 below.

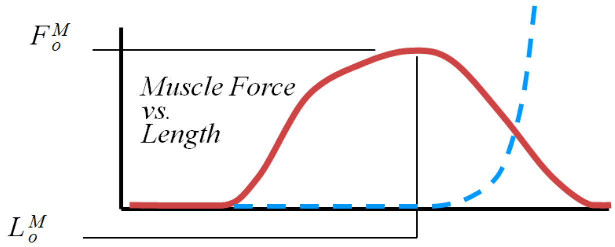

Figure 13: Muscle Force-Length Curve with peak isometric force (F_o^M) and optimal fiber length (L_o^M) positions defined

Tendon slack length (L_S^T) describes the length of tendon present in a musculotendon unit when not under a tensile load. A depiction of a musculotendon unit is shown below in Figure 14. This value is important because the amount of tendon present in a musculotendon unit changes the characteristics of the muscle. A long musculotendon unit with small amounts of tendon could be capable producing a larger range of motion than a long muscle that consists almost entirely of tendon.

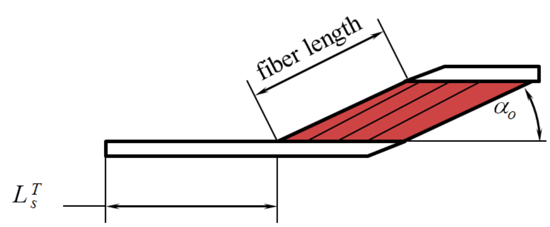

Figure 14: Depiction of musculotendon unit. Fiber length, tendon slack length (L_S^T), and pennation angle α_0 defined.

The pennation angle (α_0) is the angle between the longitudinal axis of the muscle and the muscle's fibers. In the previous model, the angle was assumed to be zero for the muscles in the shoulder girdle [24]. The pennation angle is displayed as α_0 in Figure 14 above.

The initial values used for peak isometric force, optimal muscle-fiber length, and tendon slack length were calculated previously using an optimization procedure described by Garner and Pandy [26]. The calculated values had been compared to measured values in literature, and the muscle volume, physiological cross sectional area, and peak isometric force were all larger than published values [26].

Estimation of Muscle Parameters

Garner and Pandy [26]also developed a method for estimating appropriate values for the physiological parameters of musculotendon units in the human upper limb. The purpose of this study was to develop a method for estimating the values of tendon slack length, peak isometric muscle force, and optimal muscle-fiber length for human musculotendon actuators. Pennation angles were obtained from literature and were not altered in the optimization process. A two-phase optimization was developed in which muscle volume and minimum and maximum physiological lengths of the actuator must be known to calculate the desired muscle parameters. In phase I the joint angles and muscle activation levels are found by maximizing the joint torque, and in phase II the properties of each musculotendon unit are found by comparing the joint torques to experimental joint torque values found in literature [26]. A very similar, nested two-step process will be used in the current experiment as was used by Garner and Pandy [26]. Muscle volume, PCSA, and Lom values were compared to values in literature, and had higher values than were previously published [26].

Limitations of Previous Studies

There was a particular limitation of the Garner and Pandy [25] musculoskeletal model that is relevant to the present study. While the musculoskeletal model of the upper body was validated by joint strength data from literature, published data needed for validating the shoulder girdle mechanism was unavailable. The previous musculoskeletal model was validated from the glenohumeral joint down to the hand, but the muscles actuating the shoulder girdle were unable to be validated. This lack of verification for the muscles of the shoulder girdle provided a primary motivation for this project.

Motivation

The motivation for this project was threefold. First, the computer model of the upper body that was developed by Garner and Pandy [25] was only validated for the arm and shoulder. No data was available to validate the muscles of the shoulder girdle. Data that could be used to validate the model could include muscle moment arm values for exercises of the shoulder girdle or strength data for exercises that targeted the muscles of the shoulder girdle.

Secondly, strength performance data became that was appropriate for validation of the shoulder girdle. Garner and Shim [1] performed experiments where the isometric shoulder girdle strength was measured for four different types of exercises. This experiment provided the experimental strength data necessary for validation of the computer model.

Thirdly, there was a lack of published muscle parameter data which is needed for accurate modeling of the muscles in the shoulder girdle. The muscles of the shoulder girdle have been the focus of less research than muscles of other parts of the body, therefore less published data has been available. It was our goal to provide a validated model of the shoulder girdle as well as the muscle parameters calculated for use in our musculoskeletal model.

CHAPTER FOUR

Shoulder Girdle Exercise Experiment

Design and Testing of Exercise Apparatus

In a separate venture from the modeling experiments, Garner and Shim designed and developed a device and an experimental procedure that was used to measure shoulder girdle strength [5]. The device was constructed similar to conventional exercise equipment, but a load cell was implemented into the device to measure the amount of force produced during each isometric exercise. The exercise device designed for the experiment is shown below in Figure 15. Additional figures of the device design are provided in Appendix D. After the device was designed and built, an experiment was performed to validate that the apparatus was effective for measuring shoulder girdle strengths. It was used to measure the shoulder girdle strength of nineteen subjects (nine female and ten male) during maximum isometric force exercises. Elevation, depression, protraction, and retraction exercises were performed, and a video motion captures system was used to measure the shoulder girdle position. Protocols were described for each exercise and statistical analysis of each of the exercise positions and of the peak force generated were performed. It was concluded that that the apparatus and protocol presented in this paper was effective for measuring shoulder girdle strength [5].

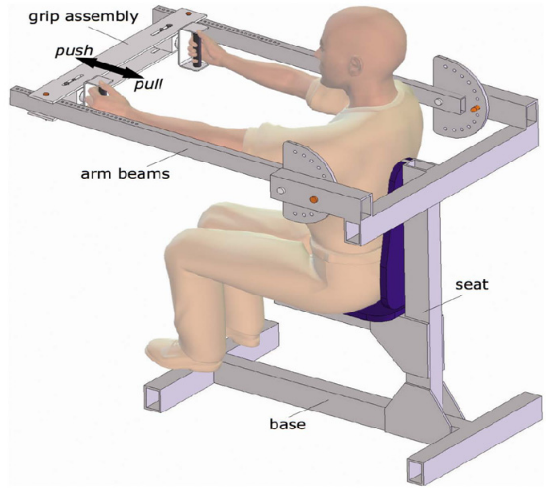

Figure 15: Exercise apparatus designed and built by Garner and Shim [1].
The apparatus is shown in the protraction/retraction exercise position.

Exercise Experiment

Garner and Shim [1] then performed an experiment to determine the average maximum isometric forces that can be generated in shoulder elevation, depression, protraction, and retraction at three different shoulder positions. An isometric exercise is an exercise where the muscle is producing force but the position of the joints of the body are unchanged (i.e. a static exercise). Because each exercise was isometric, three different positions for each type of exercise were performed to measure the static strengths across a range of motion. For elevation and depression exercises, the three positions were a low, middle, and high shoulder position. For protraction and retraction, a front, middle, and back shoulder position were assumed for each exercise. Because exercises were performed at three positions for all four types of experiments, a total of twelve maximal effort strength measurements were taken for each subject. Motion capture markers were placed on the subject and cameras were used to track the shoulder girdle position during the exercises.

For each exercise, strength was found to decrease as the shoulder girdle position was moved in the direction of the applied force. Depression and retraction forces were found to be less than elevation and protraction forces. The forces measured during each maximal isometric force exercise are shown below in Figure 16. This study provided valuable information because the results are vital for further study of the shoulder girdle.

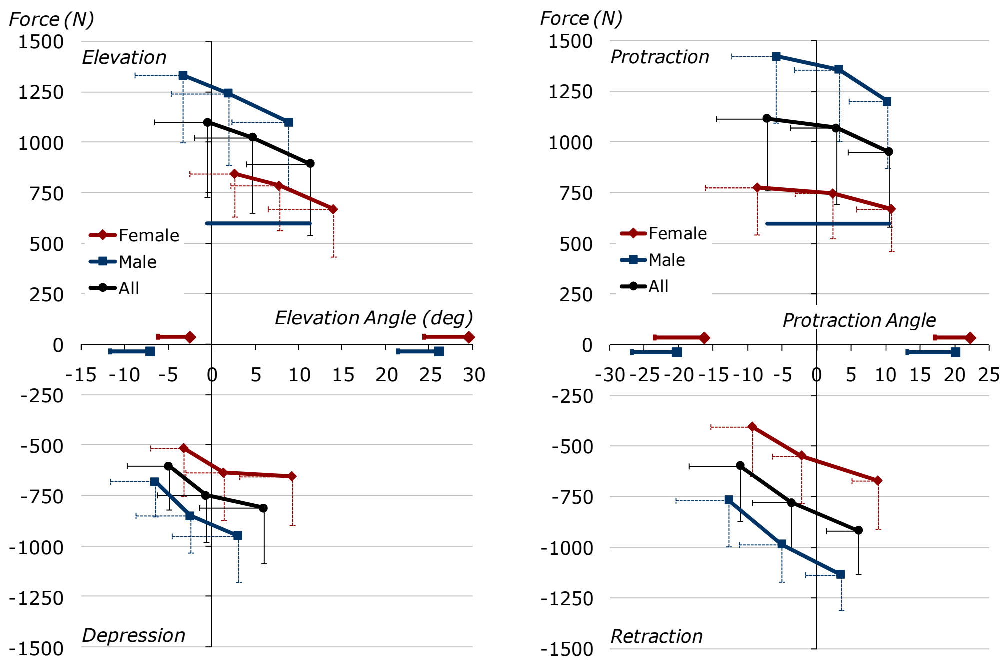

Figure 16: Forces generated at each position during all four exercise types [1]

CHAPTER FIVE

Methodology

Modeling of the Human Shoulder Girdle

While there have been many anatomical studies on the kinematic movement of the bones in the shoulder [29-31], there have not been many computer models of the musculature in the shoulder girdle. This lack of published work on the shoulder girdle provided motivation for the subject of this study. In the current study, an in depth musculoskeletal model was developed for the shoulder girdle (images of the model shown in Figure 17 below).

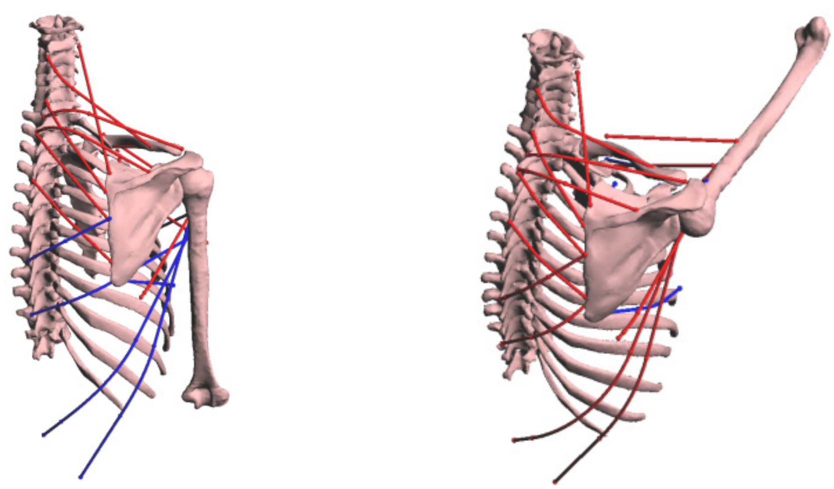

Figure 17: Posterior isometric view of constructed computer model at position for elevation exercise (L) and retraction exercise (R). Active muscles are represented as red bands and passive muscles are represented as blue bands.

The models of the bones, joints, and musculature were all derived from the same anatomical database: a set of high-resolution images and CT scans made available by the Visible Human Male project through the National Library of medicine [2]. This project will be referred to as the Visible Human Project (VHP). This model has nine degrees of freedom (DOF) and includes two holonomic constraints that were used in modeling the articulation of the scapulothoracic joint [25].

Bone-Fixed Reference Frames

There are four body coordinate systems; or reference frames, defined in this model. Each reference frame is based on anatomical features of the bone or bones in the frame. The four frames are: the thorax (also called the ground frame), clavicle, scapula, and humerus frame. Each of the frame's origins are seen in Figure 18. The origin of the thorax frame is located at the jugular notch (the dip on the superior portion of the sternum), and its orientation is aligned with the principal axes of the body, which were defined using bony landmarks on the vertebrae and sternum [32]. The thorax frame includes the vertebral column, ribs, sternum, as well as the pelvis, sacrum, and skull when they are included in the visualization of the model. These bones do not move with respect to each other because they are located at fixed positions within their frame.

The origin of the clavicle frame is located at the center of the sternoclavicular joint. The clavicle frame includes only the clavicle bone model and is allowed three rotational degrees of freedom at the sternoclavicular joint. The clavicular coordinate system is defined with the x-axis of the clavicle along the length of the bone and the z-axis pointing superiorly.

The origin of the scapular frame is located at the center of the acromioclavicular joint. The scapula frame includes only the scapula bone model and is also allowed three rotational degrees of freedom at the acromioclavicular joint. The scapular coordinate frame is based on the positions of the glenohumeral joint and the medial border of the scapula. The negative x-axis passes through the medial border of the scapula, and the negative z-axis passes through the glenohumeral joint.

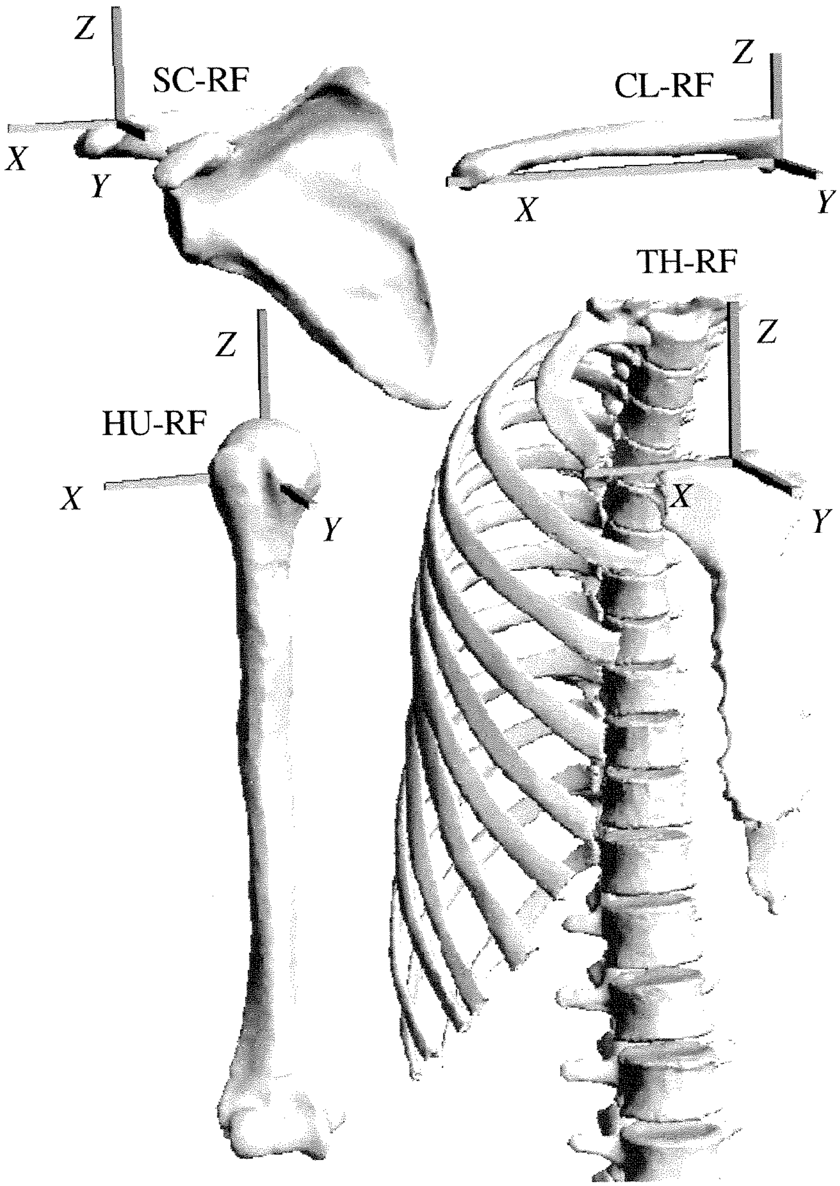

Figure 18: Locations and orientations of all bone reference frames [24]

The humerus frame rotates at the glenohumeral joint where it is connected to the scapular frame. The origin of the humerus is located at the center of the glenohumeral joint. The humerus coordinate system has the axial direction of the humerus as the z-axis, and the x-axis is defined as parallel to the plane formed by the humeroulnar joint and the z-axis, thereby defining the coordinate system with its origin at the glenohumeral joint center.

This multiple-frame linkage acts as a serial chain between the ground frame and the humerus frame, allowing for multiple degrees of freedom. The bone reference frames and the standard anatomical position for this model were based on the positions published in Garner and Pandy [24].

Joint Models

Three joints plus a constraint on the flat surface of the scapula were created to accurately represent the kinematics of the shoulder girdle. The joints modeled were the sternoclavicular joint, the acromioclavicular joint, and the glenohumeral joint. The constraint on the scapula limits two points that are offset from the interior surface of the scapula to be coincident with the surface of an ellipsoid that approximates the surface of the rib cage. The points are offset by the thickness of the musculature anterior to the scapula (i.e., between the rib cage and the scapula). The ellipsoid is set in the ground (thorax) frame, but is offset laterally and is slightly rotated in order for its surface to accurately model the surface of the ribcage. This ellipsoid was then used to create a mathematical constraint which allows the two points to move freely along the surface of the ellipsoid, which creates an effective representation of the scapulothoracic articulation. The two points (in blue) and ellipsoid are seen below in Figure 19.

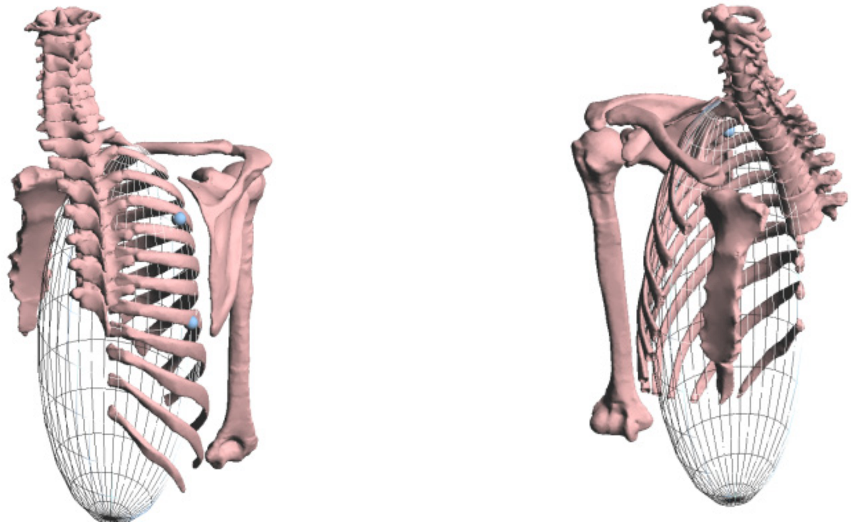

Figure 19: Model of scapulothoracic ellipsoid constraint

Muscles Modeled

Eleven muscles were included in the model of the shoulder girdle, five of which were modeled using multiple muscle bundles because of their broad fan shaped nature. Nineteen total muscle bundles were needed to accurately model the musculature of the shoulder girdle. The muscles modeled were selected because they were the primary moving muscles of the shoulder girdle. Muscles that attached the humerus to the scapula (the muscles around the glenohumeral joint) were not modeled because they should not affect shoulder girdle strength. Muscles that attached the scapula, clavicle, and humerus to the thorax body were modeled because they are used to change the position of and produce force in the shoulder girdle. A list of the muscle bundles modeled and an image of the computer model is provided in Figure 20.

Muscle Bundles Modeled

Subclavius
Subscapularis
Serratus Anterior (Superior)
Serratus Anterior (Middle)
Serratus Anterior (Inferior)
Trapezius (C1-C6)
Trapezius (C7)
Trapezius (T1)
Trapezius (T2-T7)
Levator Scapulae
Rhomboid Minor
Rhomboid Major (T1-T2)
Rhomboid Major (T3-T4)
Pectoralis Minor
Pectoralis Major (Clavicular)
Pectoralis Major (Sternal)
Pectoralis Major (Ribs)
Latissimus Dorsi (Thoracic)
Latissimus Dorsi (Lumbar)
Latissimus Dorsi (Illiac)
Teres Major

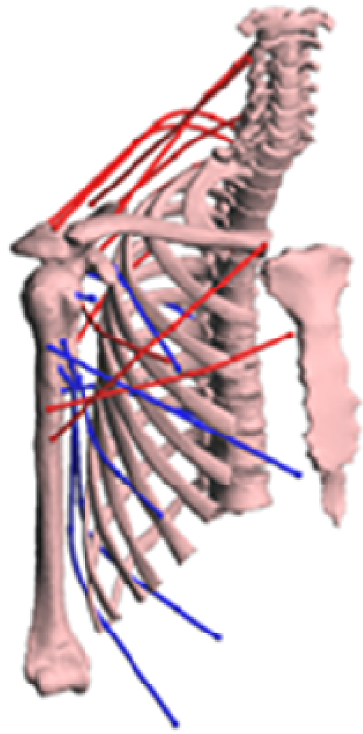

Figure 20: A list of all muscle bundles modeled in the computer model

Obstacles

The obstacle set method was utilized for defining the muscle pathways in this .model. While cylinder, double cylinder, sphere, and sphere capped cylinder obstacles are available for use in this method, the current model only used the cylinder and double cylinder obstacles. There were no cases where the other two obstacle types were needed to accurately represent the muscles of the shoulder girdle.

Muscle Parameters

The same muscle physiological model type was used to define the muscle characteristics as was used in the previous modeling studies by Garner [9, 24, 26]. The muscle parameters that needed to be defined for this model are the same variables that also had to be defined for each of the earlier models. Values of optimal muscle fiber length, tendon slack length, peak isometric force, pennation angle, and muscle volume are some of the variables that are used in this modeling method.

Pennation angles for muscles in the shoulder were assumed to be zero [8, 33, 34]. The muscle volume (Vol), slack tendon-length (LST), and optimal muscle-fiber length (LOM), values used in Garner and Pandy [9, 26] were all implemented in this model. Peak isometric muscle force (Fom) was calculated using the method described by Garner [26], which assumes that Fom is proportional to the physiological cross-sectional area (PCSA). PCSA is defined as the muscle volume divided by the optimal muscle-fiber length, as is seen below in Equation 1.

$$PCSA = \frac{Vol}{Lom} \qquad \text{Equation 1}$$

Defined muscle volumes were used to constrain the peak isometric forces for each muscle, and the maximum muscle stress was defined to be 330 kPa [25]. Previously defined tendon elasticity conditions were also assumed [25].

Constraints

In addition to the scapulo-thoracic constraint, several constraints were applied to the model to accurately simulate the shoulder exercises. These constraints included 1) setting the correct shoulder position, 2) replicating the interaction of the subject with the exercise apparatus, 3) keeping the humerus oriented properly for each exercise. The position of the shoulder girdle was unique for all twelve exercise simulations, so the model had to be placed in the correct position for each simulation. The method for achieving these positions is further described in the Exercise Simulations section below. The subject's interaction with the exercise apparatus was emulated by constraining the distal end of the model's humerus to have zero acceleration in the direction of the humeral axis. This constraint kept the model from moving when the muscles applied force, emulating an isometric exercise. Finally, the humeral orientation was constrained to be vertical for elevation/depression exercises and horizontal for protraction/retraction exercises.

Validation

Validation of computer models is an important part of the modeling research process. Unvalidated computer models are not useful for comparison in research because physiology and parameters could very easily be improperly modeled.

Garner [25] validated his musculoskeletal model from the glenohumeral joint down the arm but was unable to validate his model of the shoulder girdle because data on the subject which could be used for comparison had not been published. Garner and Shim [1] subsequently collected strength data and thus facilitated the current research project. The current project utilized the available strength data to validate the musculoskeletal model of the shoulder girdle by comparing the experimental data to data generated by simulating the same exercises using the developed computer model.

Exercise Simulations

The current computer model was used to simulate the maximal isometric strength exercises that were carried out by Garner and Shim [1, 5]. Twelve individual strength exercises were simulated using the computer model. These twelve exercises were broken up into four groups: elevation, depression, protraction, and retraction exercises.

The elevation exercises that were simulated involved the subjects sitting in a testing apparatus and pulling upward, using only their shoulder. During depression exercises the user pushed downward. During protraction exercises the subject's humerus was elevated so that it was pointing forward. They then pushed forward, moving only their shoulder. During retraction exercises the subject pulled backward using their shoulder. In each of these four groups of exercises, the exercises were carried out at three positions: low, middle, and high for the elevation and depression exercises and back, middle, and front for the protraction and retraction exercises [5]. While the exercises were being carried out, the subjects' positions were recorded using motion capture software. Images of the computer model set in all three positions for each of the four exercises are shown in Figure 21 and Figure 22 below. Each of these exercises performed were simulated using the current computer model.

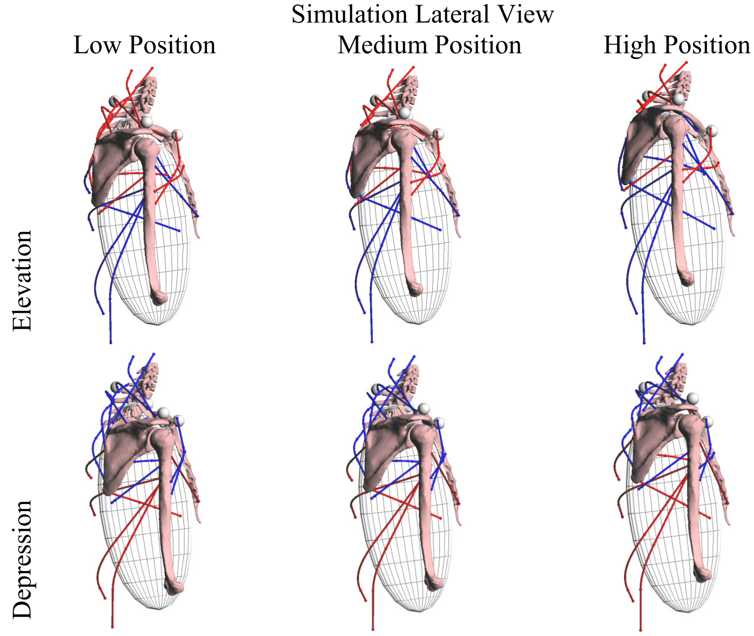

Figure 21: Lateral View of Simulated Elevation and Depression Exercises

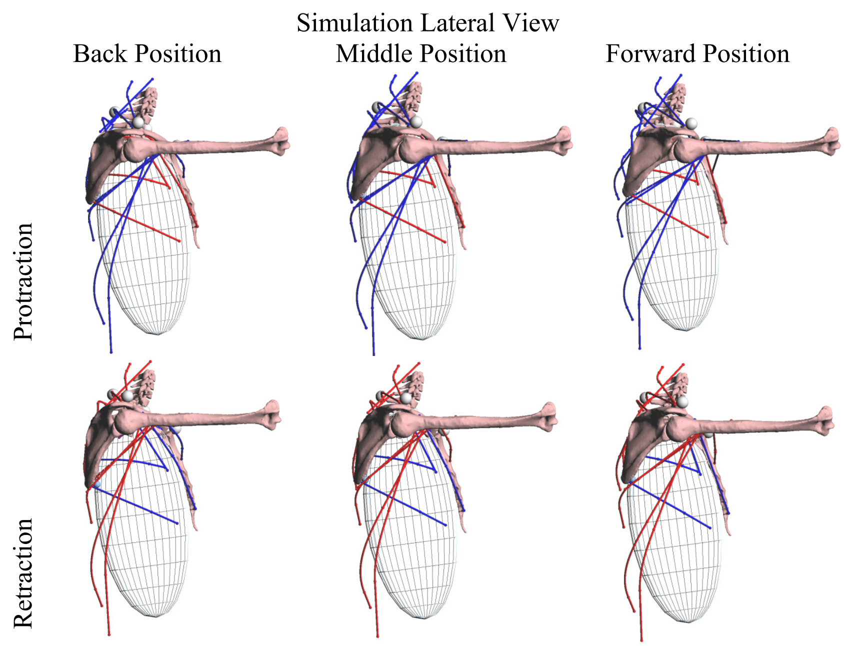

Figure 22: Lateral View of Simulated Protraction and Retraction Exercises

Muscle Activation Computation

To simulate each of the twelve exercises, the model first computed which muscles would contribute to the exercise force. Initially each muscles' level of activation was set to 50%. The model was manually placed in a position that approximated that of the respective exerice, and the muscle forces and corresponding exercise force were computed. Then, each muscle's level of activation was varied iteratively to see how it affected the exercise force, and variations were applied so as to maximize the exercise force. Eventually, all muscles contributing to the exercise were activated fully, and those opposing the exerice were deactivated fully. The result was a set of muscle activations for each simulated exercise by which exercise force was maximized.

Joint Position Computation

In like manner, the model computed the precise set of joint positions that both matched the overall elevation and protraction angles of the exercise, and permitted the production of maximum exercise force. To perform this computation, the model was initially placed in a position that approximated that of the respective exercise. The exercise was then simulated by applying to each muscle the previously-computed activation levels, and computing the resulting exercise force. Then, the joint angles of each modeled degree-of-freedom were varied, subject to constraints such as the scapulo-thoracic articulation, until the exercise elevation and protration positions (defined in Figure 23) were met and the exercise force was maximized. The result was a set of joint angles for each exercise that satisfied the various positional constraints and achieved maximum exercise force. The computations of muscle activation levels and joint positions were repeated in turn for each exercise until no further variation improved the exercise force.

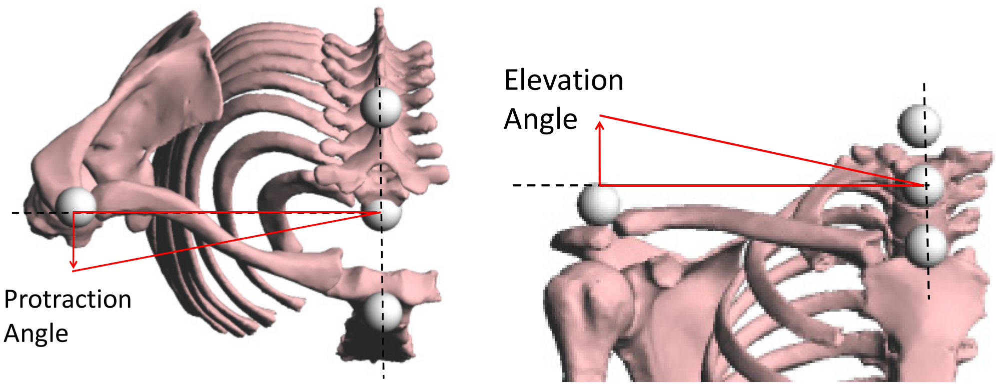

Figure 23: Elevation and protraction angles shown with superior and anterior views of shoulder girdle. Illustration used to define calculations used for protraction and elevation angles. Marker balls were used as calculation points for protraction and elevation angles.

Table 1: Target shoulder elevation and protraction angles (Radians) and target strength data (Newtons) from Garner and Shim [1]

Exercise		Exercise Force	Elevation Angle	Protraction Angle
Elevation	Lo	-1331.5	-0.05729	0.00506
	Med	-1242.2	0.03375	-0.03639
	Hi	-1098.9	0.15472	-0.02637
Depression	Lo	680.0	-0.11297	0.16558
	Med	850.4	-0.04294	0.17156
	Hi	949.6	0.05353	0.17725
Protraction	Back	-1422.7	0.06006	-0.10253
	Mid	-1358.8	0.01744	0.05667
	For	-1202.1	-0.00046	0.17847
Retraction	Back	766.4	0.18623	-0.22243
	Mid	984.1	0.168	-0.0881
	For	1133.0	0.13173	0.06084

Parameter Optimization

The male exercise strength measurements taken from Garner and Shim [1] were used as a performance comparison for the current computer model. Ideally, the exercises simulated by the model with initial muscle parameter values would provide similar strength results to the experimental measurements. But, this was not the case, and so the muscle parameters associated with the model were adjusted by an optimizer to tune the model so that it could accurately reproduce the strength results recorded during the experimental exercises. The parameters that the optimizer was allowed to adjust were the optimal muscle fiber length (Lom) and tendon slack length (Lst). When these were adjusted, the peak isometric force was also affected due to the relationship between Lom, PCSA, and the known muscle volume (see Equation 1). A simple steepest-descent optimizer was used in conjunction with numerical forward differencing. To overcome the possibility of local minima within the solution space, the optimization process was occasionally subjected to small, random perturbations (*i.e.* the solution variables were perturbed randomly).

Since the average shoulder elevation and protraction angles for the subjects were known for each exercise (shown in Table 1 above), the simulated exercises were penalized for deviations from these positions. The joint positions were defined using the elevation and protraction angle as is defined in Figure 23. For each individual exercise simulation, both the muscles' activations and the joint positions were computed. In finding the optimum way to perform an exercise, a person intuitively determines what muscles are needed to maximize the force for that specific exercise and makes minor posture and joint adjustments to place their body in the best position to produce maximum forces. For the same reasons, the muscle activations and joint positions were adjusted to maximize force for each exercise simulation. This optimization for all twelve exercises is diagrammed in below in Figure 24. Penalties were created within the joint position optimization to keep the optimization algorithm from deviating from stable joint positions. The output of each exercise simulation was the maximal isometric force produced during that exercise (the Exercise Force).

After the muscle activations and joint positions had been computed for each exercise, the error between the simulated and actual (measured) forces produced for each exercise was calculated. Each error was squared, and all of these squared errors were summed. This sum was then used as the performance criteria to simultaneously optimize the physiological parameters for all modeled muscles.

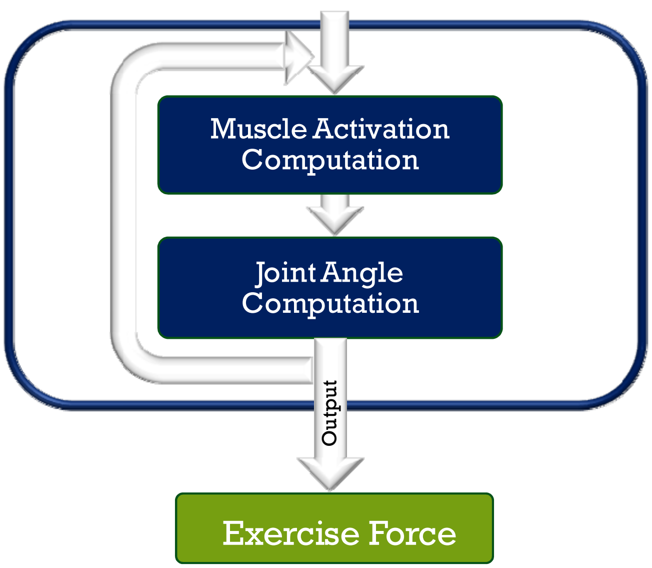

Figure 24: Optimization loop performed for each individual exercise

The physiological muscle parameter values were optimized so that the strength performance for the simulations would best match the experimental strength values. During this process, the sum of the squared errors between the experimental and simulated exercise forces was minimized. The optimizer varied the optimal muscle fiber length and the tendon slack length, which affected the peak isometric force values for each muscle. The process for calculating the overall performance is shown below in Figure 25. Once the optimizer minimized the total summed error the best solution for the muscle parameters had been calculated. This is important because the same muscle parameters are used in all 12 exercise simulations.

The muscle parameter optimizer was given manually-prescribed limits for each parameter to be optimized to ensure that the parameters stayed within reasonable bounds. A quadratic penalty was also assessed if the muscle fiber lengths deviated far from the optimal muscle fiber length. This penalty was added to help keep the muscles in the active portion of the muscle force-length curve and to keep the amount of passive force created to reasonable levels. After the optimization, each muscle parameter was checked to make sure that it did not reach either the maximum or minimum limits. All parameters remained within the allowable range.

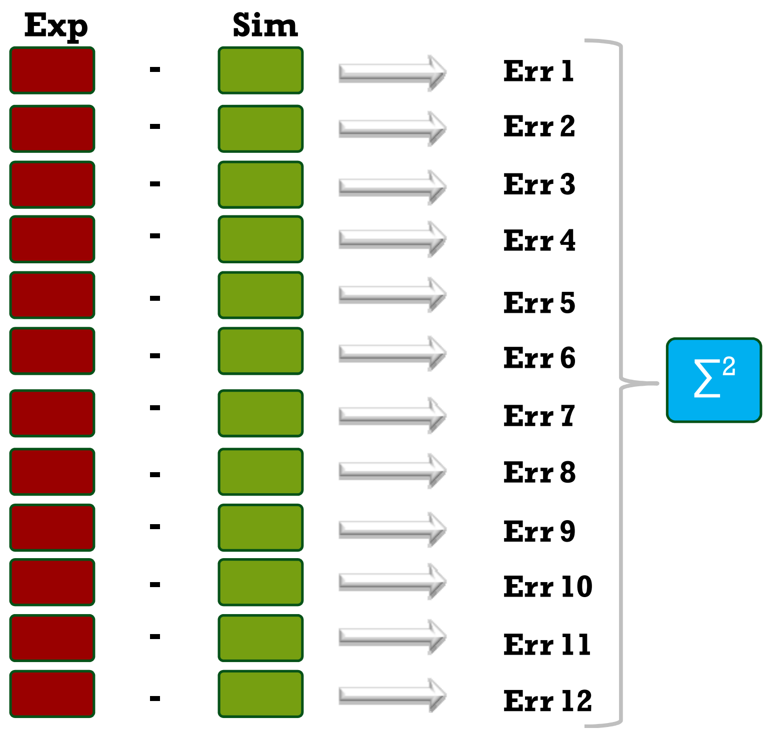

Figure 25: Full optimization performed to achieve best performance for all exercises. Each exercise error was calculated, squared, then summed. The sum of the squares of the error was then minimized.

After the muscle parameters were optimized based on the sum of the squares of the exercise force error, all the simulations were again run to compute the muscle activation levels and the joint position. The muscle activations, joint angles, and muscle parameters were compared to their previous values to ensure that they had not changed. Once the model reached a steady state the model optimization was concluded.

Through this process, the optimizer was able to first find proper values for muscle activations and joint positions and then was able to adjust the muscle parameters to find a best solution that gave the least total error between the simulated and experimental values. This model optimization process outputs the best possible muscle parameter values and also defines the contributing muscles and the best joint positions for each exercise. After the optimization process was completed, the model was able to run a good representative simulation of each exercise at all positions.

Apparatus

This model was created using a conventional desktop computer and Metrowerks CodeWarrior IDE version 5.11.1105, Austin, TX. The computer had a 2.66 GHz processor and 3.5 GB of RAM, running a Microsoft Windows XP system. After the model was created the exercise simulations were run using the same hardware. The custom software used to run the simulations was developed by Dr. Brian A. Garner and edited by Joel D. White for use during this project.

CHAPTER SIX

Results

This chapter will present the data generated from the model simulations previously described. First, results of the muscle activation and joint angle position calculations will be presented. Then, three sets of computed muscle physiological parameter solutions and the corresponding exercise forces will be given for comparison to the experimental strength data. A solution set computed from the initial model parameters, a solution set after a full optimization (based on all four exercise types), and a solution set after a half optimization (based on elevation and depression exercises only) will be presented. For each solution set, the muscles activated during each exercise, the joint positions and elevation and protraction angles achieved, the exercise forces generated, and the optimized muscle parameters will be given for further review.

Muscle Activations

The muscles that were used for each exercise are displayed below in Table 2. Each muscle had a possible activation level between 0 (not active) to 1 (full activation). Muscles that contributed to each exercise were assigned a value of 1, and muscles that detracted from a maximum exercise force for that exercise were made inactive. Inactive muscles were given activation levels of 0. Muscles that neither contributed nor detracted from the exercise are indicated in the table by a dash (-) mark. This feature was only seen in the subscapularis and serratus anterior inferior muscles for certain exercises.

In general, the activation values flip from 0 to 1 or 1 to 0 between opposing exercises (Elevation to Depression or Protraction to Retraction). However, there are times when this does not take place. Some muscles contribute minimally at one position but because of changes in joint position may change to have a negative moment arm and detract from the exercise if activated. The subclavius, serratus anterior superior, and sternal and rib bundles of the pectoralis muscles all followed this trend.

Table 2: Active muscles for each position
(1 denotes active muscles, 0 denotes passive muscles, and '–' denotes muscles that did not have any effect)

Muscles	Elevation			Depression			Protraction			Retraction		
	L	M	H	L	M	H	B	M	F	B	M	F
subclav	1	1	0	0	0	1	1	1	0	0	0	0
serants	1	1	1	0	0	0	1	1	1	-	0	0
serantm	1	1	0	0	0	1	1	1	1	0	0	0
seranti	0	0	0	1	1	1	1	-	1	0	0	0
trapc	1	1	1	0	0	0	0	0	0	1	1	1
trapc7	1	1	1	0	0	0	0	0	0	1	1	1
trapt1	1	1	1	0	0	0	0	0	0	1	1	1
trapt	0	0	0	1	1	1	0	0	0	1	1	1
lvs	1	1	1	0	0	0	0	0	0	1	1	1
rmn	1	1	1	0	0	0	0	0	0	1	1	1
rmjt2	1	1	1	0	0	0	0	0	0	1	1	1
rmjt3	1	1	1	0	0	0	0	0	0	1	1	1
pmn	0	0	0	1	1	1	1	1	1	0	0	0
pmjc	1	1	1	0	0	0	0	0	0	1	1	1
pmjs	1	1	1	0	0	0	0	0	0	0	1	1
pmjr	0	0	0	1	1	1	1	1	1	0	0	0
ltdt	0	0	0	1	1	1	0	0	0	1	1	1
ltdl	0	0	0	1	1	1	0	0	0	1	1	1
ltdi	0	0	0	1	1	1	0	0	0	1	1	1

Joint Positions

The joint degrees of freedom for all nine joints (q1 – q9) and all twelve exercises are provided below in Table 3 The zero angle for each joint was defined as that corresponding to the anatomical reference position. The only joint angles that were not allowed to be changed by the optimizer were q3 (clavicular axial rotation), q9 (humeral axial rotation), and the two scapular angles (q5 and q6) that were constrained to permit contact between the scapula and thorax. The humerus was left unrotated for all of the elevation and depression exercises and was rotated 60 degrees medially when the humerus was in the forward position to mimic the anatomical position of the subjects during the protraction and retraction exercises.

Table 3: Optimized joint positions for each exercise (Radians)

Exercise		Clavicle			Scapula			Humerus		
		q1	q2	q3	q4	q5	q6	q7	q8	q9
Elevation	Lo	0.140	0.305	0.000	0.108	-0.139	-0.098	-0.087	-0.162	0.000
	Med	0.055	0.219	0.000	0.082	-0.076	-0.058	-0.061	-0.126	0.000
	Hi	0.015	0.090	0.000	0.016	0.010	-0.038	0.006	-0.064	0.000
Depression	Lo	0.352	0.303	0.000	0.047	-0.220	-0.127	-0.071	-0.172	0.000
	Med	0.323	0.224	0.000	0.011	-0.179	-0.087	-0.052	-0.145	0.000
	Hi	0.279	0.118	0.000	-0.029	-0.128	-0.040	-0.028	-0.097	0.000
Protraction	Back	-0.029	0.212	0.000	0.066	0.006	-0.061	1.542	0.029	1.047
	Mid	0.165	0.206	0.000	-0.008	0.098	-0.083	1.679	-0.029	1.047
	for	0.308	0.176	0.000	-0.082	0.105	-0.148	1.774	-0.069	1.047
Retraction	Back	-0.191	0.118	0.000	0.067	-0.097	-0.041	1.452	0.104	1.047
	Mid	-0.052	0.097	0.000	0.048	-0.049	-0.019	1.517	0.009	1.047
	For	0.116	0.083	0.000	-0.009	0.017	-0.046	1.618	-0.054	1.047

The q values listed are the joint rotations that determine the model position. The three degrees of freedom of the sternoclavicular joint are prescribed by q1-q3 (clavicular elevation/depression, protraction/retraction, and axial rotation). The degrees of freedom at the acromioclavicular joint are prescribed by q4-q6 (scapular medial/lateral elevation, anterior/posterior elevation, and rotation about the vertical axis). The joint angles q7-q9 prescribe the rotations at the glenohumeral joint (flexion/extension, abduction/adduction, and internal/external rotation).

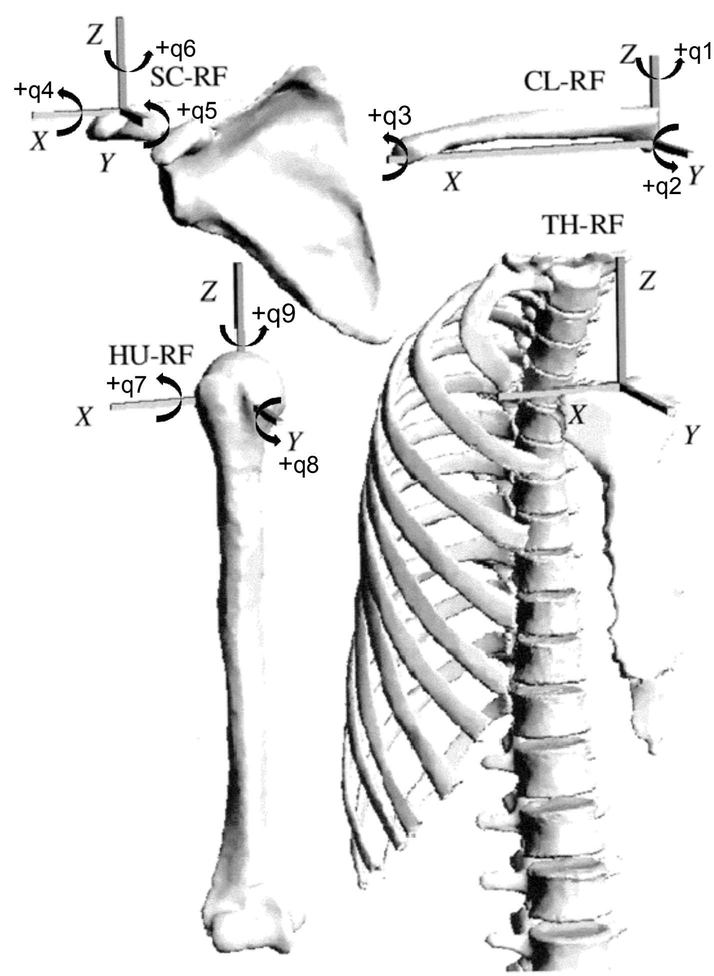

Figure 26: Kinematic model with joint degrees of freedom defined. Adapted from Garner and Pandy [24]

All values of the joint angles are relatively small because all of the exercises for the shoulder girdle do not require extremely large ranges of motion. The largest values of joint rotations, other than for the humerus rotation in the protraction and retraction exercises, are seen during depression for joint angle q1. The largest joint angle value is 0.352 which is seen for q1 is during the low depression exercise. The q1 degree of freedom rotates the clavicle inferiorly at the sternoclavicular joint, thereby creating a downward position for the whole shoulder girdle.

All of the joint angles listed in the table are a result of forcing the skeletal bodies into positions so that the elevation and depression angles of the simulations would match the target elevation and depression angles that were measured during the experimental exercises from Garner and Shim [1]. The target elevation and protraction shoulder angles were able to be achieved to within 3.5% error for every exercise that was simulated (as is seen below in Table 4). The target and achieved elevation and protraction angles are also displayed in Figure 27. Prescribing the elevation and protraction angles for the model was a satisfactory method for prescribing the shoulder model position.

Table 4: Target and Achieved Shoulder Elevation and Protraction Angles in Radians

Exercise	Target Elevation	Achieved Elevation	%Error	Target Protraction	Achieved Protraction	%Error
ElvLo	-0.0573	-0.0573	0.06	0.0051	0.0051	0.99
ElvMd	0.0338	0.0335	0.87	-0.0364	-0.0362	0.41
ELvHi	0.1547	0.1552	0.28	-0.0264	-0.0261	1.11
DepLo	-0.1130	-0.1118	1.05	0.1656	0.1662	0.38
DepMd	-0.0429	-0.0428	0.34	0.1716	0.1716	0.03
DepHi	0.0535	0.0537	0.23	0.1773	0.1773	0.02
ProBk	0.0601	0.0593	1.30	-0.1025	-0.1041	1.56
ProMd	0.0174	0.0169	3.38	0.0567	0.0568	0.18
ProFr	-0.0005	-0.0004	3.26	0.1785	0.1774	0.60
RetBk	0.1862	0.1853	0.48	-0.2224	-0.2211	0.62
RetMd	0.1680	0.1673	0.42	-0.0881	-0.0875	0.69
RetFr	0.1317	0.1315	0.16	0.0608	0.0608	0.00

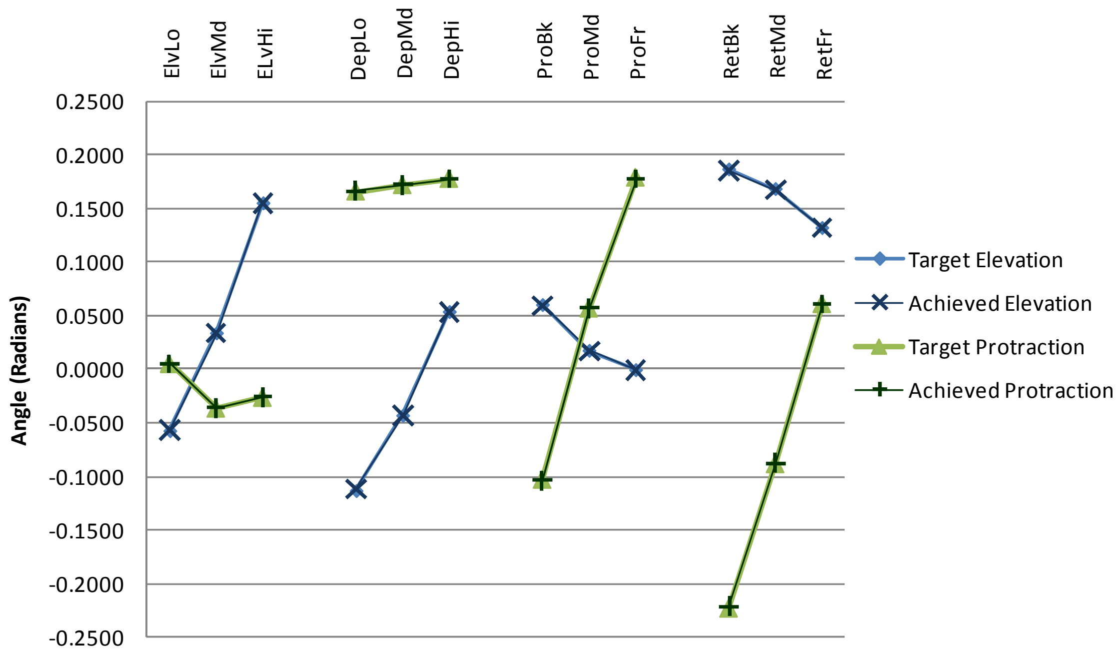

Figure 27: Target and achieved elevation and protraction angles

Exercise Force Values

The force values calculated during the simulation of all twelve exercises are provided in Table 5. The published experimental exercise force values listed below in Table 5 [1] were used as a comparison for the values calculated in the simulations. Three different simulations' exercise forces are shown. All of the simulated values were compared to the experimental force values. The first simulation was performed using published muscle physiological parameters which were used as the initial values for each of the optimizations [25]. The second optimization was calculated to find the best overall strength performance. For this optimization, the total error was minimized over all twelve exercises by adjusting muscle parameters to calculate the best overall solution for all simulations when compared to the experimental results. The total percent error for this simulation was found to be 5.91%. Nine of the twelve simulations resulted in less than 10% error between the simulated and experimental values. Only three simulations had over 10% error associated with them (all during protraction exercises). The third set of results was generated after optimizing the exercise forces only for the elevation and depression exercises. During this optimization, the values generated for the protraction and retraction exercises did not affect the optimization, the elevation and depression values only affected the performance of the optimizer.

Table 5: Exercise force values (N) for experimental data and three simulations; one with initial muscle parameters (Initial), one after optimization over all exercises (Full), and one after optimization over only the elevation and depression exercises (Elev/Dep). [1]

		Experimental	Simulated: Initial		Simulated: Full		Simulated: Elev/Dep	
Exercise		Value	Value	%Error	Value	%Error	Value	%Error
Elevation	Lo	-1331	-959	28.0	-1312	1.5	-1322	0.7
	Med	-1242	-883	28.9	-1225	1.4	-1250	0.6
	Hi	-1099	-794	27.8	-1013	7.8	-1092	0.6
Depression	Lo	680	442	35.0	636	6.5	681	0.1
	Med	850	532	37.4	845	0.6	841	1.1
	Hi	950	624	34.3	971	2.3	952	0.3
Protraction	Back	-1423	-585	58.9	-1067	25.0	-1040	26.9
	Mid	-1359	-559	58.9	-1162	14.5	-1101	19.0
	For	-1202	-501	58.3	-1019	15.2	-968	19.5
Retraction	Back	766	970	26.5	722	5.8	945	23.3
	Mid	984	1054	7.1	1060	7.7	1202	22.1
	For	1133	1115	1.6	1219	7.6	1341	18.3
TOTAL				403		96		133

Figure 28 below is given to present the experimental and simulated exercise forces. The experimental exercise forces are presented in black. The exercise forces generated using the initial (published) muscle parameters are presented in blue, the exercise forces generated after optimization for the elevation and depression exercise only are in green, and the exercise forces after optimization for all the exercises are presented in red. A substantial increase in accuracy is seen after muscle parameter optimizations in both cases. Also, while the simulated force values may not directly match the experimental values, three out of the four groups of exercises have similar trends when compared to the experimental values.

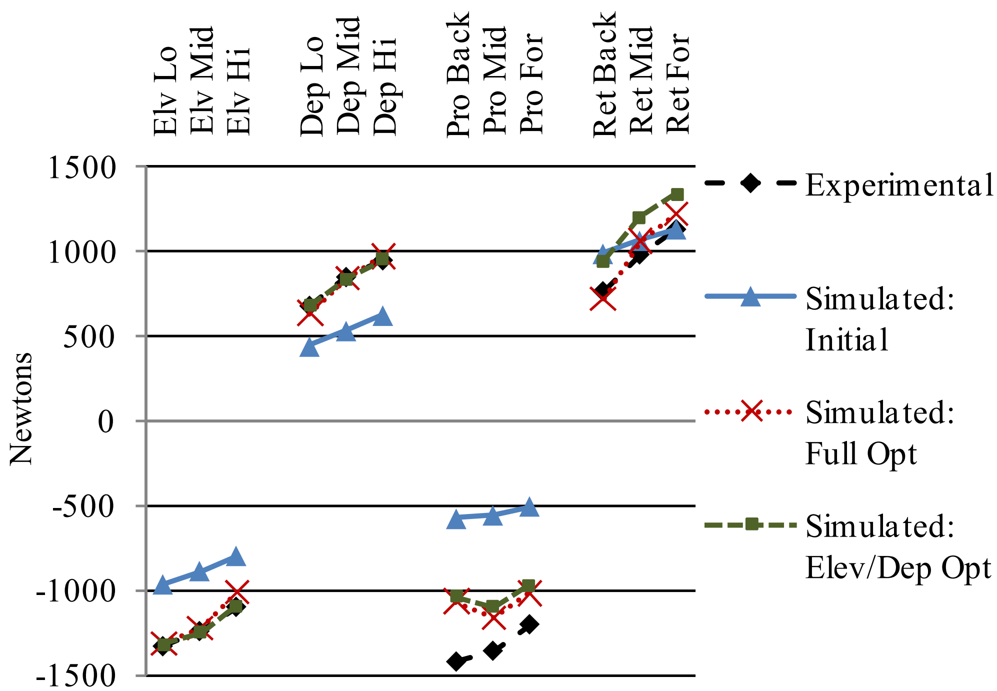

Figure 28: A Comparison of all simulated and experimental exercise forces. [1] Elevation, depression, protraction, and retraction exercises were abbreviated Elv, Dep, Pro, and Ret.

The most apparent trend is that a positive slope for each exercise's grouping of three exercise positions is seen, with the exception of the back protraction position. This occurs because as the shoulder position is moved in the direction of the applied force, the range of motion and maximum force possible is decreased. The positions with the largest range of motion in the direction of the force (front retraction, low elevation) are generally able to generate the most force, and the positions at the far range of their motion (low depression, front protraction) are able to produce the least. The highest force value for each group of exercises is generated at the position that provides the greatest range of motion in the direction of the exercise, also with the exception of the back protraction position. The force generally decreases as the range of motion in the direction of the exercises decreases, and the force reaches its minimum at the limit of the range of motion. This tendency is observed in the experimental and the simulated forces.

Muscle Parameters

The parameters describing optimal muscle-fiber length (Lom), tendon slack length (Lst), and peak isometric force (Fom) are all presented in below. Table 6 presents the values generated for the optimal muscle-fiber length for each muscle. Table 7 presents tendon slack length values for each muscle, and Table 8 below presents peak isometric force values calculated for each muscle. Each of these tables lists the initial value used (taken from literature), the parameter found after a global optimization, and the parameter value found after an optimization of only the elevation and depression exercises. The initial values listed in the chart were taken from Garner and Pandy [25] and were used as the initial values for the model muscle parameter optimization.

All parameters were affected by the optimization, however some were adjusted much more notably than others. The muscle parameters before and after optimization are shown below in Figure 29 - Figure 31.

The optimal muscle-fiber length for the subclavius muscle increased from 0.0202 m to 0.0536 m, a percent difference of 165.5%, which was by far the largest percent change in optimal fiber length. Also notable were a 64.2% decrease in length by the serratus anterior superior muscle as well as a 64.5% increase in the pectoralis minor muscle. Tendon slack length values had much larger changes in value than the optimal muscle fiber lengths. The smallest change in tendon slack length was a 28.6% difference that occurred for the rib section of the pectoralis major from 0.0958 to 0.0684 m.

Table 6: Initial and optimized optimal muscle fiber length values (m) for optimizations over all exercises and optimizations only for elevation and depression

	Lom		
Muscles	Intl	All Exercises	Elev/Dep
subclav	0.0202	0.0536	0.0537
serants	0.1135	0.0407	0.0447
serantm	0.1791	0.0954	0.0926
seranti	0.2315	0.1302	0.1272
trapc	0.1862	0.1098	0.1064
trapc7	0.2144	0.1838	0.1618
trapt1	0.1937	0.1728	0.1621
trapt	0.1591	0.1762	0.1761
lvs	0.1902	0.1399	0.1421
rmn	0.1755	0.1411	0.1360
rmjt2	0.1747	0.1743	0.1656
rmjt3	0.1833	0.1752	0.1712
pmn	0.1503	0.0533	0.0615
pmjc	0.2265	0.1870	0.1621
pmjs	0.1658	0.1797	0.1687
pmjr	0.1776	0.1599	0.1474
ltdt	0.3487	0.3857	0.3855
ltdl	0.3478	0.5189	0.5140
ltdi	0.4817	0.4124	0.3564

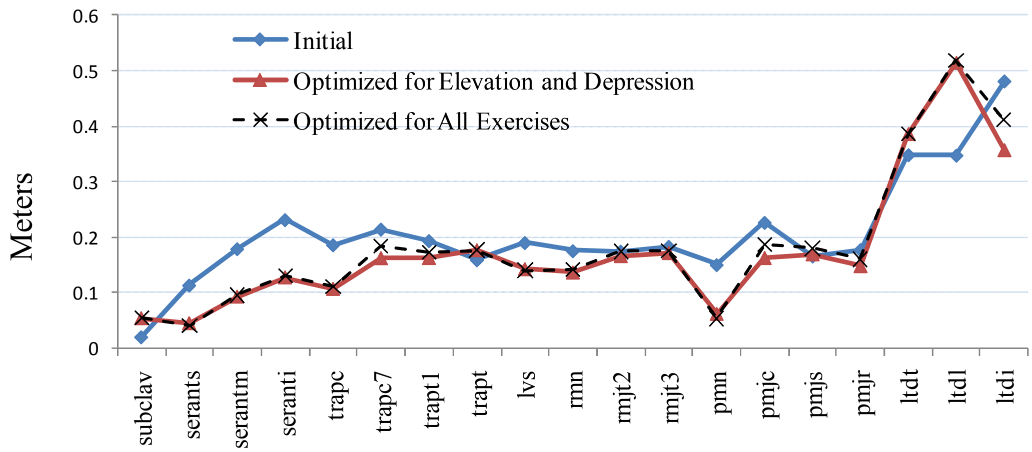

Figure 29: Optimizer Analysis for Lom Parameter

The values of the peak isometric force were not directly changed by the optimizer, but peak isometric force (Fom) was a function of the optimal muscle fiber length and the volume of the muscle. The muscle fiber lengths (Lom) generally decreased after optimization, and all stayed within the same magnitude as the initial values. Tendon slack length values least closely followed the initial values, with increases in length for all muscles except for the pectoral and latissimus dorsi muscles. The changes seen in Table 8 for the peak isometric force were below 40% for thirteen of the eighteen muscles. The largest increases in strength were generated by the serratus anterior superior muscle, and the pectoralis minor muscle, both of which also had large changes in muscle fiber length.

Table 7: Initial and optimized tendon slack length values (m)

	Lst		
Muscles	Intl	All Exercises	Elev/Dep
subclav	0.0507	0.0066	0.0066
serants	0.0027	0.0409	0.0389
serantm	0.0075	0.0592	0.0592
seranti	0.0001	0.0696	0.0696
trapc	0.0048	0.0746	0.0763
trapc7	0.0060	0.0411	0.0416
trapt1	0.0032	0.0236	0.0239
trapt	0.0042	0.0092	0.0080
lvs	0.0090	0.0238	0.0240
rmn	0.0044	0.0181	0.0184
rmjt2	0.0067	0.0148	0.0130
rmjt3	0.0024	0.0111	0.0096
pmn	0.0001	0.0480	0.0415
pmjc	0.0045	0.0371	0.0318
pmjs	0.0903	0.0385	0.0380
pmjr	0.0958	0.0684	0.0684
ltdt	0.1475	0.0386	0.0332
ltdl	0.1992	0.0669	0.0560
ltdi	0.1089	0.0477	0.0523

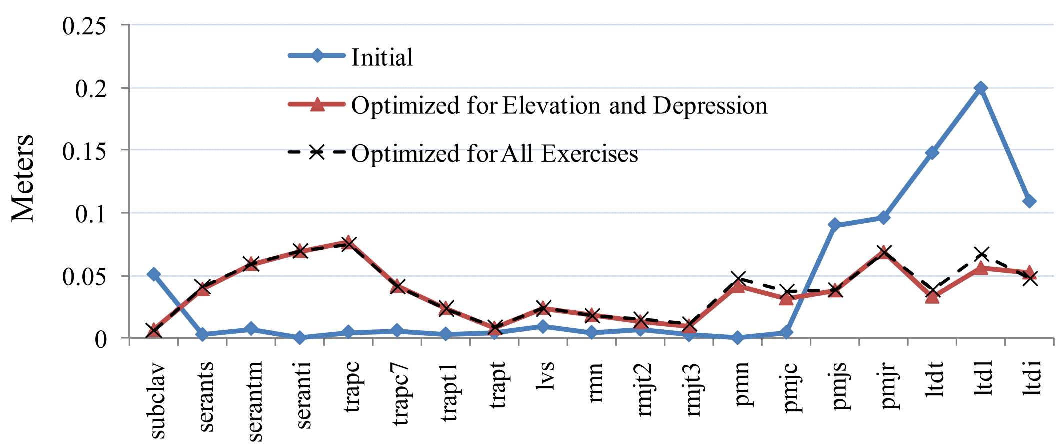

Figure 30: Optimizer Analysis for Lst Parameter

Table 8: Initial and optimized peak isometric force values (N)

		Fom	
Muscles	Intl	All Exercises	Elev/Dep
subclav	144.0	54.1	54.1
serants	268.1	748.3	681.1
serantm	132.1	248.0	255.7
seranti	277.5	493.4	504.9
trapc	206.0	349.4	360.3
trapc7	119.3	139.1	158.0
trapt1	114.0	127.8	136.2
trapt	409.2	369.3	369.6
lvs	124.8	169.6	167.0
rmn	221.5	275.4	285.9
rmjt2	136.5	136.9	144.0
rmjt3	81.9	85.7	87.7
pmn	160.6	452.6	392.7
pmjc	342.5	414.9	478.5
pmjs	484.4	446.9	476.1
pmjr	367.8	408.7	443.3
ltdt	173.4	156.8	156.9
ltdl	173.9	116.5	117.6
ltdi	125.5	146.6	169.7

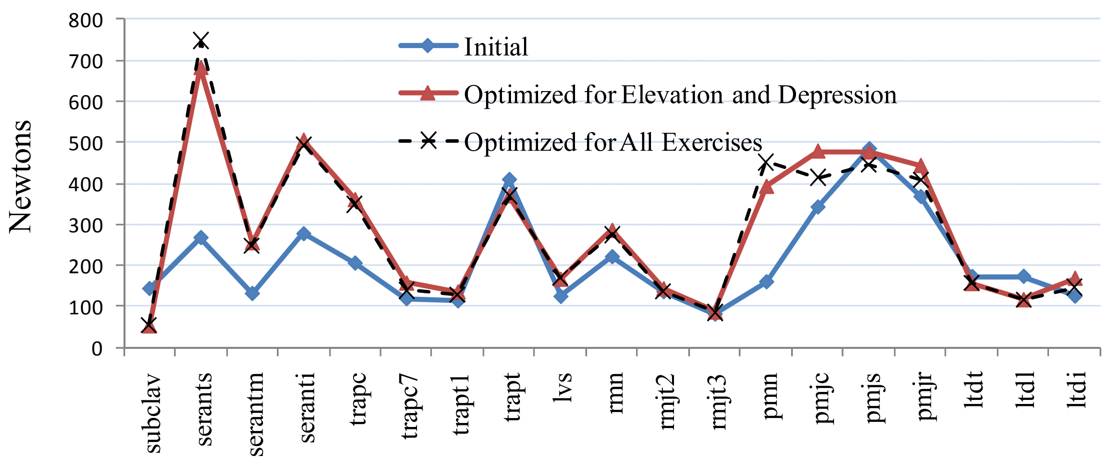

Figure 31: Optimizer Analysis for Fom Parameter

Figure 32 on the following page displays the tendon slack length and optimal muscle fiber length results for all three scenarios. The scenarios are listed in the same order, from top to bottom, for all muscles. The top scenario is the simulation with initial muscle parameters, the middle scenario is simulation after full optimization, and the bottom scenario is the simulation after optimization for elevation and depression. This figure was constructed for comparison of these muscle parameters between exercise scenarios.

Figures 33 - 35 displayed on the following pages illustrate the tendon and muscle lengths for each muscle during exercises at all twelve positions. The tendon is displayed as tan line segments in series with the red muscles. The tendon slack length and optimal muscle fiber values are also shown at the top of each muscle grouping as thicker lines. Three figures are displayed, one for each scenario.

Figures 36-38 display the passive and active force contributions of each muscle for all twelve exercises. The passive forces are displayed in blue, and the active forces are displayed in red. The peak isometric force for each muscle is also displayed at the top of each muscle grouping as a thick red line.

For each of the figures that shows the muscles for all twelve exercises, the muscles are displayed in groups of three, delineated by the black and white rectangles seen on the muscles left. The order of the exercises is the same for all figures: elevation (black) on top, followed by depression (white), protraction (black), and then retraction (white) on bottom.

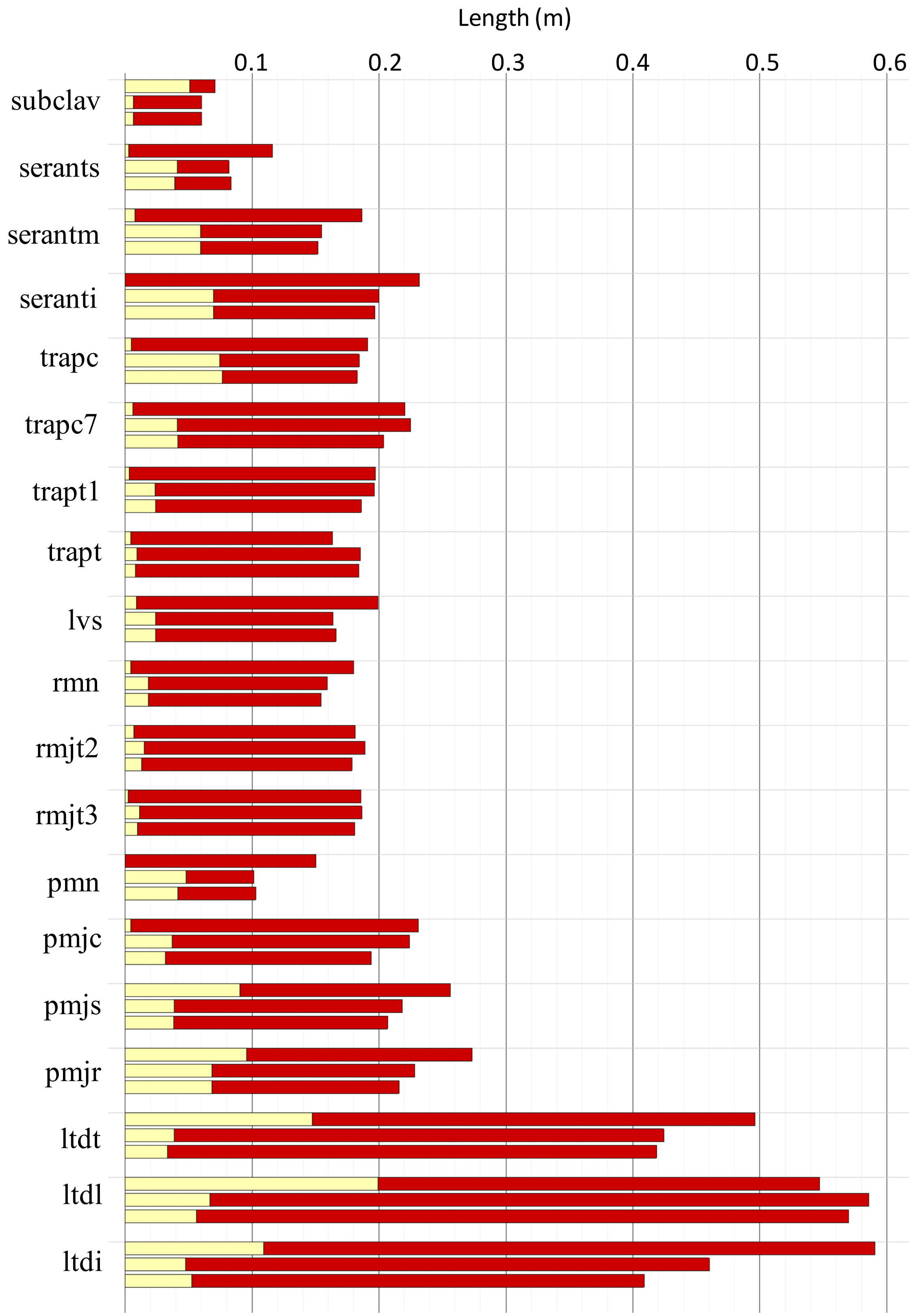

Figure 32: Tendon slack lengths and optimal muscle fiber lengths for each muscle during all three simulation types (Initial, Full Opt, and Half Opt)

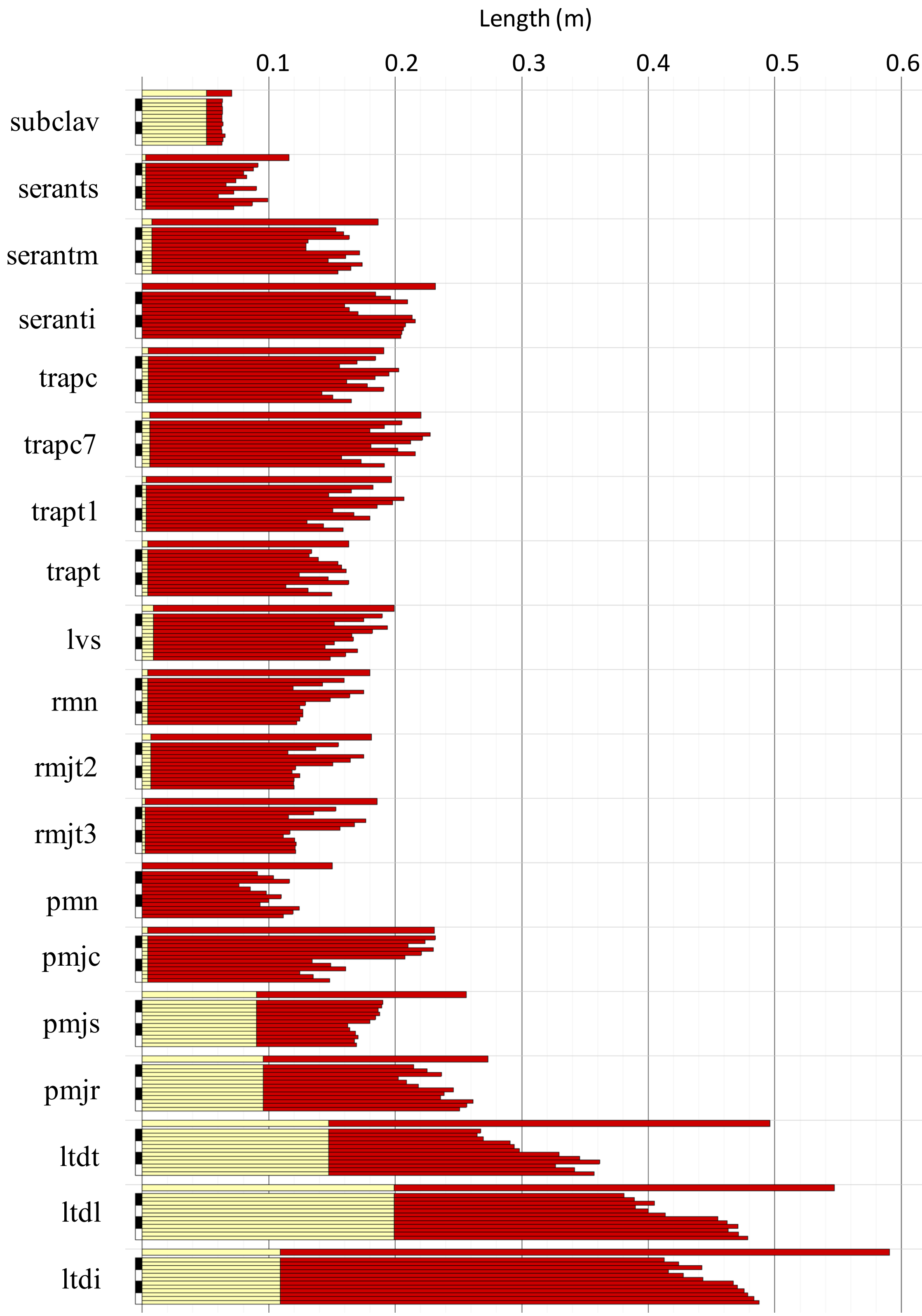

Figure 33: Actual tendon and muscle lengths for each muscle during all twelve exercises calculated with initial muscle parameter values Tendon slack length and optimal muscle fiber length shown as the thick line segments at the top of each muscle grouping.

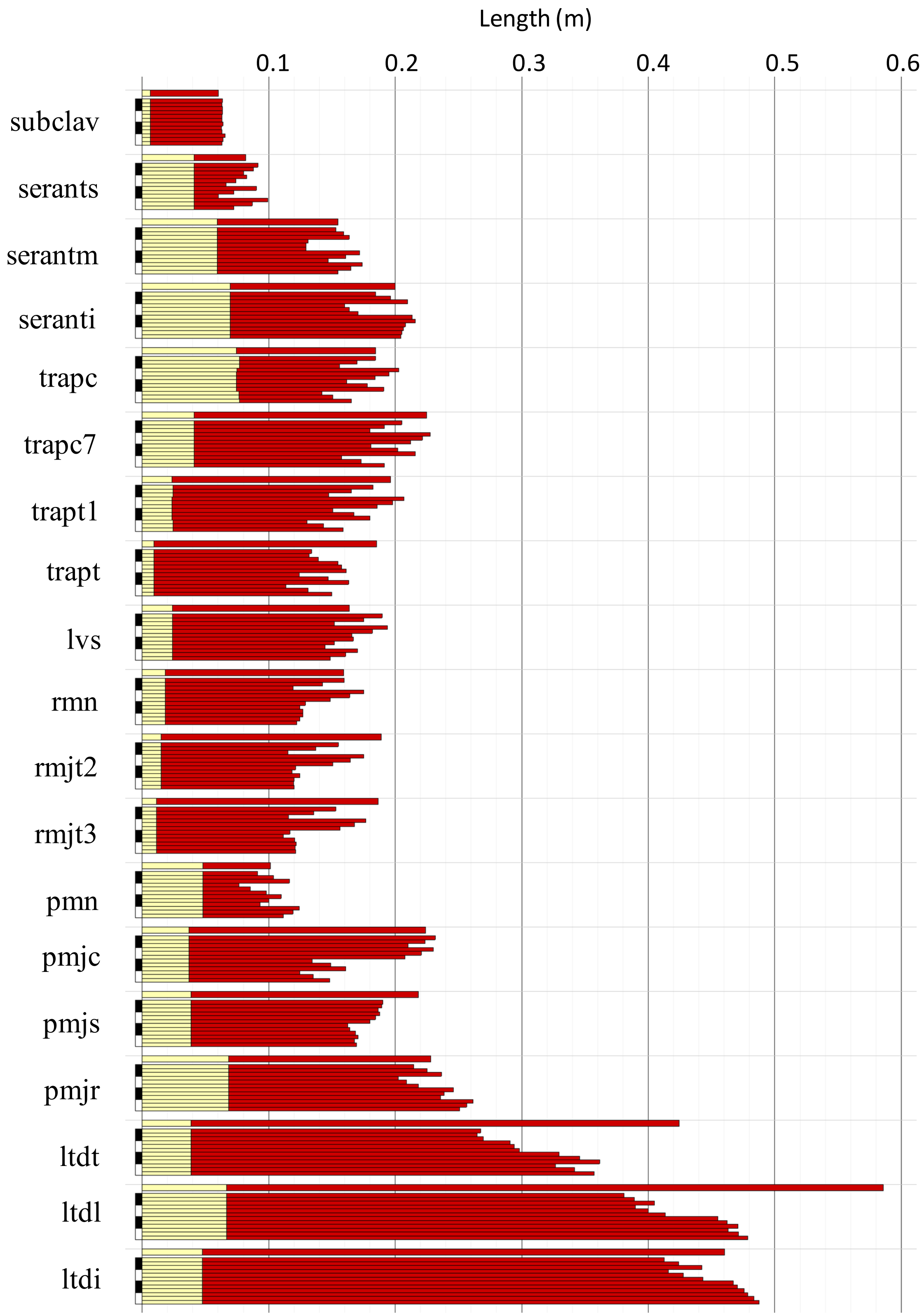

Figure 34: Actual tendon and muscle lengths for each muscle during all twelve exercises after full optimization. Tendon slack length and optimal muscle fiber length shown as the thick line segments at the top of each muscle grouping.

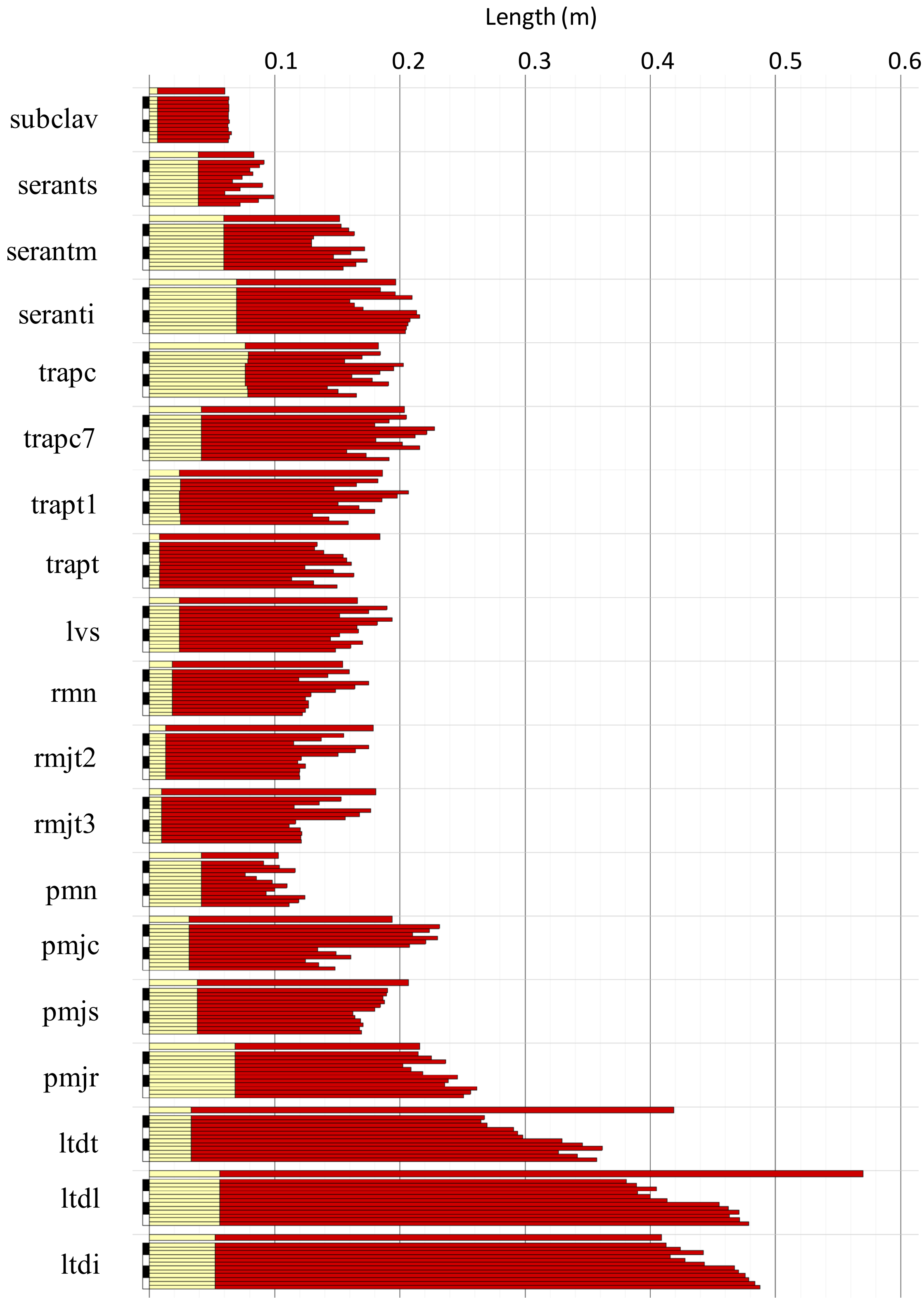

Figure 35: Actual tendon and muscle lengths for each muscle during all twelve exercises after half optimization. Tendon slack length and optimal muscle fiber length shown as the thick line segments at the top of each muscle grouping.

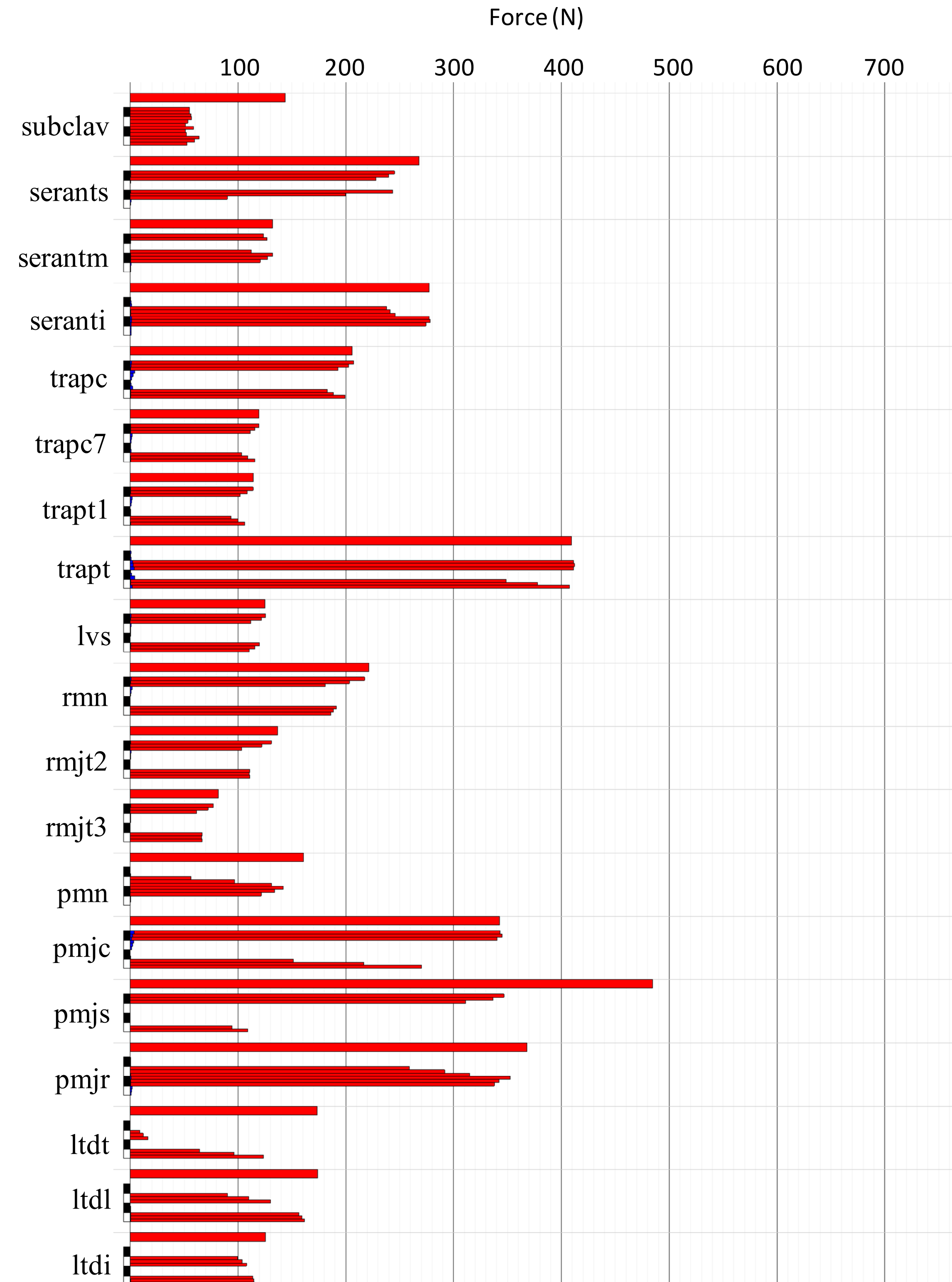

Figure 36: Passive (blue) and active (red) forces generated by muscles during each exercise using initial muscle parameters. Maximal isometric force displayed as the thick line segment at the top of each muscle grouping.

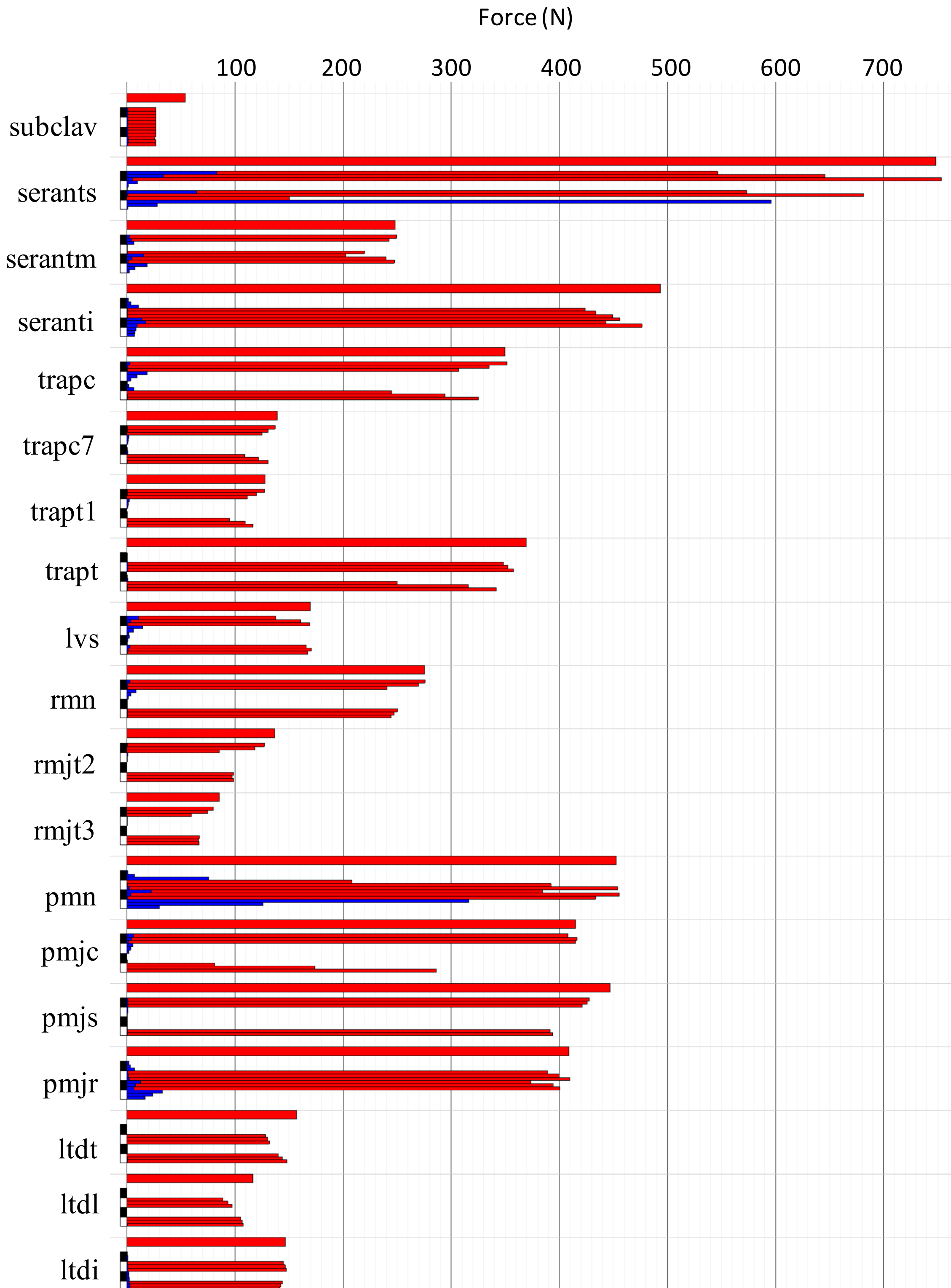

Figure 37: Passive (blue) and active (red) forces generated by muscles during each exercise after full muscle parameter optimization. Maximal isometric force displayed as the thick line segment at the top of each muscle grouping.

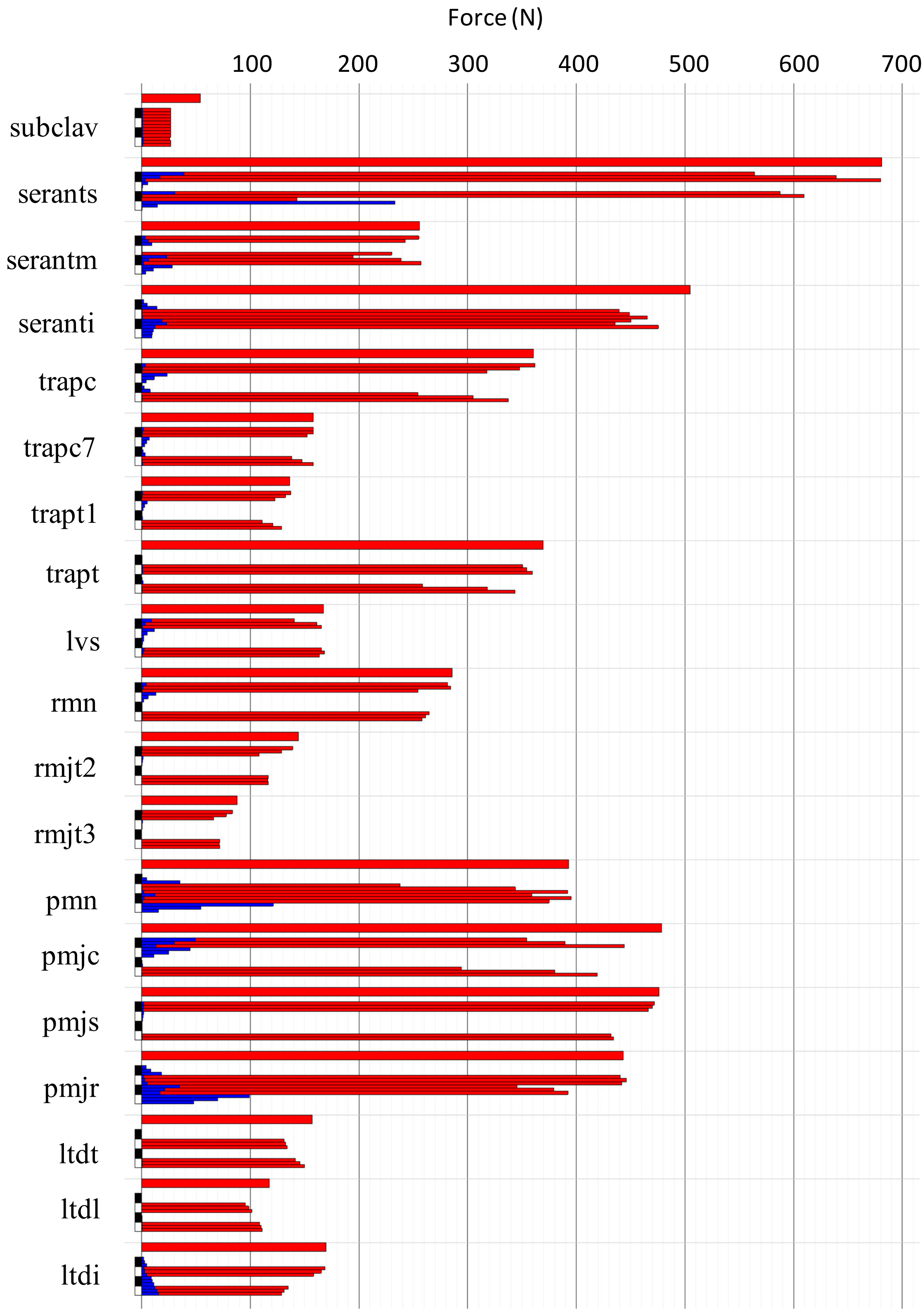

Figure 38: Passive (blue) and active (red) forces generated by muscles during each exercise after half muscle parameter optimization. Maximal isometric force displayed as the thick line segment at the top of each muscle grouping.

CHAPTER SEVEN

Discussion

Activation Values

Only one solution set for the muscle activations was displayed because the active and passive muscles were the same for all three scenarios. The model position for each exercise was the same for all three scenarios, so the muscle activations did not change between scenarios. The trends for the activation values were as expected: the activation values generally flipped between opposing exercises, though muscles that contributed minimally at one position sometimes changed to have small negative contributions at the next model position. The muscles that contributed to each exercise were verified visually in the graphics window for each simulation. Each active muscle was colored red, and the inactive muscles were colored blue to make it easy to distinguish the active muscles. For the protraction exercise shown below in Figure 39, the active muscles were located primarily in the anterior portion of the body, while many of the posterior muscles were inactive.

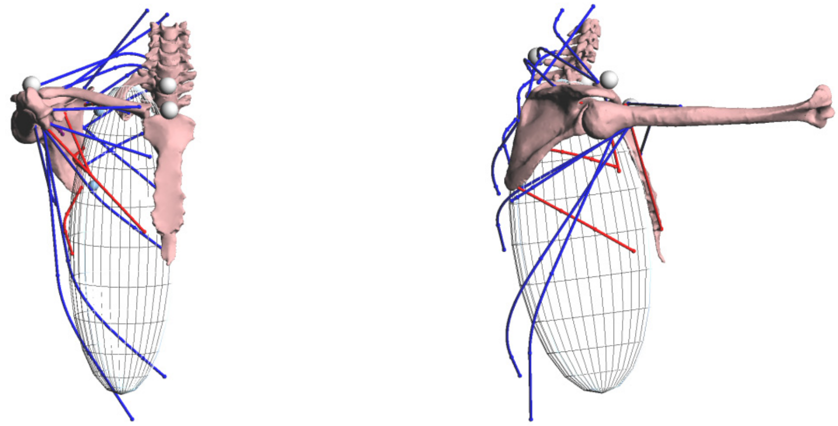

Figure 39: Anterior and medial-lateral view of shoulder model illustrating the ability to visually identify active and passive muscles used for protraction exercises

The computations that determined which muscles to activate for each exercise took into account only whether or not each individual muscle contributed to increasing the magnitude of the exercise force. The computations did not take into account joint stabilizing muscles that did not directly contribute to the exercise force. Solving exercise simulations that include joint stabilizing muscles adds significantly to the complexity of the simulation. This would also require the inclusion of the muscles that actuate the glenohumeral joint, which was not included in this model. Because of this substantial increase in complexity, the contributions and detractions of joint stabilizing muscles were not taken into account in this model. The principal purpose of this model was to simulate shoulder girdle exercises using the primary actuators contributing to the joint movement, so we feel that it is of less importance to take the stabilizing muscles into account. Some muscles did not change activation between opposing exercises because the actual model positions for each type of position (low shoulder elevation vs low shoulder depression) were not in the exact same position. Since the positions were measured during experimentation, the low position for elevation and the low position for depression were not exactly the same. This difference in model position could have affected which muscles contributed to the exercise, causing some muscles with small positive moment arms during one type of exercise to change position and have a small negative moment arm during the opposing exercise even though they are at the position with the same title.

Elevation & Protraction Angles and Joint Angles

The model was able to achieve the target elevation and protraction angles for each exercise position. The model computed the appropriate elevation and protraction angles to within ten thousandths of a radian from the target angles. The model positions were examined after the joint angle optimization to ensure that the joint positions were within reasonable bounds.

Exercise Force Values

In this section, the results from all three simulated scenarios will be compared to the experimental results presented previously and will be discussed in the sections below.

Performance with Initial Muscle Physiological Parameters

The initial performance of the model was calculated using physiological parameters that were based on previous cadaver studies, with the muscle volumes having been calculated using the VHP database by Garner and Pandy [25]. All of the initial physiological parameters were also published in the same work. After examining the results, it is evident that the simulations generate a fairly poor representation of the exercises when simulated with these muscle parameter values. The sum of the exercise error s, which gives a value associated with the performance of the model, was a total of 403%. This value should be minimized for peak model performance. As a whole, the exercise force performance was very low compared to the experimental forces. These poor results draw attention to the risks associated with directly plugging in physiological parameter values from experimental studies into musculoskeletal models without subsequent validation. This also illustrates the importance of model validation, such as by strength comparisons.

As is seen in Figure 28, the model performance for the initial parameters is not close quantitatively, but demonstrates some of the same trends as are seen in the experimental results. The slopes for each of the exercises is positive both for the experimental and simulated initial experiments. This means that the minimum and maximum forces produced for all four exercises were located at the same relative position – at the far range of their motion. The exercise force values for the elevation and depression exercises were both somewhat low. The protraction exercise forces generated were fairly low when compared to the experimental results, but the retraction exercise forces were actually higher than the experimental results.

The fact that the results generated using published experimental data do not provide an accurate model highlights the risks of using experimental data in a representative model without validation.

Performance After Full Muscle Parameter Optimization

The overall performance after the full optimization was much better than the initial performance; however there were still several problem areas. The sum of all of the exercise errors associated with the performance from the simulation after optimization for all exercises was a much reduced value of 96%. The total performance was still low compared to the experimental performance. The generated exercise force values are displayed in red in Figure 28. The exercise force values for elevation, depression, and retraction match experimental results well, but the exercise forces for the protraction exercises do not match the experimental results. The protraction exercise forces have less magnitude, and the force produced at the back protraction position does not fall along the same slope as the other two positions in the exercise. After analyzing the data, it became evident that the problems associated with matching the simulated values to the experimental values were due to an imbalance of strength during the protraction and retraction exercises. While the optimizer was able to easily solve the elevation and depression exercises to match the experimental results, the forces created in retraction were overly strong and the protraction forces were too weak. This competition between the protraction and retraction caused the optimizer to struggle to produce good results.

There are several possible reasons for this problem. First, inconsistencies in muscle volume modeling are possible. While the muscle volumes had been computed using imaging software to analyze the Visible Human Male cross-sections, the volumes for each muscle bundle were not defined. The muscle volumes were divided between the muscle bundles by comparing published physiological cross-sectional areas, which do not take into account muscle length [9]. Secondly, the muscle moment arms for the muscles contributing to the protraction and retraction exercises could need to be adjusted. The moment arms associated with some of the muscles in the back could be too large, causing higher force values, or the moment arms for the pectoral or serratus muscles may need to be slightly increased. While the muscle moment arms in the model should be similar to those in an average human body, it is possible that the male subject modeled had different body geometry than the average subject. Thirdly, it is also possible that the subject modeled had a strength profile that was dissimilar to the subjects used in the strength experiment. The muscles modeled in this experiment were chosen because they should directly contribute to the strength exercises performed; however, it is possible that the addition of more muscles or more muscle bundles could improve the performance of the model.

It has already been stated that the muscles associated with retraction are too strong and that the muscles used for protraction are unable to attain the desired strength values. In order for the optimizer to increase its overall performance (by increasing protraction strength and decreasing retraction strength), the optimizer was penalizing the retraction muscles because they were too strong, such that they were used to oppose the antagonist (protraction) exercise by driving the muscles used for retraction into their passive force-producing region (also known as the parallel elastic region), as is displayed in Figure 5. This behavior is physiologically unrealistic for these exercises, but allows the optimizer to calculate a better performance than it would otherwise be able to achieve. The passive and active force contributions to each exercise will be further examined below in the muscle parameters section.

Performance After Muscle Parameter Optimization for Elevation & Depression Exercises

In order to show the natural traits of the model, an optimization was calculated which only depended on the performance of the elevation and depression exercises. The optimizer only took into account elevation and depression exercise forces. Protraction and retraction exercises were still affected by the changes made in muscle parameters, but their exercise forces did not affect choices of the optimizer. After this optimization was finished, all twelve exercises were simulated with the new muscle parameters. The optimizer quickly solved the elevation and depression exercises, with percent errors below 1.5% for all elevation and depression positions. The resulting strength values for protraction and retraction demonstrate the innate strength profiles of the model. While the protraction and retraction forces still match the experimental results fairly well, the retraction forces naturally settled higher than experimental values, and the protraction exercises naturally settled low. The sum of the errors (133) was much lower than for the initial simulation (403), but did not reach the performance of the fully optimized simulation (96). The protraction exercises were too weak by an average error of 21.8%, and the retraction exercises were too strong by an average of 21.2%. error. In order to match the experimental and simulated strength profiles for this optimization, the average simulated forces for protraction would have to be scaled up by 1.28, and retraction would have to be scaled down by 0.83.

The overall performance of the elevation and depression optimized simulations were expected to be worse than the performance of the model optimized for all twelve exercises. However, this was not the case (see Table 5). The elevation/depression model generated a higher total strength (12,734 N) than the model that was optimized for all exercises (12,250 N). The overall performance was calculated by comparing only the sum of the magnitudes of all of the exercise forces, not by summing all of the errors for each exercise. If this was the case, the full optimization would have a better performance than the elevation/depression optimization. The full optimization was able to find a solution that had less error per exercise (a better fit for each individual exercise), but the elevation/depression optimization was able to find a solution that displayed the natural strength profile of the model and ended up with an exercise sum that came closer to the magnitude of the sum of the experimental forces.

Performance After Muscle Parameter Optimization for Elevation and Depression Exercises Strength Scaling

For illustration of the problems as well as the correct trends seen in our model, the force values for protraction and retraction were scaled by 1.28 and 0.83, respectively, and the resulting forces and errors were calculated. The results are shown in Table 9 below. The total percent error after these scaling factors are applied was calculated to be 0.11%.

Table 9: Exercise force values (N) after elevation/depression optimization and scaling

Exercise		Experimental	Optimized Elev/Dep	Scaled Elev/Dep	%Error
Elevation	Lo	-1331.5	-1321.7	-1321.7	0.74
	Med	-1242.2	-1250.0	-1250.0	0.63
	Hi	-1098.9	-1092.5	-1092.5	0.58
Depression	Lo	680.0	680.7	680.7	0.10
	Med	850.4	840.7	840.7	1.14
	Hi	949.6	952.3	952.3	0.28
Protraction	Back	-1422.7	-1039.8	-1332.2	6.36
	Mid	-1358.8	-1101.1	-1410.8	3.82
	For	-1202.1	-968.3	-1240.6	3.20
Retraction	Back	766.4	944.9	781.3	1.95
	Mid	984.1	1201.6	993.6	0.96
	For	1133.0	1340.7	1108.6	2.15
TOTAL		13019.7	12734.3	13005.0	0.11

A graph illustrating how well the simulated values matched the experimental values after scaling corrections are made is seen below in Figure 40. All of the exercise force values line up almost directly with the experimental values except for the protraction exercise values. The lack of strength at the back protraction position is still a problem. There are numerous reasons that could be affecting the force produced during this exercise, varying from the muscle parameters that change the force produced in all

18 muscles to the obstacle sets that have been defined for the muscle pathways in the model.

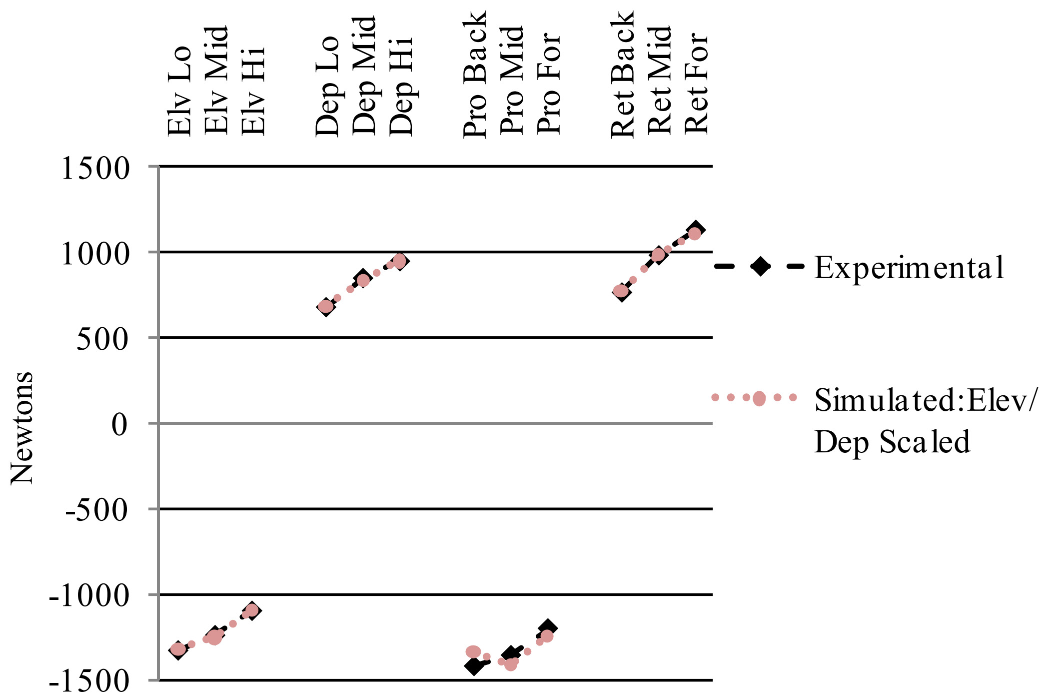

Figure 40: Exercise forces displayed after elevation and depression optimization and exercise force scaling

While we do not feel that it would be appropriate to arbitrarily scale forces to match our model, we wanted to show that after further adjustments to our model we may be able to provide a shoulder girdle model which would be able to simulate a wide variety of exercises very accurately. As was previously discussed, there are multiple reasons that could have caused the strength problems in the protraction and retraction directions. Because of the presence of these unknowns, we are pleased with the results generated by our model.

In conclusion, the model was able to be tuned to generate the experimentally-measured shoulder girdle strengths, although it required careful analysis and adjustment of variables that affected the performance of the simulations. While the model did require nurturing to direct the model to correct solutions, we feel that the adjustments made were not arbitrary or wholly unrealistic.

Muscle Parameters

The optimal muscle fiber length values generated for both the full and half optimizations trend similarly to the initial values. Both optimized scenarios give very similar results even though the half optimization was only dependent on the elevation and depression cases. This result is somewhat surprising because the elevation and depression exercises have different primary muscles used and different ranges of motion than the protraction and retraction exercises. The lengths found are within reasonable anatomical bounds.

Muscle fiber lengths were compared to the optimal muscle fiber length (Lom) to calculate relative the position on the muscle force-length curve, which was shown previously in Figure 5. The muscle fiber lengths for each muscle during all twelve exercises are displayed in Appendix C.

Table 10 below shows the averaged muscle fiber lengths generated for each muscle after the optimization was performed for all exercises. Tables listing each muscle length for all twelve exercises for the initial and two optimized cases can be found in Appendix C. The table below is an abbreviated version of Table B.2 used to show that the optimal muscle fiber length parameter stayed well within anatomical bounds. All values of the ratio of the average muscle fiber length (L0) to the optimal fiber length (Lom) were within the 60 to 140 percent muscle length range, with the largest deviation seen in the rhomboid major T2 muscle bundle with a value of 68.95. Deviations of the muscle fiber length outside this range would show that the muscle was unable to produce active force. If the ratio was significantly above 100%, then the passive contribution of the muscle force would be unrealistically high. While many muscle fiber lengths deviated below the optimal fiber length, very few deviated above the optimal length, which would significantly increase the passive force contribution. We were pleased to see that the passive force contributions were small in most cases (listed in Appendix A and displayed in Figure 36 - Figure 38).

Table 10: Average muscle fiber lengths for all exercises after full optimization

	Muscle Fiber Lengths			
Muscles	Ave L0	Std Dev	Lom	%L0/Lom
subclav	0.0568	0.0008	0.0536	105.84
serants	0.0388	0.0113	0.0407	95.42
serantm	0.0931	0.0159	0.0954	97.60
seranti	0.1242	0.0203	0.1302	95.39
trapc	0.0977	0.0196	0.1098	89.04
trapc7	0.1548	0.0216	0.1838	84.22
trapt1	0.1440	0.0234	0.1728	83.35
trapt	0.1330	0.0158	0.1762	75.45
lvs	0.1426	0.0161	0.1399	101.90
rmn	0.1203	0.0190	0.1411	85.22
rmjt2	0.1202	0.0209	0.1743	68.95
rmjt3	0.1236	0.0227	0.1752	70.51
pmn	0.0536	0.0145	0.0533	100.44
pmjc	0.1438	0.0423	0.1870	76.92
pmjs	0.1377	0.0104	0.1797	76.62
pmjr	0.1634	0.0196	0.1599	102.25
ltdt	0.2731	0.0356	0.3857	70.82
ltdl	0.3638	0.0380	0.5189	70.12
ltdi	0.4039	0.0277	0.4124	97.95

Tendon slack length values after both parameter optimization scenarios had a larger range of differences between the initial and the simulated values than the optimal muscle fiber lengths, but the tendon slack lengths achieved were still within reasonable anatomical bounds. The tendon lengths for the latissimus, trapezius, and serratus muscles are all relatively large, but the tendon lengths seem reasonable for the total length of the musculotendon unit. The initial tendon slack lengths should not be compared to as the "correct" standard, but are merely shown as a general comparison. The initial muscle parameter values were used because they allowed the previous computer model to perform decently during simulations. Both the full and the half parameter optimizations also gave very similar tendon slack length results. The values from both scenarios are very similar, especially when compared with the difference that is seen between the initial and both simulated results.

The maximal isometric force values stayed within the same range of magnitude and generally follow the same trends as the initial values. The peak isometric force for the serratus muscles were all increased, but in general the amount of force produced by each muscle did not increase or decrease substantially. Again, the results generated from both the full and half simulations were very similar. All of the force values generated also stayed within reasonable bounds. We were very pleased that the physiological parameters calculated using the optimization methods described in chapter five provided results that are anatomically realistic.

Contributions

The primary contributions of this study were threefold. First, a validated shoulder girdle model was developed that was able to match experimental strength results. This musculoskeletal model of the shoulder girdle is able to be merged with the previously validated model of the arm to provide a fully validated model of the human upper body.

This model will then be able to be used for further research in the field of musculoskeletal modeling.

Secondly, the results from this research provide insights into the roles of the shoulder girdle muscles. The muscle activations for different exercises were generated and are able to be quickly calculated using the current model. The active and passive forces produced by each individual muscle were also recorded for each exercise simulation. This information provides insight into the roles and contributions of individual muscles for numerous different exercises.

Thirdly, the muscle physiological parameters that were generated during the optimization process are extremely important for future modeling research of the muscles in the shoulder girdle. The parameters found provide insights into the physiological characteristics of each muscle, and the publication of reasonable muscle modeling parameters helps to facilitate modeling research.

Limitations

There were several limitations to this research project. The most important was the lack of published muscle moment arm data for further verification of the computer model. Published values of the muscle moment arms for most of the primary contributing muscles for the exercises were not available, and published muscle parameter data for comparison of the values used in the computer model could not be located. Electronic resources such as Medline, Inspec, Scirus, Pubmed, Elsevier, SpringerLink, Engineering Village, and Google Scholar were all used in the literature search. Keywords such as shoulder girdle, shoulder, model, muscle, strength, moment arm, computer model, muscle pathway, and muscle parameters were used. Several of the key contributing muscles were also searched for individually. There were published muscle moment arm values for several of the muscles included in the model, but in each case the muscles were not the primary muscles being studied in the experiment. This was the case in the experiments performed by Kuechle *et al* [18, 19]. The experimental exercise was a humerus elevation at several fixed scapular positions, which refers to positions and exercises unlike what was studied in our experiment. Because of the small number of muscles that had published muscle moment arm values, and because of the relatively large difference in experimental exercise format, we concluded that our model could not be further validated by the current available data. However, we believe the model that has been developed provides valuable information because the strength exercises that were simulated were able to accurately reproduce the forces from the experimental strength exercises.

Also, the muscle volume distribution between muscle bundles of the same muscle could have produced a variance in the strengths of the model in certain directions. While the total volume for each muscle was known, in muscles that were modeled with multilple muscle bundles, the total muscle volume had to be distributed across the muscle bundles. While the Johnson [35]study of distributions was used to provide volume distribution ratios for most muscles, some error could have occurred in the manual distribution of these muscle volumes.

The error in protraction and retraction strengths could be due to several limiting factors. It is possible that the VHP male that was used as the basis of this model does not reflect the average male subject that took part in the strength exercises. The VHP male could have had unproportional body strength (worked out in one direction more than the other). The muscle moment arms associated with our model could also be adjusted (increased or decreased) to provide more or less strength in certain directions. Because the moment arm values were not also validated it is possible that minor changes could need to be made. Changes in muscle volume distribution could also affect strengths for different exercises.

Future Research

There are several areas in which additional research could improve this model. First, in calculating what muscles are used during each exercise, stabilizing muscles for each exercise were not taken into account. Only muscles that directly contributed to the force produced were used in the calculation of the exercise force. Adding calculations to determine which muscles to activate for shoulder stabilization greatly increases the complexity of the calculations because of the number of variables introduced. However, if these complexities could be addressed, a more accurate computer model for each exercise could be computed.

Secondly, when the active and passive forces that contributed to the total force applied for the muscles were examined (given in Appendix A), it was noticed that several of the passive forces were larger than they should be. This is believed to have occurred because the optimizer shortened the muscle fiber length so that several muscles normally used for protraction would use their passive force contribution to detract from retraction exercise forces, thereby decreasing the retraction exercise force since it is overly strong.

A redistribution of the muscle volumes across the muscle bundles could be performed to ensure that proper strength is being given to each muscle pathway. Also, adjustment and verification of the values of muscle moment arms for each of the muscle pathways could be completed, which would further validate the musculoskeletal model.

CHAPTER EIGHT

Conclusion

The primary goal for conducting this experiment was to provide a validated musculoskeletal model and necessary preliminary data on the muscle parameters of the shoulder girdle so that continued research can be conducted to improve models of the shoulder and shoulder girdle. While there are still aspects of the model that can be improved, I believe that both of these goals have been achieved. The model that was used was able to achieve the experimental strength values within reasonable bounds when the muscle parameters were optimized, and the muscle parameter values were found to have reasonable values for the majority of the muscles. The muscles that generated large passive forces because of muscle parameter values that fell outside the hypothesized range should be re-examined as this research continues forward.

This computer model was designed so that it can be used as a platform for many different types of simulations, from simulating specific exercises to calculating muscle moment arms for ranges of motion or seeing how changes in muscle parameters effect muscle force contributions. Similar models can be used to simulate changes made in surgery, whether a tendon transfer surgery or shortening of a muscle or tendon. The changes made in the human anatomy can be calculated swiftly, allowing the user to quickly find the best possible solution for many types of problems.

We hope that future researchers will use the model that has been developed, the exercise data produced, and the muscle parameters generated as standards by which they can compare their research to in order to create more accurate models of the upper body.

APPENDICES

APPENDIX A

Forces Produced By Each Muscle

Table A.1: Total Force Produced by Each Muscle with initial muscle parameters

	Total Force Produced by Each Muscle											
Muscles	1	2	3	4	5	6	7	8	9	10	11	12
subclav	87.8	87.7	0.0	0.0	0.0	79.6	98.5	78.9	0.0	0.1	0.0	0.0
serants	245.0	239.6	227.5	0.1	0.1	0.0	243.4	199.4	89.8	0.6	0.2	0.1
serantm	123.5	126.6	0.4	0.1	0.1	111.9	131.7	127.2	120.6	0.7	0.4	0.2
seranti	0.4	0.6	1.1	237.6	241.0	246.0	277.0	278.0	274.4	0.9	0.9	0.9
trapc	207.4	202.4	192.5	3.9	2.6	1.4	0.4	1.0	2.0	182.6	188.5	199.4
trapc7	119.4	115.6	111.4	1.7	1.3	0.8	0.2	0.5	1.0	103.4	108.8	115.7
trapt1	114.0	108.4	101.7	1.9	1.2	0.6	0.1	0.2	0.5	93.4	100.2	105.9
trapt	0.6	0.6	0.9	411.2	411.9	411.3	0.3	1.5	4.1	348.8	378.0	407.6
lvs	125.4	121.6	111.6	0.9	0.5	0.2	0.2	0.1	0.1	119.6	115.4	110.4
rmn	217.3	203.2	180.9	1.7	0.9	0.4	0.1	0.1	0.1	191.0	188.5	185.7
rmjt2	130.9	121.9	103.1	0.9	0.5	0.2	0.0	0.0	0.1	110.7	110.1	110.8
rmjt3	77.1	72.1	61.5	0.5	0.3	0.2	0.0	0.0	0.0	66.7	66.2	66.5
pmn	0.0	0.1	0.2	56.3	96.7	131.0	141.8	133.7	121.5	0.3	0.2	0.1
pmjc	343.1	344.9	340.1	3.3	2.2	1.2	0.0	0.1	0.2	150.9	216.0	269.7
pmjs	329.0	318.4	291.7	0.1	0.1	0.0	0.0	0.0	0.0	0.0	89.0	102.3
pmjr	0.1	0.2	0.5	245.3	281.9	309.8	348.3	337.9	333.9	1.9	1.4	1.0
ltdt	0.0	0.0	0.0	8.8	11.7	15.9	0.0	0.0	0.0	60.6	90.9	118.5
ltdl	0.0	0.0	0.0	83.4	102.8	124.1	0.1	0.2	0.2	154.7	157.2	159.5
ltdi	0.0	0.0	0.1	98.2	103.0	107.2	0.1	0.1	0.1	113.1	114.0	114.6

Table A.2: Active force produced by each muscle with initial muscle parameters

	Active Forces Produced by Each Muscle											
Muscles	1	2	3	4	5	6	7	8	9	10	11	12
subclav	87.7	87.7	0.0	0.0	0.0	79.6	98.5	78.9	0.0	0.0	0.0	0.0
serants	244.7	239.4	227.4	0.0	0.0	0.0	243.1	199.4	89.8	0.0	0.0	0.0
serantm	123.3	126.3	0.0	0.0	0.0	111.8	131.1	126.9	120.4	0.0	0.0	0.0
seranti	0.0	0.0	0.0	237.5	240.8	245.8	275.8	276.6	273.4	0.0	0.0	0.0
trapc	206.0	201.7	192.2	0.0	0.0	0.0	0.0	0.0	0.0	182.5	188.3	198.9
trapc7	118.8	115.3	111.2	0.0	0.0	0.0	0.0	0.0	0.0	103.4	108.7	115.4
trapt1	113.5	108.2	101.6	0.0	0.0	0.0	0.0	0.0	0.0	93.4	100.1	105.7
trapt	0.0	0.0	0.0	408.8	409.1	407.7	0.0	0.0	0.0	348.6	377.4	405.9
lvs	124.7	121.3	111.5	0.0	0.0	0.0	0.0	0.0	0.0	119.3	115.2	110.3
rmn	216.6	202.9	180.8	0.0	0.0	0.0	0.0	0.0	0.0	190.9	188.4	185.6
rmjt2	130.6	121.7	103.1	0.0	0.0	0.0	0.0	0.0	0.0	110.7	110.1	110.7
rmjt3	77.0	72.1	61.5	0.0	0.0	0.0	0.0	0.0	0.0	66.6	66.2	66.5
pmn	0.0	0.0	0.0	56.3	96.6	131.0	141.7	133.7	121.5	0.0	0.0	0.0
pmjc	339.6	342.4	338.8	0.0	0.0	0.0	0.0	0.0	0.0	150.9	216.0	269.6
pmjs	328.9	318.3	291.6	0.0	0.0	0.0	0.0	0.0	0.0	0.0	89.0	102.3
pmjr	0.0	0.0	0.0	245.3	281.8	309.7	347.7	337.5	333.6	0.0	0.0	0.0
ltdt	0.0	0.0	0.0	8.8	11.7	15.9	0.0	0.0	0.0	60.6	90.9	118.4
ltdl	0.0	0.0	0.0	83.4	102.7	124.1	0.0	0.0	0.0	154.6	157.0	159.3
ltdi	0.0	0.0	0.0	98.1	103.0	107.2	0.0	0.0	0.0	113.0	113.8	114.5

Table A.3: Passive force produced by each muscle with initial muscle parameters

	Passive Forces Produced by Each Muscle											
Muscles	1	2	3	4	5	6	7	8	9	10	11	12
subclav	0.0	0.0	0.0	0.0	0.0	0.0	0.0	0.0	0.0	0.1	0.0	0.0
serants	0.3	0.2	0.1	0.1	0.1	0.0	0.3	0.1	0.0	0.6	0.2	0.1
serantm	0.2	0.3	0.4	0.1	0.1	0.1	0.6	0.3	0.1	0.7	0.4	0.2
seranti	0.4	0.6	1.1	0.1	0.1	0.2	1.3	1.4	1.0	0.9	0.9	0.9
trapc	1.4	0.7	0.3	3.9	2.6	1.4	0.4	1.0	2.0	0.1	0.2	0.5
trapc7	0.6	0.3	0.2	1.7	1.3	0.8	0.2	0.5	1.0	0.1	0.1	0.3
trapt1	0.5	0.2	0.1	1.9	1.2	0.6	0.1	0.2	0.5	0.0	0.1	0.2
trapt	0.6	0.6	0.9	2.4	2.8	3.6	0.3	1.5	4.1	0.2	0.5	1.8
lvs	0.7	0.3	0.1	0.9	0.5	0.2	0.2	0.1	0.1	0.3	0.2	0.1
rmn	0.7	0.3	0.1	1.7	0.9	0.4	0.1	0.1	0.1	0.1	0.1	0.1
rmjt2	0.3	0.1	0.0	0.9	0.5	0.2	0.0	0.0	0.1	0.0	0.0	0.0
rmjt3	0.1	0.1	0.0	0.5	0.3	0.2	0.0	0.0	0.0	0.0	0.0	0.0
pmn	0.0	0.1	0.2	0.0	0.0	0.0	0.1	0.1	0.0	0.3	0.2	0.1
pmjc	3.5	2.5	1.4	3.3	2.2	1.2	0.0	0.1	0.2	0.0	0.0	0.1
pmjs	0.1	0.1	0.1	0.1	0.1	0.0	0.0	0.0	0.0	0.0	0.0	0.0
pmjr	0.1	0.2	0.5	0.1	0.1	0.1	0.7	0.4	0.4	1.9	1.4	1.0
ltdt	0.0	0.0	0.0	0.0	0.0	0.0	0.0	0.0	0.0	0.0	0.0	0.0
ltdl	0.0	0.0	0.0	0.0	0.0	0.0	0.1	0.2	0.2	0.1	0.2	0.2
ltdi	0.0	0.0	0.1	0.0	0.0	0.1	0.1	0.1	0.1	0.1	0.1	0.1

Table A.4: Total force produced by each muscle with muscle parameters optimized for all exercises

	Total Force Produced by Each Muscle											
Muscles	1	2	3	4	5	6	7	8	9	10	11	12
subclav	52.8	52.8	1.0	1.0	0.9	53.1	52.3	53.1	0.9	1.5	1.1	0.9
serants	573.3	676.6	749.4	10.4	1.3	0.2	623.0	667.7	274.2	455.0	27.9	0.8
serantm	249.7	245.6	6.3	0.2	0.2	217.4	209.9	243.4	240.8	18.7	7.4	2.5
seranti	1.5	3.8	10.7	418.4	429.3	444.9	465.0	453.5	496.1	8.4	7.4	7.0
trapc	351.7	335.0	307.0	18.7	9.3	3.4	0.4	2.0	6.0	245.3	294.3	325.2
trapc7	136.6	129.9	124.4	1.6	1.1	0.7	0.1	0.4	0.9	107.2	121.1	129.9
trapt1	127.3	119.7	111.5	2.3	1.4	0.7	0.1	0.2	0.6	93.9	109.3	116.6
trapt	0.2	0.2	0.3	348.6	352.7	358.0	0.1	0.4	1.0	249.3	315.9	341.6
lvs	138.9	161.8	168.5	14.8	6.2	2.0	2.0	0.7	0.7	167.0	170.8	166.7
rmn	276.1	269.2	240.0	8.7	3.9	1.3	0.3	0.2	0.4	248.9	246.5	243.8
rmjt2	127.0	118.2	84.5	0.6	0.3	0.2	0.0	0.0	0.0	96.9	96.6	97.8
rmjt3	79.8	74.5	59.0	0.5	0.3	0.2	0.0	0.0	0.0	66.4	66.0	66.4
pmn	0.6	6.9	72.1	185.1	383.7	449.9	403.6	454.9	424.2	262.8	116.4	29.3
pmjc	409.7	416.8	413.9	5.7	3.4	1.7	0.0	0.1	0.1	80.5	169.1	280.6
pmjs	425.7	423.7	419.1	0.8	0.7	0.5	0.2	0.2	0.3	0.3	389.9	392.1
pmjr	1.8	3.4	6.9	385.2	396.7	408.3	380.0	398.8	404.4	32.9	23.6	16.7
ltdt	0.0	0.0	0.0	127.6	129.5	131.3	0.1	0.2	0.3	139.6	143.5	147.8
ltdl	0.0	0.0	0.0	88.0	92.6	96.9	0.1	0.1	0.1	104.9	106.1	107.2
ltdi	0.5	0.6	1.0	144.3	146.2	147.5	1.7	1.9	2.2	144.2	142.8	141.7

Table A.5: Active force produced by each muscle with muscle parameters optimized for all exercises

	Active Forces Produced by Each Muscle											
Muscles	1	2	3	4	5	6	7	8	9	10	11	12
subclav	51.9	51.9	0.0	0.0	0.0	52.2	51.3	52.3	0.0	0.0	0.0	0.0
serants	509.0	651.7	745.6	0.0	0.0	0.0	581.6	667.1	274.2	0.0	0.0	0.0
serantm	248.0	242.3	0.0	0.0	0.0	217.3	197.4	239.6	240.2	0.0	0.0	0.0
seranti	0.0	0.0	0.0	418.2	429.0	444.4	453.2	439.0	491.9	0.0	0.0	0.0
trapc	349.0	334.3	306.8	0.0	0.0	0.0	0.0	0.0	0.0	245.2	294.2	324.7
trapc7	136.2	129.7	124.3	0.0	0.0	0.0	0.0	0.0	0.0	107.2	121.0	129.7
trapt1	126.8	119.5	111.4	0.0	0.0	0.0	0.0	0.0	0.0	93.8	109.3	116.5
trapt	0.0	0.0	0.0	347.9	351.9	357.0	0.0	0.0	0.0	249.2	315.8	341.1
lvs	128.7	158.1	167.8	0.0	0.0	0.0	0.0	0.0	0.0	164.5	169.5	166.2
rmn	273.4	268.4	239.8	0.0	0.0	0.0	0.0	0.0	0.0	248.7	246.3	243.6
rmjt2	126.8	118.1	84.5	0.0	0.0	0.0	0.0	0.0	0.0	96.9	96.6	97.8
rmjt3	79.7	74.4	59.0	0.0	0.0	0.0	0.0	0.0	0.0	66.4	65.9	66.4
pmn	0.0	0.0	0.0	185.1	383.5	448.0	387.1	452.2	423.4	0.0	0.0	0.0
pmjc	403.9	413.0	412.1	0.0	0.0	0.0	0.0	0.0	0.0	80.5	169.1	280.6
pmjs	424.8	422.9	418.4	0.0	0.0	0.0	0.0	0.0	0.0	0.0	389.6	391.9
pmjr	0.0	0.0	0.0	384.5	395.6	406.4	369.0	391.9	398.9	0.0	0.0	0.0
ltdt	0.0	0.0	0.0	127.6	129.4	131.3	0.0	0.0	0.0	139.5	143.3	147.5
ltdl	0.0	0.0	0.0	88.0	92.6	96.8	0.0	0.0	0.0	104.8	106.0	107.1
ltdi	0.0	0.0	0.0	143.8	145.6	146.6	0.0	0.0	0.0	142.0	140.3	139.0

Table A.6: Passive force produced by each muscle with muscle parameters optimized for all exercises

	Passive Forces Produced by Each Muscle											
Muscles	1	2	3	4	5	6	7	8	9	10	11	12
subclav	0.9	0.9	1.0	1.0	0.9	0.8	1.0	0.8	0.9	1.5	1.1	0.9
serants	64.3	24.9	3.7	10.4	1.3	0.2	41.4	0.6	0.1	455.0	27.9	0.8
serantm	1.7	3.3	6.3	0.2	0.2	0.2	12.5	3.8	0.7	18.7	7.4	2.5
seranti	1.5	3.8	10.7	0.2	0.3	0.5	11.9	14.6	4.3	8.4	7.4	7.0
trapc	2.8	0.8	0.2	18.7	9.3	3.4	0.4	2.0	6.0	0.1	0.1	0.5
trapc7	0.4	0.2	0.1	1.6	1.1	0.7	0.1	0.4	0.9	0.0	0.1	0.2
trapt1	0.5	0.2	0.1	2.3	1.4	0.7	0.1	0.2	0.6	0.0	0.1	0.1
trapt	0.2	0.2	0.3	0.6	0.8	0.9	0.1	0.4	1.0	0.1	0.2	0.5
lvs	10.2	3.7	0.7	14.8	6.2	2.0	2.0	0.7	0.7	2.5	1.3	0.5
rmn	2.7	0.8	0.2	8.7	3.9	1.3	0.3	0.2	0.4	0.3	0.2	0.2
rmjt2	0.2	0.1	0.0	0.6	0.3	0.2	0.0	0.0	0.0	0.0	0.0	0.0
rmjt3	0.1	0.0	0.0	0.5	0.3	0.2	0.0	0.0	0.0	0.0	0.0	0.0
pmn	0.6	6.9	72.1	0.0	0.2	1.8	16.5	2.7	0.7	262.8	116.4	29.3
pmjc	5.8	3.8	1.8	5.7	3.4	1.7	0.0	0.1	0.1	0.0	0.0	0.1
pmjs	0.9	0.8	0.7	0.8	0.7	0.5	0.2	0.2	0.3	0.3	0.3	0.3
pmjr	1.8	3.4	6.9	0.7	1.1	1.9	11.0	6.8	5.5	32.9	23.6	16.7
ltdt	0.0	0.0	0.0	0.0	0.1	0.1	0.1	0.2	0.3	0.1	0.2	0.3
ltdl	0.0	0.0	0.0	0.0	0.0	0.0	0.1	0.1	0.1	0.1	0.1	0.1
ltdi	0.5	0.6	1.0	0.5	0.6	0.9	1.7	1.9	2.2	2.2	2.5	2.7

Table A.7: Total force produced by each muscle with muscle parameters optimized for elevation and depression exercises only

	Total Force Produced by Each Muscle											
Muscles	1	2	3	4	5	6	7	8	9	10	11	12
subclav	52.8	52.8	1.0	1.0	0.9	53.1	52.4	53.1	0.9	1.4	1.1	0.9
serants	589.2	657.6	671.8	5.9	0.8	0.1	625.2	599.2	180.2	204.6	14.4	0.6
serantm	256.7	247.5	9.1	0.3	0.2	227.2	201.9	244.0	254.7	27.9	10.7	3.5
seranti	1.9	4.8	14.1	434.5	444.1	460.0	460.7	446.8	493.8	11.0	9.7	9.1
trapc	362.1	347.7	317.8	23.4	11.5	4.1	0.5	2.3	7.4	254.5	304.9	337.4
trapc7	158.3	157.6	151.5	7.1	4.8	2.7	0.4	1.4	3.5	137.2	146.8	157.6
trapt1	137.2	132.3	122.6	4.9	2.9	1.3	0.2	0.4	1.0	110.5	120.5	128.9
trapt	0.2	0.2	0.3	350.7	354.4	359.5	0.1	0.4	1.1	257.4	318.2	343.7
lvs	141.6	161.9	164.8	12.1	5.1	1.6	1.7	0.6	0.4	166.0	168.1	162.8
rmn	282.2	284.0	253.5	13.5	5.8	1.9	0.4	0.3	0.5	263.4	260.5	257.4
rmjt2	138.8	128.7	107.1	1.2	0.6	0.3	0.0	0.0	0.1	115.6	115.3	116.0
rmjt3	83.4	77.6	65.9	0.7	0.4	0.2	0.0	0.0	0.0	71.6	71.2	71.5
pmn	0.6	4.4	34.3	219.6	338.8	388.4	369.8	393.4	369.9	112.6	52.7	15.4
pmjc	357.6	393.4	447.4	44.0	24.9	11.3	0.1	0.3	0.6	285.9	376.4	417.5
pmjs	470.1	468.4	464.1	1.5	1.3	1.0	0.4	0.4	0.5	0.6	429.6	432.2
pmjr	4.1	8.5	18.1	437.0	444.9	444.2	353.5	388.0	401.3	97.0	67.8	47.0
ltdt	0.0	0.0	0.0	130.7	132.1	133.6	0.2	0.2	0.4	141.1	145.1	149.5
ltdl	0.0	0.0	0.0	95.0	98.1	100.9	0.1	0.1	0.2	108.1	109.4	110.5
ltdi	1.9	2.6	4.4	169.2	165.9	159.0	8.7	9.6	11.2	135.9	132.3	129.5

Table A.8: Active force produced by each muscle with muscle parameters optimized for elevation and depression exercises only

	Active Forces Produced by Each Muscle											
Muscles	1	2	3	4	5	6	7	8	9	10	11	12
subclav	51.9	51.9	0.0	0.0	0.0	52.2	51.4	52.3	0.0	0.0	0.0	0.0
serants	559.0	644.8	669.4	0.0	0.0	0.0	604.8	598.8	180.2	0.0	0.0	0.0
serantm	254.3	242.8	0.0	0.0	0.0	227.0	183.2	238.6	253.6	0.0	0.0	0.0
seranti	0.0	0.0	0.0	434.3	443.7	459.5	444.9	427.4	485.7	0.0	0.0	0.0
trapc	358.8	346.8	317.6	0.0	0.0	0.0	0.0	0.0	0.0	254.4	304.7	336.9
trapc7	156.7	156.9	151.2	0.0	0.0	0.0	0.0	0.0	0.0	137.1	146.6	156.9
trapt1	136.1	131.9	122.5	0.0	0.0	0.0	0.0	0.0	0.0	110.4	120.4	128.6
trapt	0.0	0.0	0.0	350.0	353.6	358.5	0.0	0.0	0.0	257.3	318.0	343.1
lvs	133.3	158.9	164.3	0.0	0.0	0.0	0.0	0.0	0.0	163.9	167.0	162.3
rmn	278.2	282.8	253.3	0.0	0.0	0.0	0.0	0.0	0.0	263.1	260.2	257.1
rmjt2	138.5	128.6	107.1	0.0	0.0	0.0	0.0	0.0	0.0	115.6	115.2	116.0
rmjt3	83.2	77.6	65.9	0.0	0.0	0.0	0.0	0.0	0.0	71.5	71.2	71.4
pmn	0.0	0.0	0.0	219.5	338.6	387.0	360.3	391.4	369.2	0.0	0.0	0.0
pmjc	310.7	365.1	435.1	0.0	0.0	0.0	0.0	0.0	0.0	285.8	376.3	417.3
pmjs	468.4	466.8	462.8	0.0	0.0	0.0	0.0	0.0	0.0	0.0	429.2	431.7
pmjr	0.0	0.0	0.0	435.5	442.5	439.7	322.6	369.7	386.6	0.0	0.0	0.0
ltdt	0.0	0.0	0.0	130.6	132.1	133.6	0.0	0.0	0.0	141.0	144.9	149.1
ltdl	0.0	0.0	0.0	95.0	98.0	100.9	0.0	0.0	0.0	108.0	109.2	110.4
ltdi	0.0	0.0	0.0	167.2	163.2	154.8	0.0	0.0	0.0	124.4	119.0	114.6

Table A.9: Passive force produced by each muscle with muscle parameters optimized for elevation and depression exercises only

	Passive Forces Produced by Each Muscle											
Muscles	1	2	3	4	5	6	7	8	9	10	11	12
subclav	0.9	0.9	1.0	1.0	0.9	0.8	1.0	0.8	0.9	1.4	1.1	0.9
serants	30.2	12.9	2.3	5.9	0.8	0.1	20.3	0.4	0.0	204.6	14.4	0.6
serantm	2.4	4.7	9.1	0.3	0.2	0.2	18.7	5.5	1.1	27.9	10.7	3.5
seranti	1.9	4.8	14.1	0.2	0.3	0.5	15.7	19.4	8.2	11.0	9.7	9.1
trapc	3.3	0.9	0.2	23.4	11.5	4.1	0.5	2.3	7.4	0.1	0.1	0.6
trapc7	1.6	0.7	0.3	7.1	4.8	2.7	0.4	1.4	3.5	0.1	0.2	0.7
trapt1	1.1	0.4	0.1	4.9	2.9	1.3	0.2	0.4	1.0	0.0	0.1	0.2
trapt	0.2	0.2	0.3	0.7	0.8	1.0	0.1	0.4	1.1	0.1	0.2	0.5
lvs	8.3	3.0	0.6	12.1	5.1	1.6	1.7	0.6	0.4	2.1	1.1	0.5
rmn	4.0	1.1	0.2	13.5	5.8	1.9	0.4	0.3	0.5	0.4	0.3	0.3
rmjt2	0.3	0.1	0.0	1.2	0.6	0.3	0.0	0.0	0.1	0.0	0.0	0.0
rmjt3	0.2	0.1	0.0	0.7	0.4	0.2	0.0	0.0	0.0	0.0	0.0	0.0
pmn	0.6	4.4	34.3	0.0	0.2	1.4	9.5	2.0	0.7	112.6	52.7	15.4
pmjc	46.8	28.3	12.3	44.0	24.9	11.3	0.1	0.3	0.6	0.1	0.1	0.3
pmjs	1.7	1.6	1.3	1.5	1.3	1.0	0.4	0.4	0.5	0.6	0.4	0.5
pmjr	4.1	8.5	18.1	1.5	2.4	4.5	30.9	18.3	14.7	97.0	67.8	47.0
ltdt	0.0	0.0	0.0	0.1	0.1	0.1	0.2	0.2	0.4	0.1	0.2	0.3
ltdl	0.0	0.0	0.0	0.0	0.0	0.1	0.1	0.1	0.2	0.1	0.2	0.2
ltdi	1.9	2.6	4.4	2.0	2.8	4.3	8.7	9.6	11.2	11.5	13.3	14.9

APPENDIX B

Exercise Force Graphs

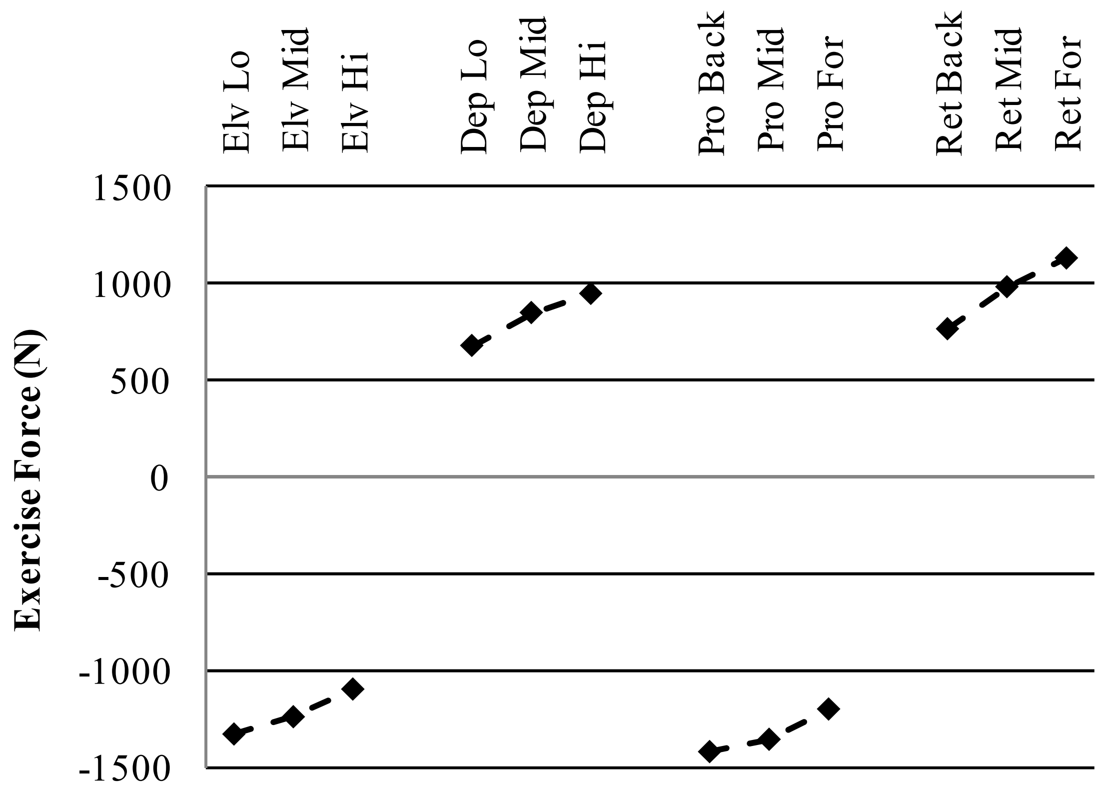

Figure B.1: Graph of exercise forces measured experimentally in Garner and Shim [1]

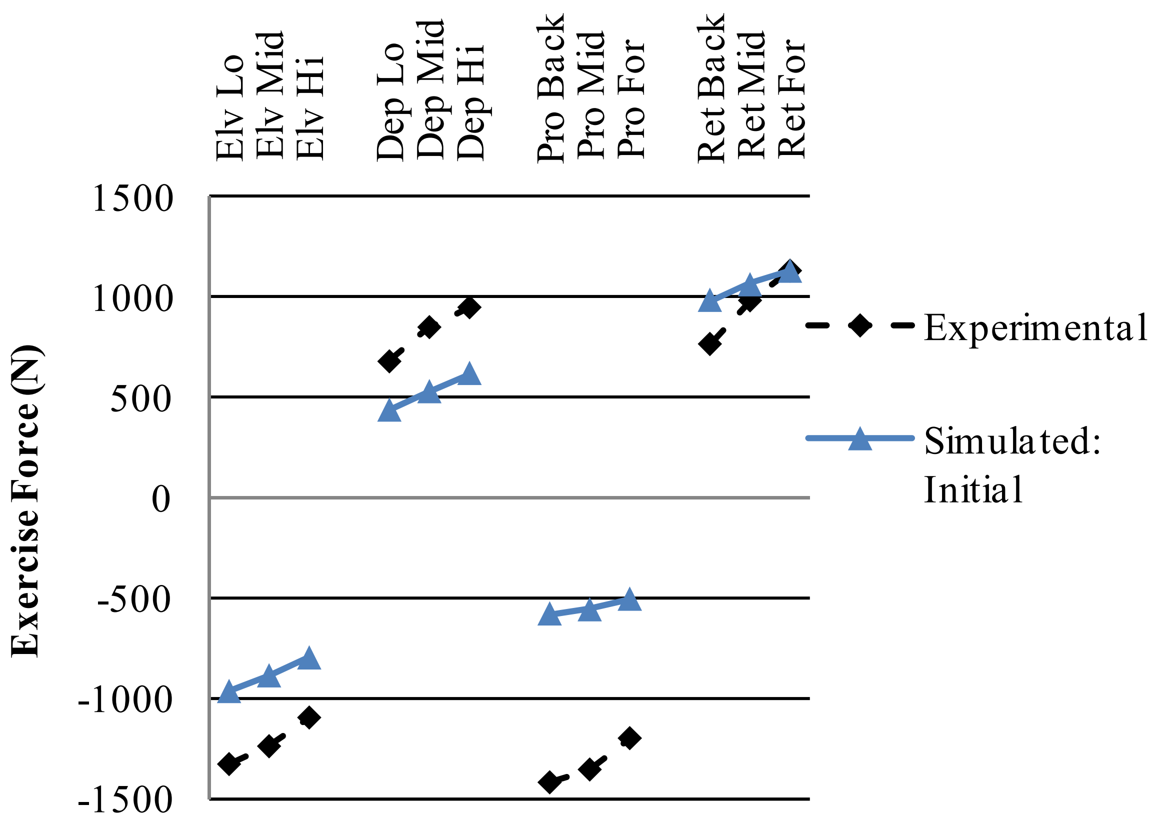

Figure B.2: Graph of exercise forces generated through exercise simulation using initial muscle parameter values. Experimental exercise force values listed for comparison.

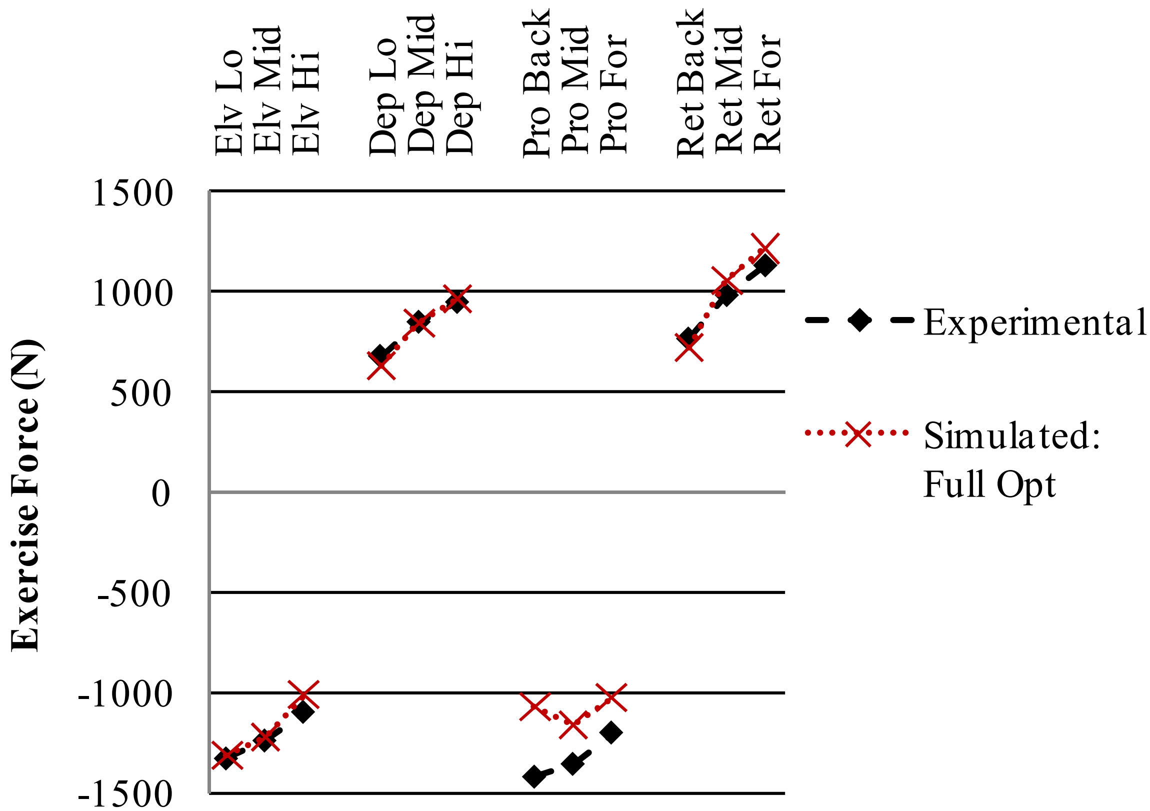

FigureB.3: Graph of exercise forces generated through exercise simulation using muscle parameters after full optimization. Experimental exercise force values listed for comparison.

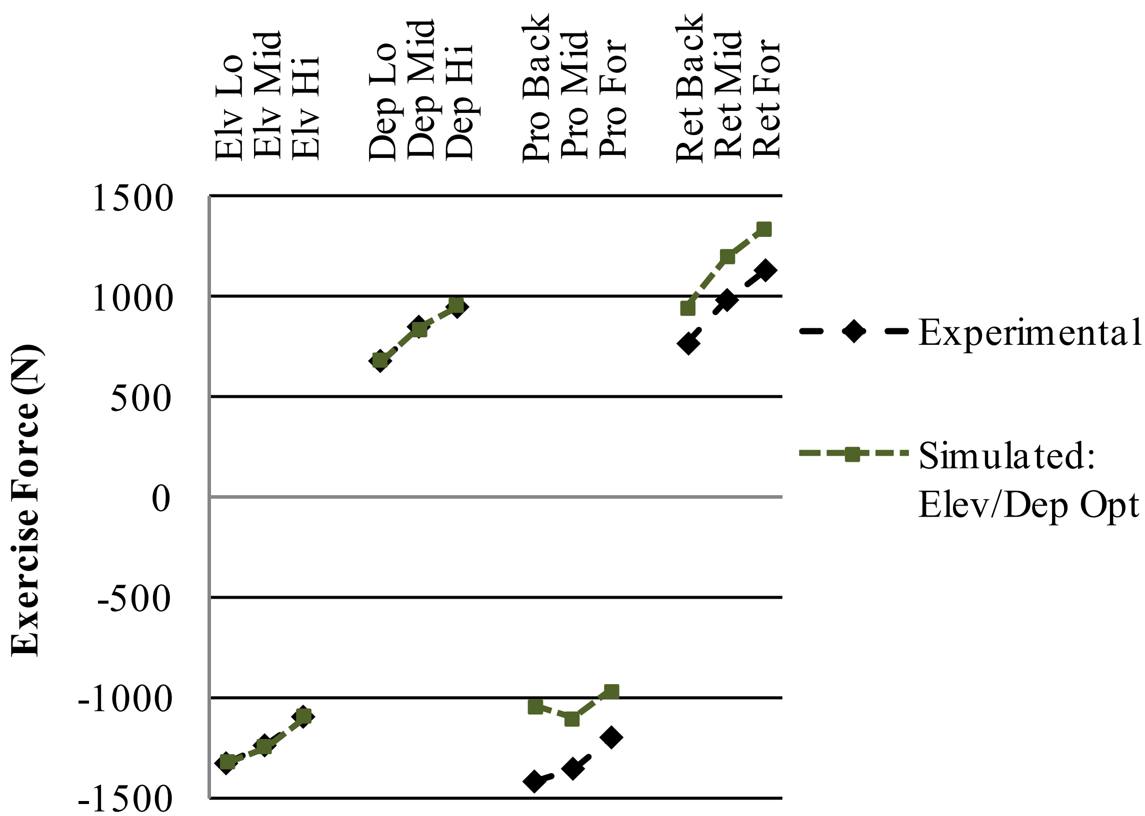

Figure B.4: Graph of exercise forces generated through exercise simulation using muscle parameters after half (elevation & depression only) optimization. Experimental exercise force values listed for comparison.

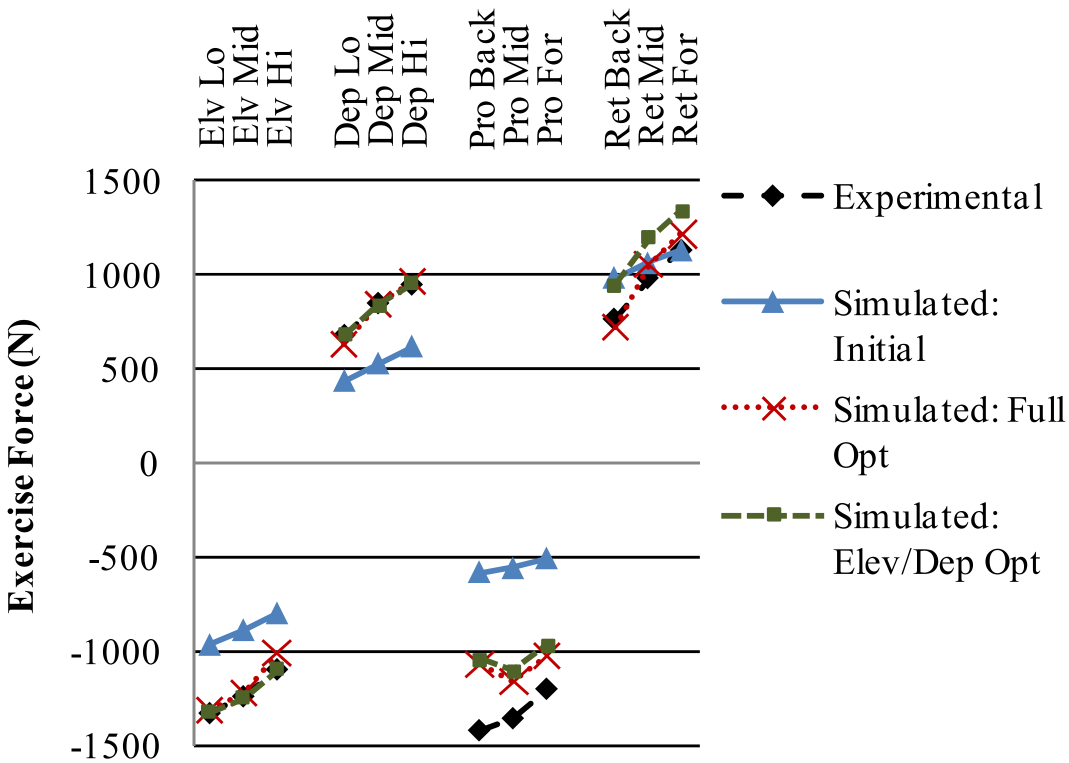

Figure B.5: Graph of exercise forces generated through all exercise simulations. Experimental exercise force values listed for comparison.

APPENDIX C

Muscle Lengths

Table C.1: Individual muscle lengths for every exercise with initial muscle parameters

Muscles	1	2	3	4	5	6	7	8	9	10	11	12	Ave	Std Dev	Lom	%L0/Lom
subclav	0.012	0.012	0.013	0.013	0.012	0.011	0.012	0.011	0.012	0.015	0.013	0.012	0.012	0.001	0.0202	61.2
serants	0.089	0.085	0.077	0.080	0.071	0.064	0.088	0.070	0.057	0.097	0.084	0.070	0.078	0.012	0.1135	68.4
serantm	0.145	0.152	0.156	0.124	0.122	0.122	0.164	0.153	0.139	0.167	0.158	0.147	0.146	0.016	0.1791	81.3
seranti	0.184	0.196	0.210	0.160	0.164	0.170	0.213	0.216	0.208	0.206	0.205	0.204	0.195	0.020	0.2315	84.1
trapc	0.179	0.165	0.151	0.198	0.190	0.179	0.157	0.173	0.186	0.137	0.146	0.160	0.169	0.019	0.1862	90.5
trapc7	0.199	0.185	0.174	0.222	0.215	0.206	0.175	0.196	0.210	0.151	0.167	0.185	0.190	0.021	0.2144	88.8
trapt1	0.179	0.162	0.144	0.203	0.195	0.183	0.147	0.164	0.177	0.127	0.140	0.156	0.165	0.023	0.1937	85.1
trapt	0.130	0.128	0.135	0.150	0.153	0.157	0.120	0.143	0.159	0.109	0.127	0.146	0.138	0.016	0.1591	86.8
lvs	0.180	0.166	0.143	0.185	0.173	0.157	0.158	0.143	0.136	0.161	0.152	0.140	0.158	0.016	0.1902	82.9
rmn	0.155	0.138	0.115	0.171	0.160	0.144	0.125	0.120	0.123	0.123	0.120	0.118	0.134	0.019	0.1755	76.5
rmjt2	0.148	0.130	0.108	0.168	0.158	0.144	0.114	0.112	0.118	0.113	0.113	0.113	0.128	0.021	0.1747	73.5
rmjt3	0.151	0.133	0.113	0.174	0.165	0.154	0.114	0.109	0.118	0.119	0.119	0.119	0.132	0.023	0.1833	72.2
pmn	0.091	0.104	0.116	0.076	0.086	0.098	0.110	0.100	0.093	0.124	0.119	0.111	0.102	0.014	0.1503	68.1
pmjc	0.227	0.219	0.206	0.226	0.216	0.203	0.130	0.145	0.156	0.120	0.131	0.144	0.177	0.042	0.2265	78.1
pmjs	0.098	0.097	0.094	0.097	0.094	0.090	0.072	0.074	0.078	0.080	0.077	0.078	0.086	0.010	0.1658	51.8
pmjr	0.119	0.130	0.141	0.104	0.111	0.120	0.147	0.140	0.137	0.166	0.161	0.155	0.136	0.020	0.1776	76.5
ltdt	0.120	0.117	0.122	0.143	0.146	0.150	0.182	0.198	0.214	0.177	0.192	0.207	0.164	0.035	0.3487	47.1
ltdl	0.181	0.190	0.206	0.187	0.197	0.210	0.256	0.263	0.272	0.258	0.266	0.274	0.230	0.037	0.3478	66.1
ltdi	0.304	0.315	0.334	0.304	0.316	0.331	0.358	0.362	0.367	0.366	0.371	0.375	0.342	0.027	0.4817	71.0

Table C.2: Individual muscle lengths for every exercise with muscle parameters optimized for all exercises

Muscles	1	2	3	4	5	6	7	8	9	10	11	12	Ave	Std Dev	Lom	%L0/Lom
subclav	0.056	0.056	0.057	0.057	0.056	0.056	0.057	0.056	0.056	0.059	0.057	0.056	0.057	0.001	0.0536	105.8
serants	0.049	0.046	0.038	0.042	0.033	0.025	0.048	0.030	0.019	0.058	0.046	0.032	0.039	0.011	0.0407	95.4
serantm	0.092	0.098	0.104	0.072	0.070	0.068	0.111	0.100	0.086	0.115	0.106	0.095	0.093	0.016	0.0954	97.6
seranti	0.115	0.127	0.140	0.088	0.092	0.099	0.142	0.144	0.136	0.137	0.136	0.135	0.124	0.020	0.1302	95.4
trapc	0.107	0.093	0.079	0.128	0.121	0.110	0.087	0.103	0.116	0.066	0.074	0.088	0.098	0.020	0.1098	89.0
trapc7	0.163	0.149	0.138	0.187	0.180	0.171	0.140	0.161	0.175	0.115	0.131	0.149	0.155	0.022	0.1838	84.2
trapt1	0.158	0.141	0.123	0.183	0.174	0.162	0.127	0.144	0.156	0.106	0.119	0.135	0.144	0.023	0.1728	83.4
trapt	0.125	0.123	0.130	0.145	0.148	0.152	0.115	0.138	0.154	0.104	0.122	0.141	0.133	0.016	0.1762	75.4
lvs	0.165	0.151	0.127	0.170	0.158	0.142	0.143	0.128	0.121	0.146	0.136	0.124	0.143	0.016	0.1399	101.9
rmn	0.141	0.124	0.100	0.157	0.146	0.131	0.111	0.106	0.109	0.108	0.106	0.104	0.120	0.019	0.1411	85.2
rmjt2	0.140	0.122	0.100	0.160	0.150	0.136	0.106	0.104	0.110	0.105	0.105	0.105	0.120	0.021	0.1743	68.9
rmjt3	0.142	0.124	0.104	0.166	0.157	0.145	0.106	0.100	0.109	0.110	0.110	0.110	0.124	0.023	0.1752	70.5
pmn	0.043	0.056	0.068	0.028	0.036	0.048	0.060	0.050	0.044	0.075	0.071	0.063	0.054	0.015	0.0533	100.4
pmjc	0.193	0.185	0.172	0.193	0.184	0.171	0.097	0.112	0.124	0.087	0.098	0.110	0.144	0.042	0.1870	76.9
pmjs	0.151	0.149	0.147	0.149	0.146	0.141	0.124	0.126	0.130	0.132	0.128	0.130	0.138	0.010	0.1797	76.6
pmjr	0.146	0.157	0.168	0.132	0.138	0.148	0.176	0.168	0.165	0.193	0.188	0.182	0.163	0.020	0.1599	102.2
ltdt	0.229	0.226	0.231	0.251	0.254	0.259	0.291	0.307	0.323	0.287	0.302	0.318	0.273	0.036	0.3857	70.8
ltdl	0.314	0.322	0.338	0.321	0.331	0.345	0.388	0.395	0.404	0.394	0.402	0.410	0.364	0.038	0.5189	70.1
ltdi	0.365	0.376	0.395	0.367	0.378	0.394	0.419	0.423	0.428	0.429	0.434	0.438	0.404	0.028	0.4124	97.9

Table C.3: Individual muscle lengths for every exercise with muscle parameters optimized for elevation and depression exercises

Muscles	1	2	3	4	5	6	7	8	9	10	11	12	Ave	Std Dev	Lom	%L0/Lom
subclav	0.056	0.056	0.057	0.057	0.056	0.056	0.057	0.056	0.056	0.059	0.057	0.056	0.057	0.001	0.054	105.7
serants	0.051	0.048	0.040	0.044	0.035	0.027	0.050	0.032	0.021	0.060	0.048	0.034	0.041	0.011	0.045	91.4
serantm	0.092	0.098	0.104	0.072	0.070	0.068	0.111	0.100	0.086	0.115	0.106	0.095	0.093	0.016	0.093	100.6
seranti	0.115	0.127	0.140	0.088	0.092	0.099	0.142	0.144	0.136	0.137	0.135	0.135	0.124	0.020	0.127	97.6
trapc	0.105	0.091	0.078	0.126	0.119	0.108	0.085	0.102	0.114	0.064	0.072	0.087	0.096	0.020	0.106	90.1
trapc7	0.162	0.148	0.137	0.186	0.180	0.171	0.139	0.160	0.174	0.115	0.130	0.149	0.154	0.022	0.162	95.3
trapt1	0.158	0.140	0.123	0.183	0.174	0.162	0.127	0.143	0.156	0.106	0.119	0.134	0.144	0.023	0.162	88.7
trapt	0.126	0.124	0.131	0.147	0.149	0.153	0.116	0.139	0.155	0.105	0.123	0.142	0.134	0.016	0.176	76.2
lvs	0.165	0.150	0.127	0.170	0.158	0.142	0.143	0.128	0.121	0.146	0.136	0.124	0.142	0.016	0.142	100.2
rmn	0.141	0.123	0.100	0.157	0.146	0.130	0.111	0.106	0.109	0.108	0.106	0.103	0.120	0.019	0.136	88.2
rmjt2	0.142	0.124	0.102	0.162	0.152	0.138	0.108	0.105	0.112	0.107	0.106	0.107	0.122	0.021	0.166	73.7
rmjt3	0.143	0.126	0.106	0.167	0.158	0.147	0.107	0.102	0.111	0.112	0.111	0.112	0.125	0.023	0.171	73.1
pmn	0.050	0.062	0.075	0.034	0.043	0.055	0.067	0.057	0.050	0.082	0.077	0.070	0.060	0.015	0.061	98.0
pmjc	0.199	0.191	0.177	0.198	0.189	0.176	0.103	0.117	0.129	0.092	0.103	0.116	0.149	0.042	0.162	92.0
pmjs	0.151	0.150	0.147	0.150	0.146	0.142	0.125	0.126	0.130	0.132	0.129	0.130	0.138	0.010	0.169	81.9
pmjr	0.146	0.157	0.168	0.132	0.138	0.148	0.176	0.168	0.165	0.193	0.188	0.182	0.163	0.020	0.147	110.9
ltdt	0.234	0.232	0.237	0.257	0.260	0.264	0.296	0.313	0.328	0.292	0.308	0.323	0.279	0.036	0.385	72.3
ltdl	0.325	0.333	0.349	0.332	0.342	0.356	0.399	0.406	0.415	0.405	0.414	0.421	0.375	0.038	0.514	72.9
ltdi	0.360	0.372	0.390	0.362	0.374	0.389	0.415	0.418	0.423	0.425	0.430	0.434	0.399	0.028	0.356	112.0

APPENDIX D

Exercise Apparatus Figures

Figure D.1: Subject Demonstrating Elevation Exercise on Custom Apparatus [5]

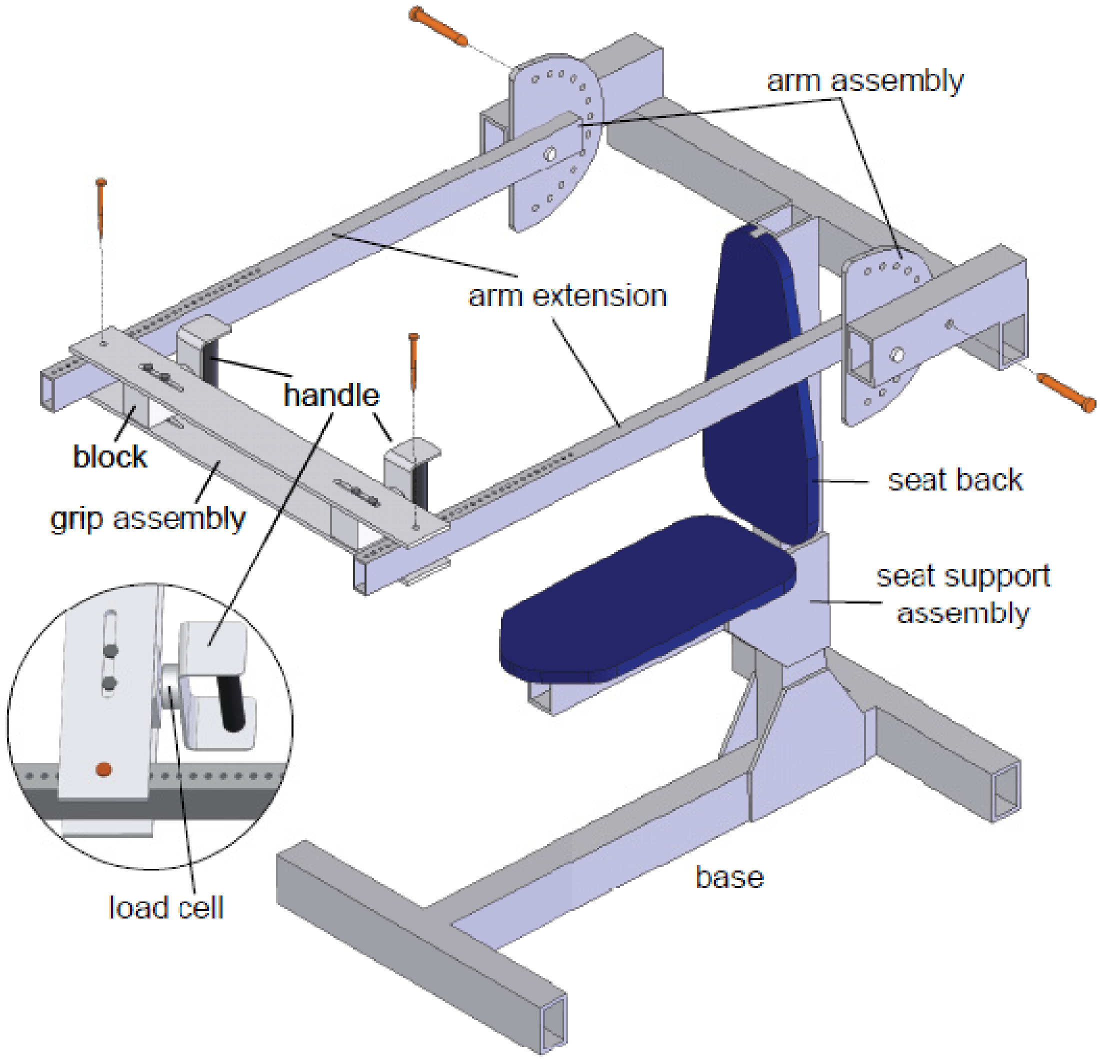

Figure D.2: Design of Custom Apparatus Used in Garner and Shim Exercise Experiment [5]

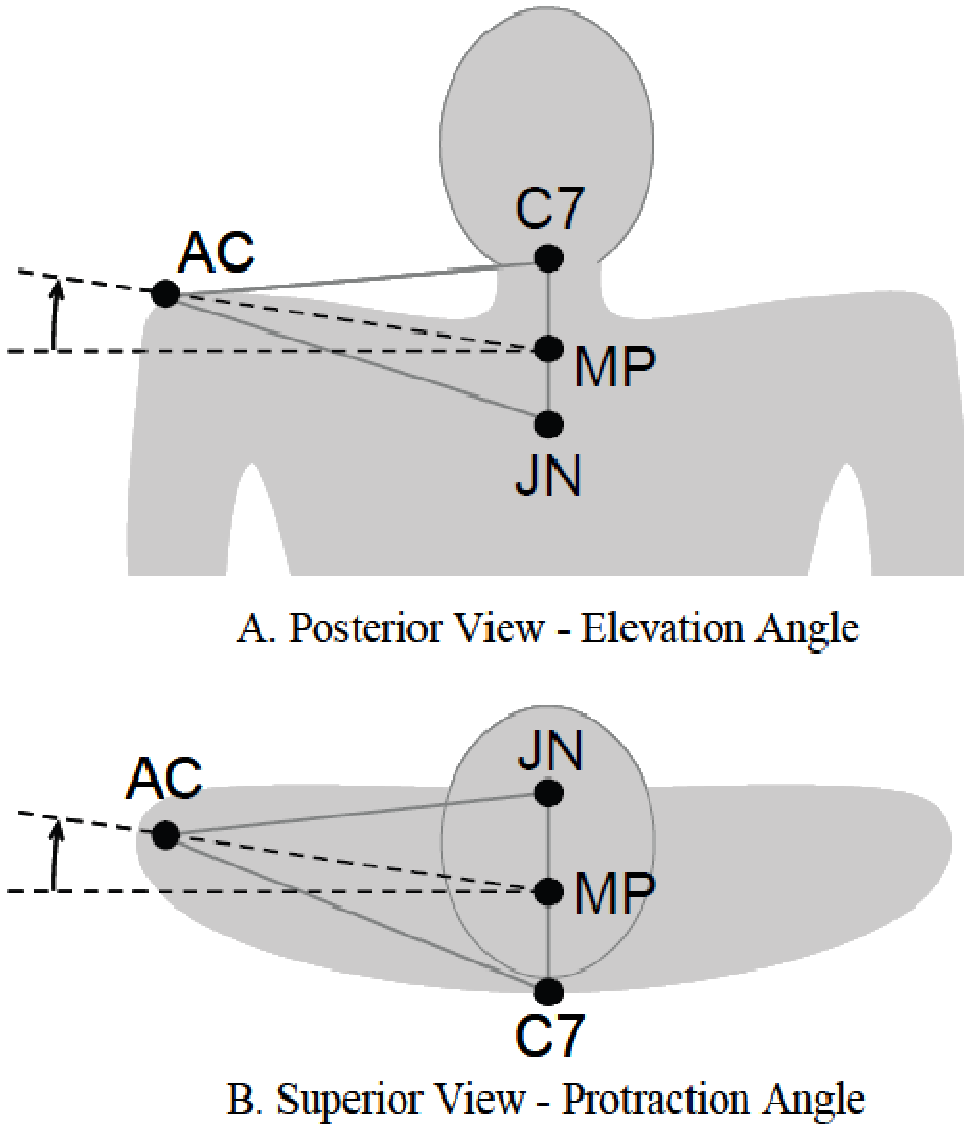

Figure D.3: Elevation and Protraction Angle Illustration [5]

REFERENCES

[1] Garner, B. A., and Shim, J., 2008, "Isometric Shoulder Girdle Strength of Healthy Young Adults," Clinical Biomechanics, **23**(1) pp. 30-37.

[2] US National Library of Medicine, 2010, "The Visible Human Project," **2010**pp. 1.

[3] Gao, F., Damsgaard, M., Rasmussen, J., 2002, "Computational Method for Muscle-Path Representation in Musculoskeletal Models," Biological Cybernetics, **87**pp. 199-210.

[4] Maurel, W., and Thalmann, D., 2000, "Human Shoulder Modeling Including Scapulo-Thoracic Constraint and Joint Sinus Cones," Computers & Graphics, **24**pp. 203-218.

[5] Garner, B. A., and Shim, J., 2006, "An Apparatus and Protocol to Measure Shoulder Girdle Strength," Journal of Medical Devices, Transactions of the ASME, **1**(4) pp. 246-253.

[6] Klopčar, N., and Lenarčič, J., 2006, "Bilateral and Unilateral Shoulder Girdle Kinematics during Humeral Elevation," Clinical Biomechanics, **21**pp. 20-20-26.

[7] Klopčar, N., Tomšič, M., and Lenarčič, J., 2007, "A Kinematic Model of the Shoulder Complex to Evaluate the Arm-Reachable Workspace," Journal of Biomechanics, **40**(1) pp. 86-91.

[8] Breteler, K., Spoor, C. W., and van der Helm, F. C. T., 1999, "Measuring Muscle and Joint Geometry Parameters of a Shoulder for Modeling Purposes," Journal of Biomechanics, **32**(11) pp. 1191-7.

[9] Garner, B. A., 1998, "A Musculoskeletal Model of the Upper Limb Based on the Medical Image Dataset of the Visible Human Male," .

[10] Hanson, J.T., and Lambert, D.R., 2005, "Netter's Clinical Anatomy," ICON Learning Systems, pp. 688.

[11] Williams, N., 2007, "Power and Strength - the Physical Parameters and Relationships that Exist," **2011**(January) pp. 1.

[12] Audenaert, A., and Audenaert, E., 2008, "Global Optimization Method for Combined Spherical-Cylindrical Wrapping in Musculoskeletal Upper Limb Modelling," Computer Methods and Programs in Biomedicine, **92**(1) pp. 8-19.

[13] Scepi, M., Faure, J. P., and Ridoux, N., 2004, "A Three-Dimensional Model of the Shoulder Girdle. Forces Developed in Deltoid and Supraspinatus Muscles during Abduction," Surgical and Radiological Anatomy, **26**pp. 290-296.

[14] Winters, J. M., and Strak, L., 1988, "Estimated Mechanical Properties of Human Joints," Journal of Biome, **21**pp. 1027-1041.

[15] Favre, P., Sheikh, R., Fucentese, S., 2005, "An Algorithm for Estimation of Shoulder Muscle Forces for Clinical use," Clinical Biomechanics, **20**pp. 822-833.

[16] An, K. N., Takahashi, K., Harrigan, T. P., 1984, "Determination of Muscle Orientations and Moment Arms," Journal of Biomechanics, **106**pp. 280-282.

[17] Ruckstuhl, H., Krzycki, J., Petrou, N., 2009, "Shoulder Abduction Moment Arms in Three Clinically Important Positions," Journal of Shoulder and Elbow Surgery, **18**(4) pp. 632-638.

[18] Kuechle, D. K., Newman, S. R., Itoi, E., 1997, "Shoulder Muscle Moment Arms during Horizontal Flexion and Elevation," Journal of Shoulder and Elbow Surgery, **6**pp. 429-439.

[19] Kuechle, D. K., Newman, S. R., Itoi, E., 2000, "The Relevance of the Moment Arm of Shoulder Muscles with Respect to Axial Rotation of the Glenohumeral Joint in Four Positions," Clinical Biomechanics, **15**(5) pp. 322-329.

[20] Veeger, H. E. J., and van der Helm, F. C. T., 2007, "Shoulder Function: The Perfect Compromise between Mobility and Stability," Journal of Biomechanics, **40**pp. 2119-2119-2129.

[21] Williams, D. A., Roush, J. R., and Davies, G. J., 2009, "Alternative Methods for Measuring Scapular Muscles Protraction and Retraction Maximal Isometric Forces," North American Journal of Sports Physical Therapy, **4**(4) pp. 200-209.

[22] Langenderfer, J., Jerabek, S. A., Thangamani, V. B., 2004, "Musculoskeletal Parameters of Muscles Crossing the Shoulder and Elbow and the Effect of Sarcomere Length Sample Size on Estimation of Optimal Muscle Length," Clinical Biomechanics, **19**pp. 664-670.

[23] Garner, B. A., and Pandy, M. G., 2000, "The Obstacle-Set Method for Representing Muscle Paths in Musculoskeletal Models," Computer Methods in Biomechanics and Biomedical Engineering, **3**pp. 1-30.

[24] Garner, B. A., and Pandy, M. G., 1999, "A Kinematic Model of the Upper Limb Based on the Visible Human Project (VHP) Image Dataset," Computer Methods in Biomechanics and Biomedical Engineering, **2**pp. 107-107-124.

[25] Garner, B. A., and Pandy, M. G., 2001, "Musculoskeletal Model of the Upper Limb Based on the Visible Human Male Dataset." Computer Methods in Biomechanics and Biomedical Engineering, **4**(2) pp. 93.

[26] Garner, B. A., and Pandy, M. G., 2003, "Estimation of Musculotendon Properties in the Human Upper Limb," Annals of Biomedical Engineering, **31**(2) pp. 207-220.

[27] Lorensen, W. E., and Cline, H. E., 1987, "Marching Cubes: A High Resolution 3D Surface Construction Algorithm," Computer Graphics, **21**pp. 163-169.

[28] Bo Xu, T., 2008, "A Linked-Plane Obstacle-Set Algorithm for Modeling Broad Muscle Paths: Application to the Deltoid Muscle," .

[29] Bagg, S. D., and Forrest, W. J., 1988, "A Biomechanical Analysis of Scapular Rotation during Arm Abduction in Scapular Plane," American Journal of Physical Medicine, pp. 238-245.

[30] Borstad, J. D., and Ludewig, P. M., 2002, "Comoparison of Scapular Kinematics between Elevation and Lowering of the Arm in the Scapular Plane," Clinical Biomechanics, **17**pp. 650-659.

[31] Karduna, A. R., McClure, P. W., and Michener, L. A., 2000, "Scapular Kinematics: Effects of Alterning the Euler Angle Sequence of Rotations," Journal of Biomechanics, **33**pp. 1063-1068.

[32] van der Helm, F. C. T., and Dapena, J., "Shoulder Joints: Definition of Joint Coordinate Systems, Joint Motions and Joint Torques," **1994**.

[33] Lemay, M. A., and Crago, P. E., 1996, "A Dynamic Model for Simulating Movements of the Elbow, Forearm, and Wrist," Journal of Biomechanics, **10**pp. 1319-1330.

[34] Zajac, F. E., 1989, "Muscle and Tendon: Properties, Models, Scaling, and Application to Biomechanics and Motor Control," **17**(4) pp. 359-411.

[35] Johnson, G. R., Spaldin, D., Nowitzke, A., 1996, "Modelling the Muscles of the Scapula: Morphometric and Coordinate Data and Functional Implications," Journal of Biomechanics, **29**pp. 1039-1051.